Thesis Report

Techno-economic analysis of ammonia decomposition for large-scale hydrogen production

Author: Alexander Tkach

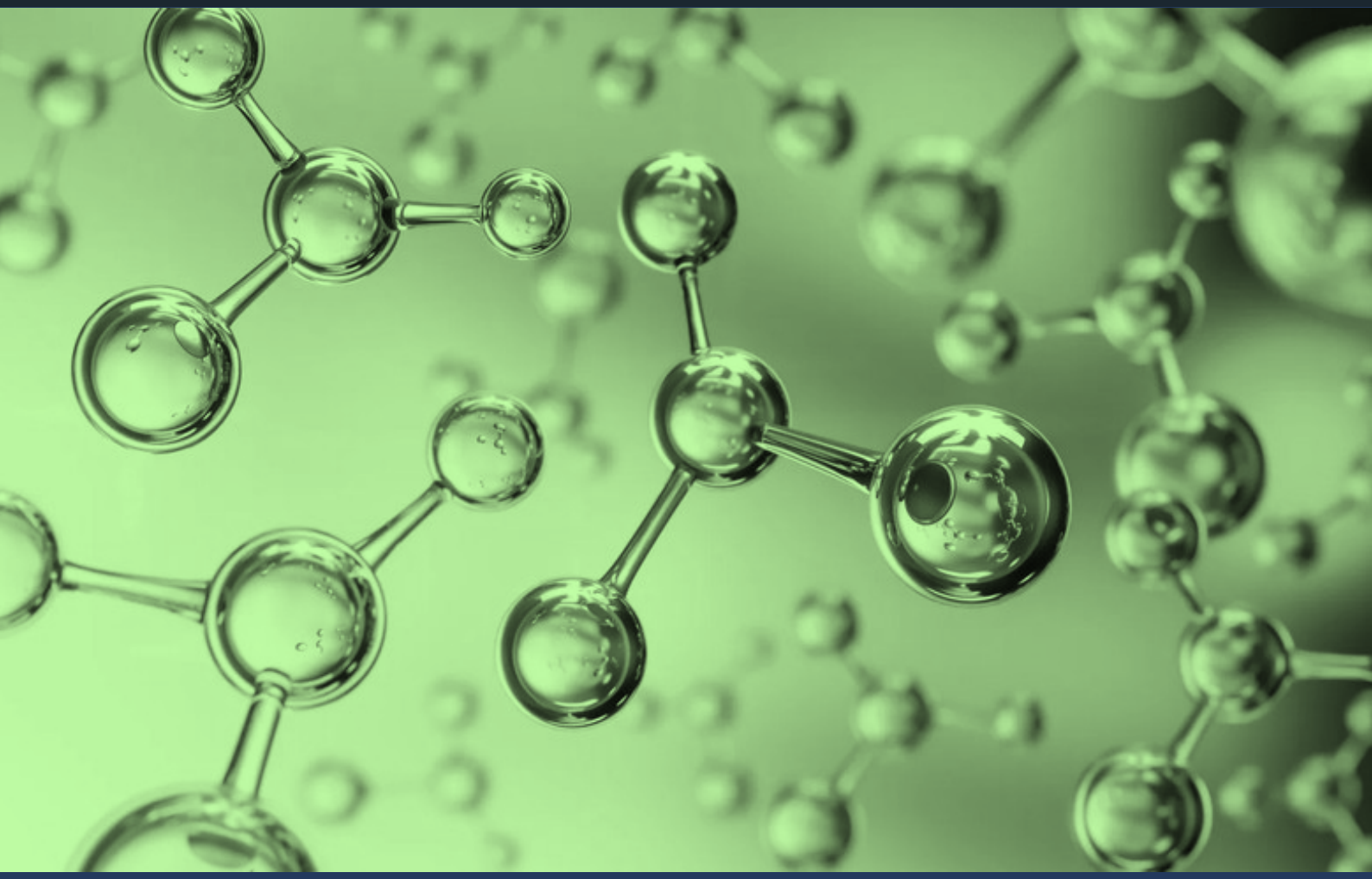

TU Delft

PROTON VENTURES

Thesis Report

Techno-economic analysis of ammonia decomposition for large-scale hydrogen production

Author: Alexander Tkach

University Supervisor: Prof.dr.ir Earl Goetheer (TU Delft)
Company Supervisor: Dr.ir. Gerard van Zee (Proton Ventures)
Project Duration: 10th of January 2023 - 28th of November 2023
Student number: 4694686

Faculty of Mechanical Engineering · Delft University of Technology

Acknowledgements

I want to express my appreciation to TU Delft and Proton Ventures for the provided opportunity to conduct my graduation thesis research within their organisations. I am greatly thankful to my academic supervisor, Prof. Dr. Earl Goetheer, for his expertise, constant encouragement and constructive feedback. His mentorship was a continuous source of inspiration during this research period. A special acknowledgment is reserved for my company supervisor, Dr. Gerard van Zee, for providing expert insights and tremendous help in shaping my ideas and elevating the quality of this research. I extend my gratitude to all my peers at TU Delft, among whom I've found the best friends of my life and with whom I have shared this journey. I also want to thank the Proton Ventures team. During my time at this company, I witnessed an outstanding working culture and an exceptional group of professionals. I am forever grateful for the professional development opportunities and the help I have received. I would also like to express my individual appreciation to MSc. Valentina Cechetto from TU Eindhoven for sharing her expertise on the membrane reactor technology, which was an invaluable help for this study.

Abstract

In the transition towards a renewable energy-powered industrial sector in the Netherlands, hydrogen plays a pivotal role. The anticipated increase in hydrogen demand by 2030 is projected to exceed the anticipated capacity of domestic green hydrogen production, hindered by the high costs and fluctuations of local renewable electricity generation. To address the growing demand, the consideration of importing more cost-effective green hydrogen is regarded as an appealing option. Storing and transporting hydrogen as green ammonia emerges as a compelling choice for hydrogen importation, given high volumetric hydrogen density of ammonia, coupled with its effective storage and well-established infrastructure. An essential element in the importation of hydrogen through green ammonia lies in the decomposition of green ammonia back into hydrogen.

This research evaluates the techno-economic feasibility of hydrogen production using an ammonia cracking process plant in the context of the Netherlands. Two process plant configurations were developed and evaluated on their performance. Both of the plants are set to generate 100 TPD of hydrogen at 50 bar pressure for the Dutch hydrogen grid. The first configuration is designed for the ammonia-to-hydrogen process plant using existing technologies applicable on a large scale by 2030, with a particular focus on the ammonia cracking reactor configuration as the central component. The second configuration is formulated based on the emerging technology of employing the membrane-assisted reactor for ammonia decomposition and is used for comparison with the existing technology configuration in the context of the year 2040.

Economic evaluation of both configurations indicates that the Levelized Cost of Hydrogen (LCOH) derived from green ammonia is primarily driven by the market price of green ammonia. Evaluating the conventional technology at 2030 market predictions, it is established that hydrogen production from imported green ammonia can compete with domestic green hydrogen production and potentially emerge as the most cost-effective option for green hydrogen import if optimistic predictions regarding green ammonia costs materialize. In comparing the conventional and emerging technology configurations for LCOH by 2040, it was determined that the membrane-assisted reactor configuration does not significantly outperform the conventional technology, even when considering the most optimistic scenarios regarding the robustness and scalability of this emerging technology.

Contents

1

Introduction

1.1. Background

1.1.1. The Transition to Renewable Energy Economy

The Paris Agreement, signed in 2015 by 195 nations, requires participating states to reduce carbon emissions by roughly 50% in order to prevent the temperature increase to exceed a maximum of 1.5°C above pre-industrial levels by 2030 [1]. The Netherlands gave its approval to the accord. The Netherlands is now investing in the production of green electricity from renewable energy sources, such as its offshore wind farms and solar farms.

Electric power can be stored by using electricity to generate hydrogen from water electrolysis. The big industrial businesses of the Netherlands have also agreed to reconfigure a significant part of their conventionally natural-gas powered production to hydrogen-powered operations.
Because the need for hydrogen would increase substantially as a result of this transition, it is anticipated that some of the necessary supply will have to be imported.The lower electricity costs for the generation of green hydrogen in the states with more abundant renewable energy sources, where prospective hydrogen production might potentially surpass local demand, are another driving force behind the necessity for hydrogen import. However, the majority of these countries, which could act as exporters of hydrogen, are located too far away from the Netherlands to allow for transportation of hydrogen via pipeline systems[2]. As a result, the Netherlands conduct exploratory research on the import of green hydrogen through its ports in collaboration with more than ten potential exporting nations, including Iceland [3], Morocco [4] , Australia[5] and Chile [6]. To facilitate efficient import of hydrogen from overseas, efficient method of hydrogen storage and transportation is required.

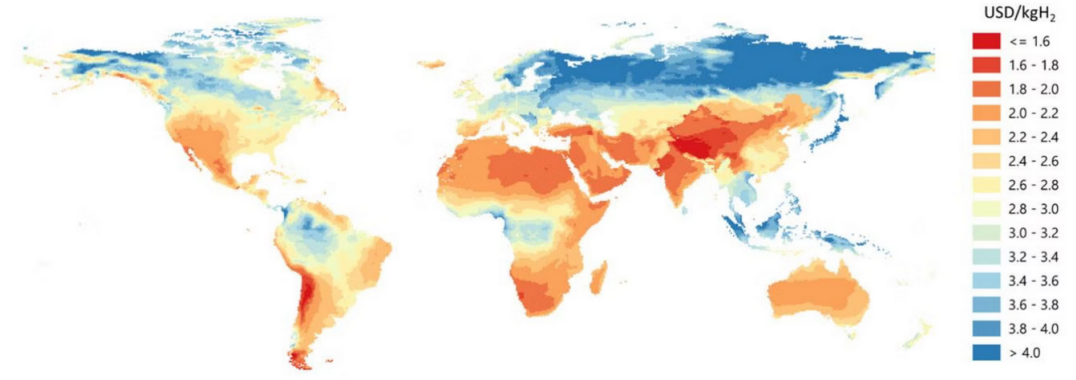

Figure 1.1: Anticipated hydrogen costs from hybrid onshore wind and solar systems by 2050[2]

1.1.2. Hydrogen Import Routes

As there is a great distance between the exporter and the importer, shipping hydrogen in tankers would be the most cost-effective way to enable the large-scale transportation of hydrogen due to its geographic advantage over the pipeline, trucks, and railway transportation. Due to very low volumetric energy density (10.05 MJ/m^3 at 1atm, 15°C)[7] hydrogen has to be stored in the tank in either compressed or liquefied form. Despite much research, both liquefaction and compression of hydrogen have substantial drawbacks. The volumetric energy density of compressed hydrogen (CH2) is still rather low after compression, which is accompanied by high storage tank costs. Hydrogen liquifaction (LH2) is an expensive and energy intensive process (the liquefaction temperature of hydrogen is −252.9 °C) . More than 30% of the energy content of the hydrogen is consumed using today's liquifaction technology [8]. Besides, some of stored hydrogen will be lost through boil-off from the storage tank in order to keep the tank pressure at a safe level [9].
The storage and transportation of hydrogen in the form of a hydrogen carrier, which would have a more developed and energy efficient transportation and storage technology, is a solution that solves these limits and is the topic of intense research. Since the purpose of importing hydrogen is to decarbonize the industry, only the green carriers, which are produced using green hydrogen, can be taken into consideration. Various hydrogen carriers are currently being investigated [10], with ammonia as one of the promising candidates [11].

1.2. Ammonia as Hydrogen Carrier

Ammonia, as a hydrogen carrier, is proposed as an efficient medium for hydrogen storage and transportation. Ammonia has multiple beneficial characteristics, when compared with other methods of hydrogen transportation:

- Ammonia can liquefy under reasonably mild conditions by either cooling to -33°C at atmospheric pressure or compressing to 8 bar at 20°C. Compared to hydrogen, this makes ammonia transport more economical.
- There is a well-established global infrastructure for the manufacturing, delivery, and storage of ammonia, with about 200 port terminals now in use. The technology and history record for safe handling of ammonia is well established. Annually, 18-20 Mt-NH_3 is shipped around the world [12].
- The hydrogen gravimetric density of liquid ammonia is 17.8% by weight. Its volumetric hydrogen density (123kg-H_2/m^3 at 1MPa) is higher than that of other hydrogen transport mediums, such as methanol (99kg-H2/m3 at 1 MPa), liquid hydrogen (71kg-H2/m3 at 1 MPa), and metal hydrides (25kg-H2/m3 at 1 MPa). This translates into a lower cost per unit of stored energy[11].
- CO_2 is not used for green ammonia production. CO_2 does not get released when decomposing ammonia back to hydrogen, unlike methanol.
- The chance of fire accidents during storage is unlikely due to narrow flammability range of ammonia (15-28% in air)[12].

Due to all of these properties, ammonia is considered a front-runner in clean and secure supply of renewable hydrogen and is a reasonable candidate for a large-scale hydrogen import medium. The following Figure 1.2[13] illustrates the whole value chain of centralized hydrogen production and distribution using green ammonia.

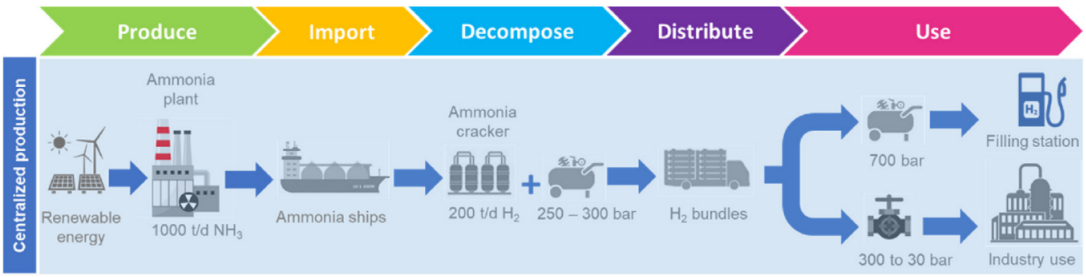

Figure 1.2: The value chain of centralized hydrogen production and distribution using green ammonia[13]

1.3. Ammonia Production

Renewable ammonia is produced from nitrogen (N_2) obtained by air separation and hydrogen (H_2) obtained by electrolysis using renewable electricity. In industry, this process is carried out using a metal catalyst and high temperatures and pressures to react nitrogen with hydrogen to produce ammonia (NH_3). This process of ammonia synthesis is known as the Haber-Bosch process and is well established in the industry.
According to latest projections, renewable ammonia will account for 8% of the current ammonia market by 2030. By then, all announced renewable ammonia plants are expected to have a combined annual production capacity of 15 Mt (by comparison, less than 0.02 Mt of renewable ammonia was produced in 2021)[12]. Thus, the long-term potential for renewable ammonia as hydrogen carrier to become a major renewable energy transportation commodity is significant.

1.4. Ammonia Decomposition

Once ammonia reaches its destination port, there are multiple steps for hydrogen production which have to be conducted to reach the prescribed quality requirements (see Figure 1.3). During the decomposition process, ammonia, coming from the storage terminal, is converted into hydrogen and nitrogen. The decomposition of ammonia is an endothermic process and requires high operating temperatures, making it highly energy intensive. The decomposition of ammonia can be greatly improved by using a catalyst. Most effective catalysts available today are made from noble metals (such as ruthenium) and are therefore quite expensive, making them difficult to apply on a large scale. The development of an efficient and affordable catalyst is a subject of intense research [14].The product gas of the reactor will contain a gas mixture of hydrogen, nitrogen, and also ammonia, unless full conversion of ammonia is achieved. Ammonia and nitrogen must be separated in order to get hydrogen up to the necessary application purity standard. Also, high recovery of hydrogen is required, to avoid product loss. The separation of gases such as nitrogen and hydrogen is an energy intensive process. Therefore, both the ammonia decomposition process and hydrogen purification are major technical barriers to hydrogen production from imported ammonia that need to be investigated.

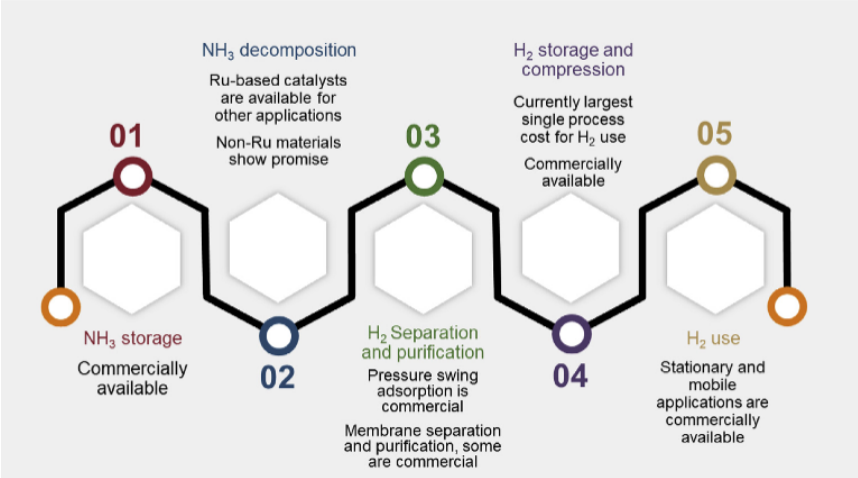

Figure 1.3: The five steps of hydrogen production through ammonia decomposition. [14]

1.5. Hydrogen Network

The level of hydrogen purification has to be in correspondence with the defined application purity standards. To use the produced hydrogen from the imported ammonia, it must be pre-treated to be admitted to the Dutch hydrogen distribution grid. Gasunie, a Dutch natural gas infrastructure company, has started a significant initiative to facilitate the national hydrogen infrastructure as 2030 draws closer. This project involves switching portion of the natural gas pipeline network along the Dutch North Sea coastline to the hydrogen gas network[15]. The hydrogen network will be used by industrial businesses in the Netherlands as they switch to hydrogen-powered operations. The port of Rotterdam, the busiest port in Europe and the largest import hub in the Netherlands, could be a suitable site to for an ammonia decomposition plant.

There, the produced hydrogen would be connected to the Dutch industry cluster through the new hydrogen network pipeline, which is expected to be operational by 2025 [16].

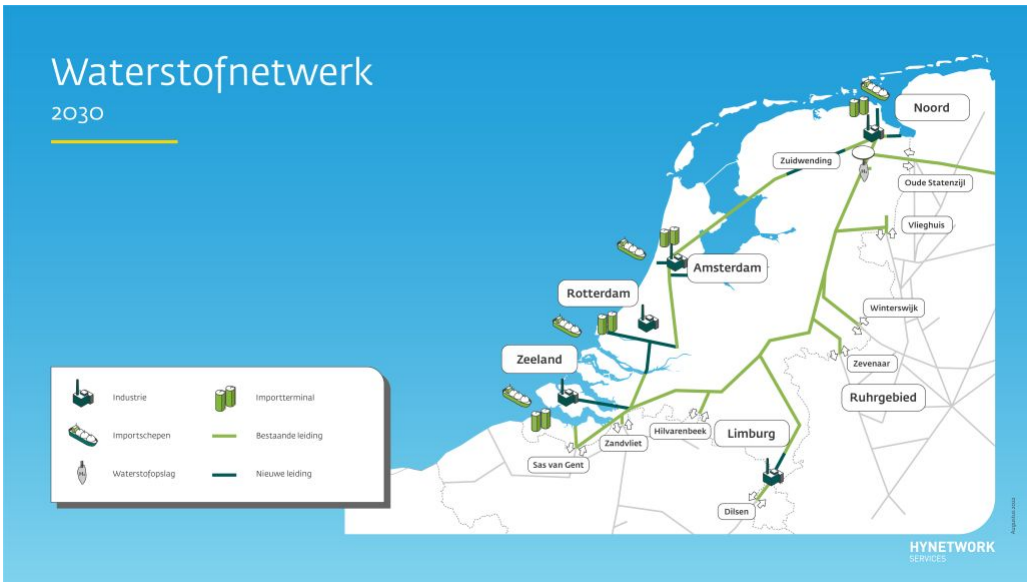

Figure 1.4: 2030 Hydrogen Network by Gasunie [15]

1.5.1. Product Requirements

The operational pressure regime of the hydrogen network is 50 bar. The hydrogen network purity standards of the industrial grade hydrogen are in accordance with the market and producers, and are visualized in Figure 1.5 [17]. Since hydrogen will mainly be used as a replacement for natural gas in industrial incinerators, a purity of 98% was chosen to be acceptable. The concentration of ammonia in the product cannot exceed 10ppm for the purpose of NO_X emission prevention during hydrogen incineration. The concentration of nitrogen must not exceed 2%, as the inert gas will interfere with the usability of hydrogen as incineration fuel in the industrial process. Therefore, the remaining ammonia and nitrogen in the reactor product stream must be separated from the produced hydrogen. Ammonia from the separated waste stream can be reused in the process either for reuse in the cracking reactor or as a fuel for ammonia reforming or as a reducing agent to remove NO_X.

Constituents	Unit	Min.	Max.
Hydrogen (H_2)	mol/mol %	98	
Total sum of hydrocarbons including CH_4 (CXHY)	mol/mol %		1,5
Oxygen (O_2)	µmol/mol (ppm)		10
Total sum of inerts (N_2, He, Ar)	mol/mol %		2,0
Carbon dioxide (CO_2)	µmol/mol (ppm)		20
Carbon monoxide (CO)	µmol/mol (ppm)		20
Total sulphur including H2S (S)	µmol/mol (ppm)		3
Formic acid (CH_3OOH)	µmol/mol (ppm)		10
Formaldehyde (CH_2O)	µmol/mol (ppm)		10
Ammonia (NH_3)	µmol/mol (ppm)		10
Halogenated compounds	µmol/mol (ppm)		0,05
Water dewpoint (H_2O)	°C @ 70 bara		-8
Hydrocarbon dewpoint	°C @ 1 - 70 bara		-2
Wobbe index	MJ/m³ (n)	44,85	48,35
All other impurities	Shall not contain solid, liquid or gaseous material that might interfere with the integrity or operation of pipes or any gas appliance		

Figure 1.5: Quality specification of the hydrogen network[17]

1.6. Research Questions

The primary aim of this study is to assess the economic viability of a green ammonia-to-hydrogen process plant by 2030. Also the improvement of the viability of such plant employing emerging technologies is investigated with a time horizon of the year 2040. The objectives of this study are approached by seeking the answer to following research questions and subquestions:

Research Question: What is the anticipated cost of hydrogen from large-scale green ammonia decomposition in the Netherlands once the national hydrogen network is fully operational?

The following subquestions emerge from the main research question:

1. Which established technologies are applicable on industrial scale for ammonia decomposition process?
2. Which emerging technologies for ammonia decomposition show potential to enhance the process on an industrial scale?
3. What key factors affect the process costs, and how are they expected to change in the next 20 years?

The formulated methodology for answering the aforementioned questions is given in Section 1.7 on the next page.

1.7. Methodology Outline

To answer the research question formulated in the previous section, various process configurations are considered, encompassing both established industrial technologies and emerging research-based approaches with promising potential.

The central parameter for the production cost assessment is the Levelized Cost of Hydrogen (LCOH). From LCOH, the Net Present Value (NPV) is calculated for an anticipated 15-year operational period of the process plant. The resulting configurations are then compared based on these two key metrics.

The methodology steps undertaken to address the formulated research question are outlined in the table 1.1 below:

Table 1.1: Research Methodology

Step	Description
1	**Literature Review (Chapter 2):** • Conducting a thorough literature review to identify best suitable technologies for ammonia decomposition. • Comparing these technologies based on maturity and their applicability potential at a large scale.
2	**Cases Defininition (Chapter 3):** Based on literature, the basis of design is formulated for two cases, with difference in approach to ammonia decomposition and the market conditions: • Case I intends to represent a process designed for the near future (2030) and is based on existing industry-standard technologies. • Case II is formulated around the assumption that a highly promising emerging technology for ammonia cracking will be ready by 2040.
3	**Process Simulation (Chapters 4 & 5):** • Sizing and optimization of major equipment for each defined case. Performing sensitivity analysis of major process factors to ensure robustness. • Entire process simulation with designed equipment for each case.
4	**Economic Model (Chapter 6):** • Model for process equipment cost estimation. • Project capital (CAPEX) and operating (OPEX) expenditures estimation. • Model for LCOH & product market price Calculation.
5	**Results and Discussion (Chapter 7):** • Comparison of defined cases by levelized-cost-of-hydrogen (LCOH). • Sensitivity analysis of LCOH with respect to major cost factors for both configurations. • Determining market price of the product from Net Present Value (NPV) of the project. • Comparison of the determined LCOH with the alternative hydrogen production routes.
6	**Conclusions and Recommendations (Chapter 8):** • Drawing conclusions from the determined results.

2

Literature Review

The first section is dedicated to the fundamentals of the core process of the plant: ammonia decomposition. The next three sections delve into the technologies behind the required subprocesses for hydrogen production through ammonia cracking, as introduced in the opening section (refer to Section 1.4). The fifth section focuses on examining predictions in the future energy market. To provide a quick overview, these sections are summarized:

Section 2.1:Ammonia Decomposition: Ammonia decomposition process fundamentals are reviewed, with mentioning the alternative ways of ammonia decomposition. The ammonia decomposition technologies are reviewed. Ammonia decomposition catalysts are reviewed.

Section 2.2:Ammonia Cracker The ammonia cracker configurations, with potential for large-scale application, are reviewed.

Section 2.3: Hydrogen Product Purification The separation technologies for hydrogen production and unconverted ammonia recovery are reviewed.

Section 2.4: Hydrogen Compression In this chapter the technologies of hydrogen compression are reviewed.

Section 2.5: Market Predictions In this chapter the main market predictions vital for ammonia decomposition plant are reviewed.

2.1. Ammonia Decomposition

The ammonia decomposition reaction and major factors to its kinetics are described in **Subsection 2.1.1**. In **Subsection 2.1.2** ammonia cracking technologies are reviewed and compared. **Subsection 2.1.3** is dedicated to the ammonia decomposition catalyst properties.

2.1.1. Decomposition Reaction

Ammonia decomposition is the reverse of ammonia synthesis and requires energy input in an endothermic reaction at a relatively high temperature when operated at standard pressure. The following formula (Eq. 2.1) presents the reaction of ammonia decomposition, together with enthalpy at 298K.

$$NH_3 \rightarrow 1.5H_2 + 0.5N_2,\ \Delta H_{298} = 46KJ/molNH_3 \tag{2.1}$$

As shown in Figure 2.1, at ambient pressure equilibrium ammonia conversion goes beyond 99% above 400°C. However, the slow reaction kinetics are the limiting factor of ammonia decomposition [18]. In current industrial practice (such as production of forming gas in steel treatment [19]), almost complete ammonia conversion is achieved at high temperatures of 850-950 °C in the presence of an industrial nickel catalyst [20]. For high conversion at lower temperatures a more effective catalyst is required.

Temperature (°C)	250	300	350	400	450	500	600	700
NH_3 conversion (%)	89.20	95.70	98.10	99.10	99.50	99.70	99.90	99.95

Figure 2.1: NH_3 equilibrium conversion at different temperatures at ambient pressure[21]

Being an endothermic reaction, ammonia decomposition increases with temperature, while according to Le Chatelier's Principle, increasing pressure favors the side of the reaction with fewer molecules, thereby slowing down ammonia decomposition. The drop in conversion at elevated pressures is especially strong for low temperatures (see Figure 2.2) [22]. Therefore, low pressures and high temperatures are preferred for higher conversion rate.

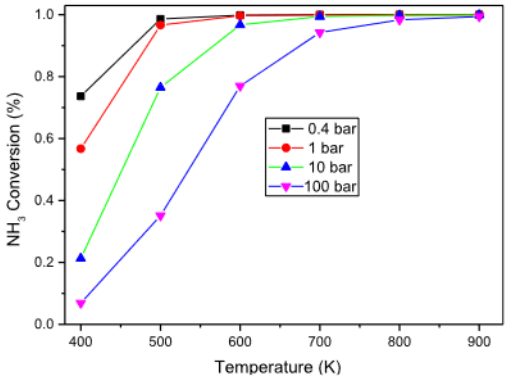

Figure 2.2: NH_3 conversion as function of temperature for different pressures. From experimental measurements by [22], using Ru-Na/CNT catalyst

The catalyst kinetics for ammonia decomposition are traditionally expressed by the Temkin-Pyzhev equation:

$$r = \alpha(\frac{pNH_3^2}{pH_2^3})^\beta \tag{2.2}$$

with r as decomposition rate, α as a temperature-dependent reaction-rate constant, β as catalyst specific exponent [23], and pNH_3 and pH_2 are the partial pressures of ammonia and hydrogen [21].

In summary, ammonia decomposition kinetics can be improved by :

- Temperature increase
- Reduction of partial pressure of the ammonia decomposition reaction product (thermodynamic shift).
- Utilization of more effective catalyst

2.1.2. Decomposition Route: Thermal Ammonia Cracking

Thermal cracking is a typical way to generate hydrogen from ammonia and was first operated in 1933[21]. It is a proven and scalable technology, with a similar working principle to industrial steam-methane-reforming. Such ammonia-to-hydrogen technologies are already commercially available. As example, Duiker Combustion Engineering claims that their cracker design is capable to produce 7-700 TPD of H_2 with NH_3 input capacity of 50-5000 MTPD, reaching more than 95% of NH_3 conversion [24]. Thermal catalytic decomposition route is currently the most studied route for large-scale hydrogen production from ammonia.

Alternative methods for converting ammonia to hydrogen are also actively researched. However, in comparison to ammonia cracking, these technologies are in early stage of development. The brief description of reviewed decomposition routes is given in Table 2.1. For more details on alternative technologies, please consult the Appendix A.1.

Table 2.1: Comparison of Ammonia Decomposition Technologies

Technology	Description	Properties
Thermal Cracking	Ammonia is decomposed in the heated catalytic packed bed reactor.	• **Advantages:** – Proven and easily scalable technology. – Can utilize fuel combustion for heat supply. • **Disadvantages:** – Produced hydrogen must undergo purification to meet product standards.
Electrochemical Decomposition	Ammonia is decomposed into hydrogen and nitrogen using an electrochemical cell.	• **Advantages:** – Fast response time and high energy conversion efficiency [25]. • **Disadvantages:** – Requires continuous electricity supply to maintain electric potential [26]. – Electrodes prone to damage at ammonia concentration above 3000 ppm[26]. – Low production rate (max. 25L/h reported). [26]
Photocatalytic Decomposition	Employs metal-loaded photocatalysts activated by light radiation to convert ammonia to hydrogen and nitrogen.	• **Advantages:** – Operates at atmospheric conditions. • **Disadvantages:** – Low efficiency of the photocatalyst. [27] – Reported research only at low ammonia concentrations.[27]

Based on the properties of reviewed technologies, thermal cracking is perceived as the only existing ammonia decomposition method suitable for large-scale hydrogen production. Therefore, further review is focused on ammonia cracking configurations only.

2.1.3. Ammonia Cracking Catalyst

To overcome the kinetic limitations of the endothermic decomposition reaction of ammonia, an effective and affordable catalyst is required. The effectiveness of the catalyst is defined by its adsorption and desorption properties for the reaction molecules, as shown in Figure 2.3 (see Appendix A.2 for detailed working principle description). The affordability of the catalyst is defined by its active metal component and the complexity of production. In this section, the latest developments in the ammonia decomposition catalysts are reviewed on their decomposition performance and affordability.

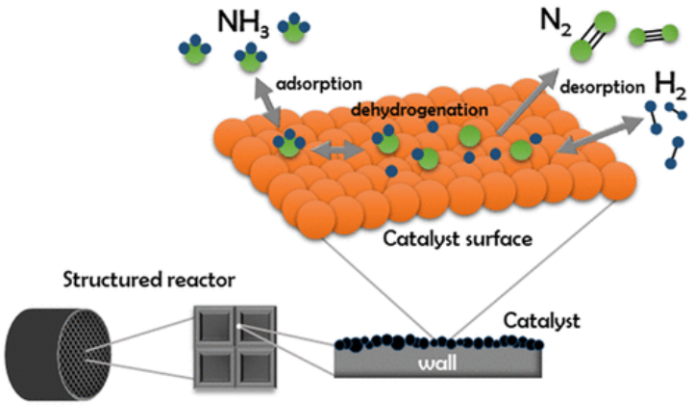

Figure 2.3: Working principle of the catalytic ammonia decomposition[28]

Catalyst Performance Parameters
It is important to note, that the best catalyst for ammonia synthesis is not necessarily the best ammonia decomposition catalyst, due to different reaction mechanisms involved[29]. The catalyst efficiency is defined by the following factors: the choice of the active metal component, the implemented catalyst supports and the use of promoters[30]. See Table 2.2 for key considerations for these factors:

Table 2.2: Key Considerations for Catalyst Performance Parameters

Performance Factors	Description	Key Considerations
Active Metal Component	Responsible for catalytic conversion.	- Main factor for catalytic activity and the cost of the catalyst (Detailed comparison in Appendix A.3) - Activity order: Ru > Ni > Rh > Co > Ir > Fe,Pt > Cr > Pd > Cu,Te.[31] - Noble metals are too expensive and scarce for large-scale application.
Support Structures	Enhance catalyst dispersion and increase surface area.	- Must be stable at process temperatures. - High specific surface area is crucial.[28] - State-of-the-art: Carbon structures nanotubes (CNTs) show best performance. Expensive and have stability issues [28] - Oxides are industry-standard due to cost and stability [28].
Promoters	Intermediate agents to inhibit sintering of active metal particles.	- Promotional effect depends on active metal choice. - Increases catalyst cost due to additional manufacturing step - Example: Promotion by K^+ ions from KOH on ruthenium.[30]

Catalyst of Choice

The catalyst chosen for large-scale ammonia cracking must strike a balance between effectiveness and affordability. The **Ni/Al_2O_3** catalyst is defined as a suitable catalyst configuration, considering the factors mentioned in Table 2.2, due to following reasons:

- **Active metal component**: Given the scarcity and costliness of noble metals on a large scale, the most effective non-noble catalyst, **Nickel**, is selected for ammonia cracking.
- **Support structure**: The industry-standard oxide, specifically **Al_2O_3**, is chosen as the support material for nickel particles due to its widespread use.
- **Promoter**: As the addition of promoters significantly complicates catalyst production and raises costs, it is **opted against** for large-scale applications.

2.2. Ammonia Cracker

As discussed in the previous section, thermal cracking stands out as the sole mature method for producing hydrogen from ammonia that holds potential for large-scale implementation. In this section, two most promising reactor configurations for large scale are reviewed. **Subsection 2.2.1** reviews the internals of the large-scale ammonia cracking unit with a conventional packed bed reactor. **Subsection 2.2.2** reviews the emerging membrane-assisted packed bed reactor technology.**Subsection 2.2.3** reviews heat supply routes to the ammonia cracker.

2.2.1. Packed Bed Reactor

The most straitforward method of facilitating endothermic reaction of gasses is by splitting the packing over multiple long tubes (multitubular packed bed reactor) and heat them by the combustion flue gas. The working principle is very similar to a fired heater configuration. This method is already used for industrial route of hydrogen production by steam methane reforming which accounts for 60% of worldwide hydrogen synthesis[32]. Modern units can reach thermal efficiency up to 95% due to its effective heat recuperation design. This technology can also be configured for ammonia cracking purposes [33].

The heat supply to process fluid in a large-scale cracker consists out of two parts: a firebox where the reforming reaction takes place, and a convection box where heat recovery from the product stream occurs before leaving through the stack. This configuration is visualized in Figure 2.4.

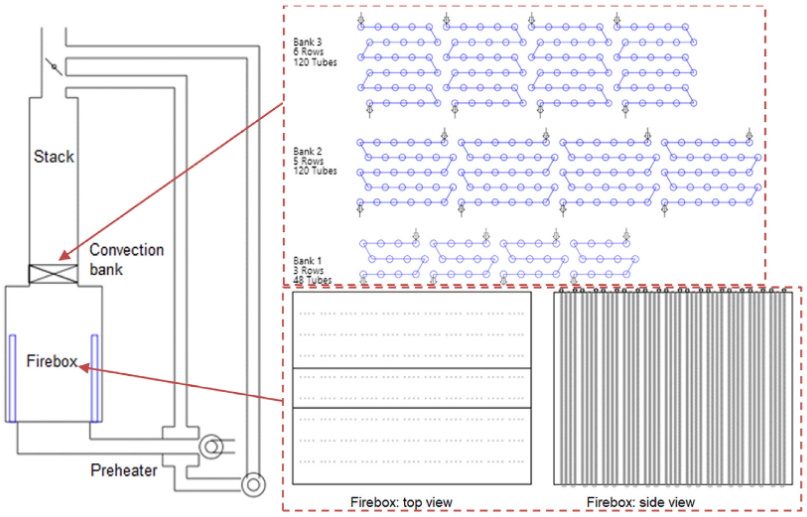

Figure 2.4: Simplified visualization of a fired-heater based ammonia cracker [13].

- **Firebox**: Radiation heat transfer section of the ammonia cracker, where the reaction occurs. Rectangular configuration is generally used for large duties and cylindrical ones for small duties. The inside of the firebox consists out of hundreds vertically arranged reforming tubes, packed with an ammonia decomposition catalyst. Between the reforming tube rows, several top-fired burners are placed within uniformed distance. The top-fired arrangement is attractive due to created uniform temperature profile along the reactor tubing and the ease of maintenance, as the combustion zone and catalytic reaction zone are split [34].

- **Convection Banks**: The heat from the flue gas leaving the firebox is recovered in the convection banks with finned tubes.

While both methane reforming and ammonia cracking are similar processes, there is a lack of published data on sizing the ammonia cracker. Only one publication has currently offered a model of a large scale ammonia cracker for the purpose of estimation of levelized cost of produced hydrogen (LCOH) for large scale production[13]. It was designed for production of fuel cell grade hydrogen with capacity of 200 MTPD (metric tons per day), with its thermal efficiency reaching 93.1%. It was designed to operate at temperatures below 400°C using a noble catalyst (Ru/Al_2O_3) bed.

The main issue of the described configuration is the requirement of the downstream purification of the hydrogen containing reactor product mixture up to the set purity requirements. The emerging technology designed to tackle this issue is reviewed in the next subsection.

2.2.2. Membrane Assisted Packed Bed Reactor

A promising technology for eliminating downstream hydrogen purification is to assist ammonia cracking packed bed reactor with integrated membrane structure. The removal of hydrogen from the reactor is facilitated by selective permeation of hydrogen molecules through membrane (visualised in Figure 5.2).

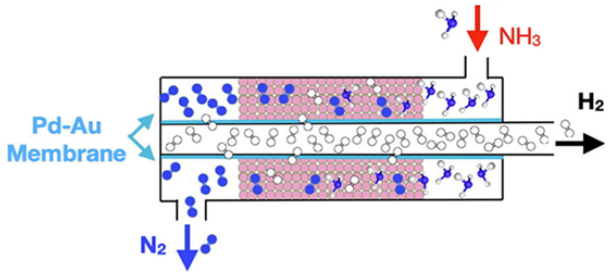

Figure 2.5: Working principle of the membrane assisted packed bed reactor[35]

The driving force for hydrogen flow through membrane is the hydrogen partial pressure difference between the retentate and permeate of membrane. The membrane performance is characterized by the ratio of Damkohler and Peclet non-dimensional numbers [36], qualitatively described below:

- Da (Damkohler) = $\frac{\text{reaction rate}}{\text{convective mass transfer rate}}$
- Pe(Peclet) = $\frac{\text{Convection mass transfer rate through catalyst bed}}{\text{Diffusive mass transfer through membrane}}$
- The higher is the Da/Pe ratio, the more effective is the membrane performance.

The following factors influence the membrane performance. Also their impact on the cost of the entire process are reviewed:

- **Retentate-to-permeate pressure ratio**:
  - **Thermodynamic shift:** As the driving force for hydrogen diffusion through membrane is the partial pressure gradient of hydrogen, the flux of hydrogen is increasing with increase in pressure ratio between retentate and permeate. Due to the removal of hydrogen product from the reactor mixture by selective permeation, thus reducing partial pressure of hydrogen, the thermodynamic equilibrium will shift in favor of ammonia decomposition, enhancing the ammonia conversion. Even at temperatures as low as 400°C near-full conversion of ammonia can be achieved with high pressure ratio in the membrane reactor, exceeding the thermodynamic equilibrium. This phenomenon is depicted in Figure 2.6(left)[37].

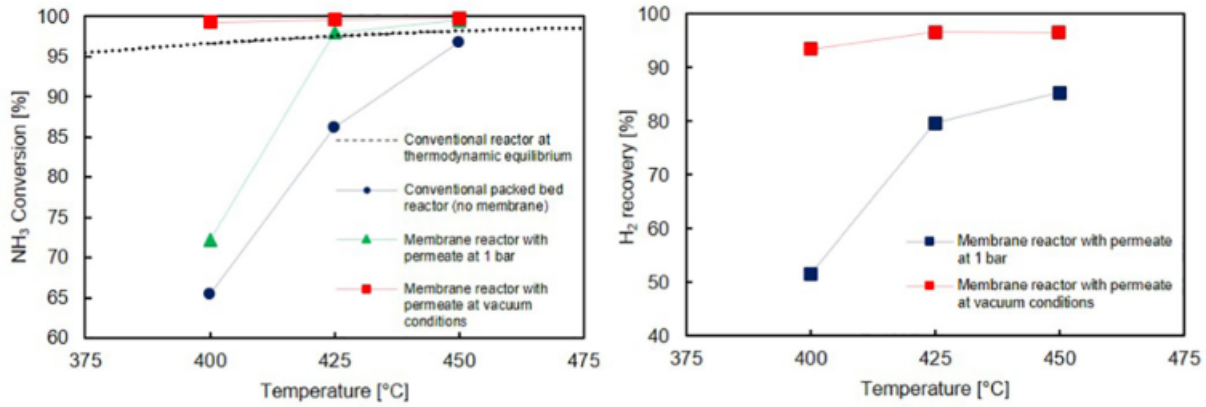

Figure 2.6: The shift from thermodynamic equilibrium in the membrane assisted reactor. The shift is enhanced by increasing the retentate-permeate pressure ratio increase by reducing the permeate pressure (left), leading to higher NH_3 conversion. Hydrogen recovery also increases with pressure ratio increase (right).

- **Hydrogen Recovery:** The increase in partial pressure ratio increases the driving force for permeation. Due to increasing driving force, hydrogen recovery is also shown to be increasing, as depicted in Figure 2.6(right).
- **Downstream Compression:** To achieve the desired pressure ratio, the permeate side of the membrane must operate at significantly lower pressure than the retentate side. This entails either maintaining high pressures on the retentate side of the membrane or maintaining low pressures on the permeate side. However, in the case of low permeate pressures, the permeate stream must undergo a highly energy-intensive compression process to reach required product pressure.
  Previous research on Packed-Bed Catalytic Membrane Reactors (PMCMRs), as demonstrated by Cerrillo et al. [38], showcased the potential for energy savings through the utilization of pressurized permeate streams (with permeate pressure ranging from 1 to 20 bar). This approach significantly reduces the energy consumption needed for subsequent hydrogen compression (refer to Figure 2.7). For instance, when compressing hydrogen up to 25 bar, maintaining a permeate pressure of 5 bar slashes compression energy requirements by 50%. This strategy, however, necessitates a higher retentate pressure in the reactor, which is easily attainable due to the relative simplicity and affordability of pressurizing ammonia compared to pure hydrogen.

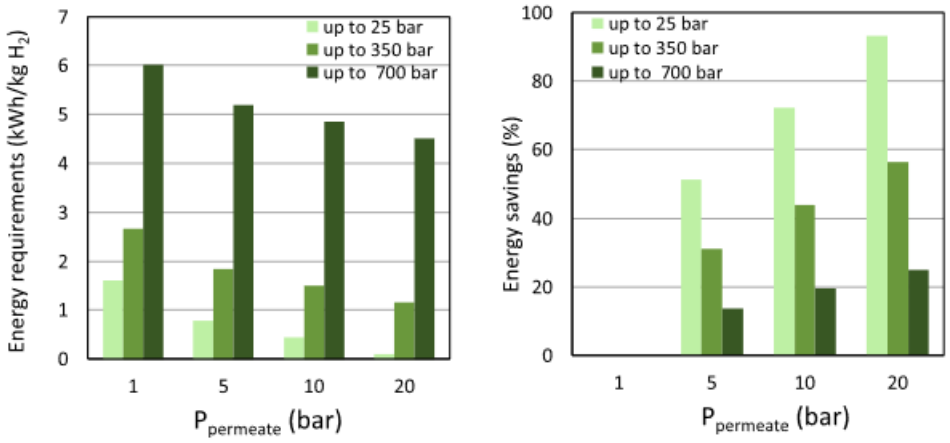

Figure 2.7: Energy requirement predictions for compression of permeate stream in range between 1 and 20 bar up to required pressure (left), and the corresponding compression energy savings[38]

- **Membrane material and thickness**:
  - **Material**: In all of the reviewed papers for ammonia cracking membrane reactors for hydrogen production[37, 37, 39, 35, 40] the palladium-based membranes are used due to their exceptional hydrogen permeation performance coupled with high H_2/N_2 and H_2/NH_3 selectivity. Only Pd-membranes currently have sufficient selectivity of hydrogen to ammonia out of all reviewed membrane types (refer to Subsection 2.3.2). Adding silver (Ag) into Pd-membrane structure has shown to improve the stability of the membrane in the presence of certain compounds [41].The main issue with utilising palladium membrane is its deterioration at temperatures above 500°C[42].
  - **Thickness**: It was experimentally determined that thinner membranes improve H_2 recovery, but also increase the NH_3 concentration in the permeate due to lower selectivity (see Table 2.3)[39]. While thicker palladium layer can improve the selectivity, it also strongly increases the cost of the membrane, as palladium is an expensive metal (€35.40/gram in 2023). A cheaper alternative could be a downstream purification unit to remove the NH_3 traces from the membrane reactor product stream (reviewed in chapter 2.3)[37].

Thickness selective layer (μm)	H_2 recovery (%)	NH_3 concentration in the permeate (ppm)
$\sim$1	93.2	47 ($\mp$2.1)
$\sim$6-8	84.8	<0.75

Table 2.3: The impact of membrane thickness on H_2 recovery and NH_3 concentration in the permeate (ppm) at T=500°C, P = 4 bar(a), ammonia feed flow rate 0.5 L_N/min [39].

– **Durability and Recyclability:** To this day, the durability of the Pd-membrane for ammonia cracking applications has never been tested above 1000h of operation. In a published research found [35], the Pd-membrane did not reduce its performance after 1000h of operation. However, to determine the maximum durability of such membrane, longer running tests are required. Assuming the limited lifetime of the membrane, its recyclability is expected to play a major role in the capital investment for the process plant. The paper published by L. Toro [43] investigates the economics of membrane recyclability. It reports that for the plant lifetime of 15 years, the cost of membrane utilization drops by 9% for membrane with recycled ceramic support layer. In case of recycling up to 90% of the selective palladium layer (4μm in the paper), the cost of membrane has potential to drop by 70%. See Figure 2.8 for visualisation.

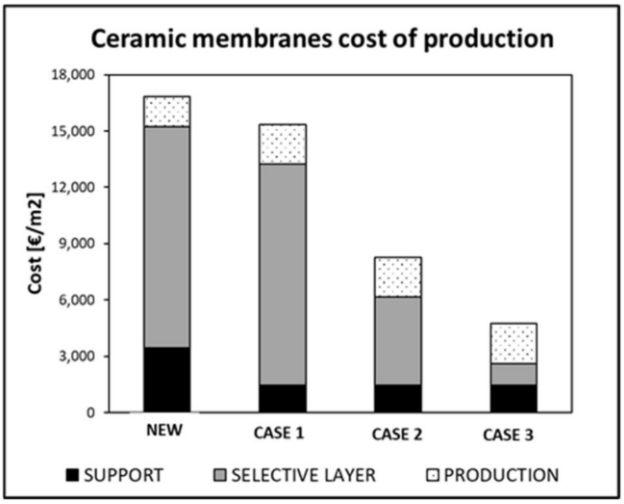

Figure 2.8: Reduction of membrane cost by the extent of recycling [43]. NEW: non-recyclable membrane, CASE 1: recycling of support layer, CASE 2: recycling of support layer and 60% of selective Pd-layer, CASE 3: recycling of support layer and 90% of selective Pd-layer

State-of-the-art Prototype

The research by (Kim T., 2022)[40] shows the state-of-the-art prototype of the membrane-assisted PBR for ammonia cracking, which is stated to be on the road to commercial application. There, the Pd-membrane module is inserted into the reactor tube of 450 mm height and 12.7 mm diameter, filled with the Ru/SiO_2 catalyst. The separation is assisted by the trans-membrane pressure difference of 100 kPa. At the pressure of 500 kPa and temperature of 472°C, the 99.6% ammonia conversion was observed, with H_2/N_2 selectivity of 8050, which is admissible for hydrogen of PEM-cell grade. The flow rate was measured to be 16.22 $mLcm^{-2}min^{-1}$[39].

Membrane-Assisted PBR vs. Catalytic Membrane Reactor

The alternative to a membrane-assisted packed bed reactor is a catalytic membrane reactor (CMR), where the catalyst is integrated into the membrane structure. However, the catalytic membrane reactors require a more complex multi-step fabrication process, leading to high fabrication costs and uncertainties in both reproducability and long term stability[40]. See Appendix A.4 for a more detailed comparison of two technologies.

2.2.3. Heat Supply to Ammonia Cracking Reactor

Conventionally, the large-scale endothermic reactions are getting their heat supply from the natural gas burning. As the ammonia decomposition plant is required to be carbon-emission free, alternative heating methods are required. The most apparent alternatives are carbon-free fuel combustion or electric heating.

Carbon-free Fuel Combustion

Ammonia, aside from serving as a hydrogen carrier, is gaining traction as a promising carbon-free fuel, particularly in the realm of ammonia-fueled gas turbines [44]. However, its utilization as fuel in ammonia cracking plants comes with challenges:

- **NO_X Emissions and Reduction:** Burning ammonia yields a notable proportion of NO_X emissions, including NO and N_2O. To mitigate these emissions, methods for NO_X reduction are imperative. One common approach is Selective Catalytic Reduction (SCR) [45]. In SCR, ammonia is introduced to the flue gas stream containing NO_X, leading to catalytic conversion into nitrogen (N_2) and water (H_2O). Modern SCR units can reduce NO_X emissions by 70-95% and are widely employed in large-scale processes.

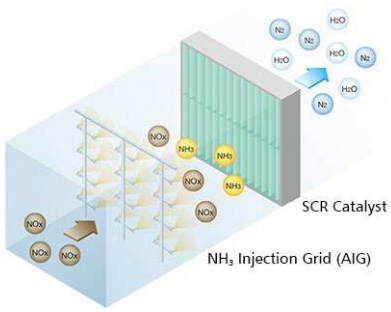

Figure 2.9: Selective Catalytic Reduction working principle [46]

It's worth noting that the equivalence ratio (ϕ), which represents the ratio of oxygen content in the oxidant supply to that required for complete stoichiometric combustion, significantly affects NO_X formation. A study by [44] demonstrates (Figure2.10) that an optimal ϕ of 1.1 minimizes both NO and NH_3 emissions. It's observed that flame temperature is 100-200K lower for ammonia/air compared to methane/air flame at the same ϕ.

- **Flame Speed Stabilization and Radiation Intensity:** Ammonia exhibits a lower laminar flame speed than hydrocarbons, resulting in a thicker flame and unstable burning [47]. Blending ammonia with hydrogen has shown to increase the flame speed of the fuel (Figure 2.11)[44]. A 70% ammonia and 30% hydrogen ratio is suggested for improved stability and radiation intensity[48][49], comparable with natural gas burning.

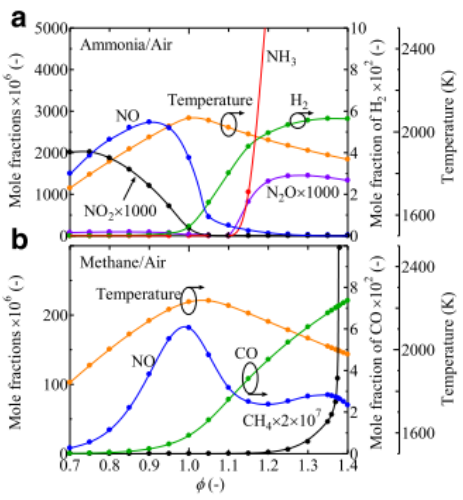

Figure 2.10: Emission characteristics for NH_3/Air and CH_4/Air [44]

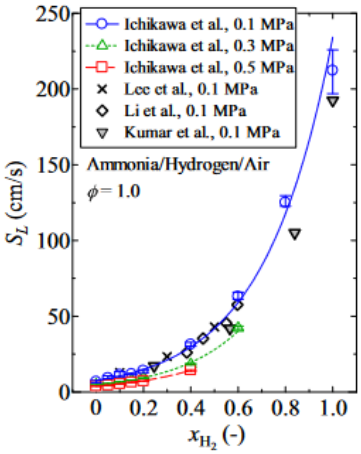

Figure 2.11: Relationship between volumetric hydrogen fraction in the fuel and flame speed[44]

Ammonia's application as a carbon-free fuel offers significant potential, albeit with considerations for emissions and combustion stability. Addressing these challenges is essential for maximizing the benefits of this promising fuel source.

Electric Heating

Alternatively, ammonia cracking reactor could also be powered by renewable electricity. Various types of electric heating methods exist, such as resistance heating, arc/plasma heating, electromagnetic heating, shock wave heating and more [50] (refer to Appendix A.5 for more details on electric heating methods).

The great advantage of electric heating of the reactor is its high thermal efficiency. Compared to traditional gas powered furnaces with 50% thermal efficiency of the firebox, the resistance heaters are showing 90% thermal efficiency[51]. Another advantage for large-scale is that the start-up/shut-down of the electrified reactor is in order of seconds, compared to several hours duration for traditional fossil fuel reactors. It would make the process plant much more adaptive to the change in ammonia import requirements. Some small-scale ammonia crackers are sometimes electrically heated, e.g. the ones used in the metallurgy industry to produce forming gas utilized in steel treatment[19].

However, in the industry there are currently no industrial cases known where the resistance heating is used for large-scale endothermic reactors. The application of electric heating has never been realised on the large scale due to absent infrastructure and high fluctuations in renewable electricity generation, what creates a barrier for large-scale ammonia cracker heating application, which requires continuous and stable heat supply. **Therefore, the ammonia-hydrogen fueled heating is perceived as a more rational choice for ammonia cracking heat supply.**

2.3. Hydrogen Purification

After ammonia cracking, hydrogen has to be separated from nitrogen and unconverted ammonia to reach to the required purity level. Meanwhile, unconverted ammonia has to be recovered. Therefore, depending on the selected decomposition route, different purification procedures are required. In this section various purification technologies are reviewed and compared on their performance at large-scale application. **Subsection 2.3.1** reviews ammonia removal and recovery routes. **Subsection 2.3.2** reviews hydrogen purification technologies.

2.3.1. Ammonia Removal and Recovery

After ammonia cracking, the first component to be removed from the product has to be ammonia, as it is heavier than other mixture components. There are two straight-forward ways of removing and recovering ammonia:

- **Absorption**: There are various types of solvents, which can absorb ammonia. The extent of traces removal depends on the absorption pressure and the amount and purity of the solvent. Water is a common and cheap ammonia solvent [52]. Ammonia dissolves easily in water and forms ammonium hydroxide, a caustic solution and weak base. The stripped ammonia can then be recovered and reused in the process, while the regenerated solvent cycles back to the absorption unit [53]. Water is also an attractive solvent as it is already present in the ammonia feed tank for stress corrosion cracking prevention (at least 0.2%)[54]. Therefore, no new impurities are introduced to the process stream during water absorption. The traces of water can then be removed from the hydrogen product by a downstream drying unit filled with desiccant[55].
  Another method of ammonia absorption developed is by using calcium- or magnesium chloride salts[56][57]. There, ammonia is taken into a solid salt by the reaction to form a crystal. However, compared to liquid absorption, this type of separation can not operate in steady state and requires operation with pressure swing (PSA)[56] or with temperature swing cycles (TSA)[56][57], which are slow and increase the process control complexity.
- **Adsorption**: Alternative way to recover ammonia is by dry adsorption. Various materials, such as zeolites are selectively adsorbing ammonia onto the surface, while nitrogen and hydrogen are not adsorbed. Just as for absorption salts, the temperature oscilation is required for adsorbent regeneration. During the research on membrane reactor by V. Chechetto, it was indicated that while adding complexity of the process, implementing the zeolite 13X adsorption unit can prove more economically attractive than using a thicker membrane for a more selective ammonia removal [42]. There, while adsorbing ammonia from permeate stream at 450°C from reactor assisted with a thin membrane (1μm), the purity of NH_3 below 0.75 ppm was reached[42]. Sitar et al. conducted experiments showcasing that residual ammonia impurities in the hydrogen stream can be diminished from around 1000 ppm to levels below 0.025 ppm[42][58]. They achieved this using the readily available zeolite clinoptilolite as an adsorbent material for ammonia removal[58].

2.3.2. Hydrogen Purification Technologies

In this section the hydrogen purification technologies, potentially feasible for large-scale, are reviewed for the purpose of hydrogen separation from nitrogen after ammonia has been recovered. The properties of each method are described and compared in the Table 2.4. See Appendix A.6 for details on working principle of each technology:

Table 2.4: Comparison of Hydrogen Purification Technologies

Purification Method	**Description**	**Advantages/Disadvantages**
Pressure Swing Adsorption	Separation of gases by preferential adhesion to adsorbent material. • PSA operates at ambient temperature and with pressure swing cycles (at least two columns) for sorbent regeneration. Adsorption at 10-40bar pressures [59], desorption at low pressures. • High adsorption pressure reduces downstream compression costs of hydrogen product. Common adsorbents: 13X and 5A zeolites[60].	**Advantages:** • Well-established industrial gas purification technology. Large throughputs capacity (>28000m^3/h)[60] • Low capital investment costs. • Reaching ultra-purity (>99.99%)[61] with larger column system (more then 12 columns)[61] • Up to 90% recovery [62]. **Disadvantages:** • Trade-off between recovery and purity. • Increase of control complexity with more towers
Cryodistillation	Uses differences in boiling points of gases for separation. Requires very low temperatures, making it suitable for large quantities of gas, high purities, and high pressures [63]. The fundamental processes of cryodistillation are: (i) compression of gas mixture, (ii) gas purification, (iii) heat exchange, (iv) distillation and finally (v) the compression of product gas to required pressure (see Figure A.12 in Appendix)	**Advantages:** • Well-established technology. • Can achieve high purity H_2 (e.g., 99.999%) [64] and recovery up to 95%. • **Disadvantages:** • Energy intensive cooling and separation processes due to very low operating temperatures. • Larger footprint, compared to PSA [65] • Higher capital investment [65],compared to PSA
Membrane Separation	Depends on the molecular structure of the membrane. Different types include polymeric, molecular sieve, and metallic membranes (Pd-based) (compared in Appendix C. Pd membranes are the only reported membranes with both sufficient H_2/N_2 and H_2/NH_3 selectivity [66] (research Figure in Appendix A.13 shows H_2/N_2 and H_2/NH_3 selectivity below 70 and 15 for alternative membranes[66])	**Advantages:** • High selectivity and permeability for Pd-based membranes [42]. • Energy efficient and environmentally friendly.[42] • Compact and minimal footprint.[42] • Pd-based membrane H_2/N_2 selectivity up to 68960 [37] for . • Facilitate thermodynamic shift in ammonia reaction, when integrated into ammonia cracker (see subsection 2.2.2). **Disadvantages:** • High costs and scarcity of Pd for large-scale application [37]. • Low pressure of hydrogen in the permeate. • Deterioration phenomena when exposed to temperatures > 500°C [42]

Comparison of hydrogen purification technologies
(i) PSA is the most mature process, used in most of the hydrogen purification units worldwide. Also, the use of PSA is more favorable due to recovery improvements at larger scale.

(ii) Cryogenic distillation is also a mature process, frequently used for gas separation. However, its application for hydrogen purification is much more rare due to very low boiling points of hydrogen and nitrogen, requiring very low temperatures, to attain desired purity. This makes it a highly energy intensive process.

(iii) Membrane separation is economically challenging for large scale production mainly due to high costs of membranes and required pressurization costs. Its most efficient application would be in synergy with the reaction in a membrane reactor.

2.4. Hydrogen Compression

To be admitted to hydrogen network, purified hydrogen has to be pressurized up to 50 bar [17]. The required pressure ratio is dependent on the exit pressure of the purification unit. Also, the target for large-scale hydrogen production capacity of ammonia cracking plant is set at 100 tons/day, which is around 50000 Nm^3/h, which is at comparable scale to the large-scale electrolysis plant production. Therefore, the selection of a applicable compression technology is required, which is able to handle such throughputs. In this section the technologies with a potential for large-scale hydrogen distribution by pipeline are reviewed. All of the reviewed technologies are reviewed and compared in Table 2.5. For more details on each compression type, please refer to Appendix A.7.

Table 2.5: Comparison of Mechanical and Electrochemical Compression

Compression Type	Description	Advantages/Disadvantages
Mechanical Compression (Reciprocating)	Uses a piston to compress gas, suitable for high pressure ratios.	**Advantages:** • Can handle high pressure ratios. • Suitable for highly compressed hydrogen production[7]. • Can reach very high pressures (up to 1000 bar with multi-stage configuration[67]) . • Modern compressors are reported at the maximum flowrates up to 34000 m^3/h (by Howden [68]) **Disadvantages:** • Larger and heavier components needed for large scale. • Requires lower operating speeds at large scale due to increasing mechanical stresses. • Complex manufacturing, high maintenance costs [69]. • Pressure variations causing vibrations, noise, and potential safety issues [7]. • Ineffective cooling during compression [69]

Continued on next page

Table 2.5 – *Continued from previous page*

Compression Type	Description	Advantages/Disadvantages
Mechanical Compression (Centrifugal)	Uses rotating impellers to compress gas, suitable for high flow rates[7].	**Advantages:** • Can handle very high flow rates (up to 50,000 Nm^3/h[7]). **Disadvantages:** • Unsuitable for very high compression in one stage(pressure ratio limit of 1.05 - 1.2). • Requires higher speeds and/or many compression stages for high pressurization [7]. • Complex and expensive for high compression [7].
Electrochemical Compression	Works on the principle of a PEM fuel cell, using a solid polymer electrolyte membrane [67]. The process of compression consists out of three main steps: 1. Low-pressure hydrogen is directed to the anode side, where it splits into protons and electrons (Eq.A.4): $H_2 \rightarrow 2H^+ + 2e^-$ (2.3) 2. Protons move through the solid polymer electrolyte membrane to the cathode, while electrons flow through an external circuit driven by an electric power source. 3. Protons and electrons recombine at the cathode (Eq. A.5), leading to increased pressure: $2H^+ + 2e^- \rightarrow H_2$ (2.4)	**Advantages:** • More efficient than mechanical alternatives at moderate pressures and low flow rates [67]. • No moving parts, eliminating vibrations and noise [67]. • Simultaneously purifies hydrogen from impurities [70]. **Disadvantages:** • Did not reach the level of maturity and reliability of mechanical alternatives. Limited proton exchange membrane lifetime (currently below 5 years) [71]. • Higher voltage required due to membrane resistance [67]. • Permeation of molecular hydrogen at high pressure ratios reduces efficiency [67].

Comparison of compression technologies
The mechanical compression is currently the only method which can handle large gas throughputs. The compression can either be facilitated by multiple reciprocating compressors operating in parallel or by the series of centrifugal compressor stages. Both of this configurations have their disadvantages as the reciprocal compression faces mechanical limitations at high through-puts, while centrifugal compression requires high speeds and many compression stages.

At this moment, while the research into centrifugal compression optimization for hydrogen pressurization is a hot topic[72], they are deemed unsuitable for high pressurization and are mainly applied for the pipeline application [7]. Reciprocating compressors in parallel are considered a compressor of choice due to required product pressures. They are also currently employed for the largest renewable hydrogen production plants currently being built in the Netherlands (such as two large reciprocating compressors supplied by Howden for the Holland Hydrogen One green hydrogen production facility with 60 TPD production capacity, currently developed by Shell[73]).

2.5. Market Predictions

In this section the market predictions are performed. In **Subsection 2.5.1** the market development for main process utilities, green ammonia and electricity, is reviewed. **Subsection 2.5.2** provides the review of recent predictions of levelized cost of hydrogen (LCOH) for various sustainability-oriented hydrogen production routes in the Dutch setting.

2.5.1. Major Utilities Cost Prediction

- **Green Ammonia** The high cost of green ammonia as hydrogen carrier is currently the main barrier for large scale import, currently floating in the range of $700-1400/ton[12], which is at least six times higher than natural gas/coal-based ammonia, which is in the range of $110-340/ton with market fluctiations.
  However, while the market for green ammonia was valued to $36 mln in 2021, it is anticipated to grow to $5480 mln by 2030[74]. By the year 2030, according to International Renewable Energy Agency (IRENA), with the new green ammonia projects currently in development, the price of green ammonia is expected to drop down to $475-900 /tonne (€$_{2023}$430-820/tonne)[12] (Figure 2.12). By the year 2050, with further expansion of green ammonia market due to its potential future applications as hydrogen medium and shipping fuel, the renewable ammonia is predicted to fall within the price range of $310-610/tonne (€$_{2023}$280-555/tonne)[12].

  To reach such cost reduction for green ammonia, the innovation is required in new electrolyzer technology. Also, global electrolyzer production capacity has to increase by 20 times, from 2.1GW per year upto 42GW per year, to achieve the targeted cost of green ammonia production by 2050[75]. The increase in renewable electricity generation scale is required to enable the required production capacity for the electrolyzers. To facilitate the capacity increase, new governmental policies and regulations are required for transition from conventional carbon-emitting processes in the industry towards carbon-neutral alternatives.

Table 2.6: Green Ammonia Cost Projections

Year	Projected Green Ammonia Cost (in $/ton)	Remarks
2022	700-1400	Current cost range[12].
2030	475-900	Anticipated cost with green ammonia projects in development[12].
2050	310-610	Predicted cost with further market expansion and potential future applications of green ammonia as hydrogen carrier or direct fuel[12].

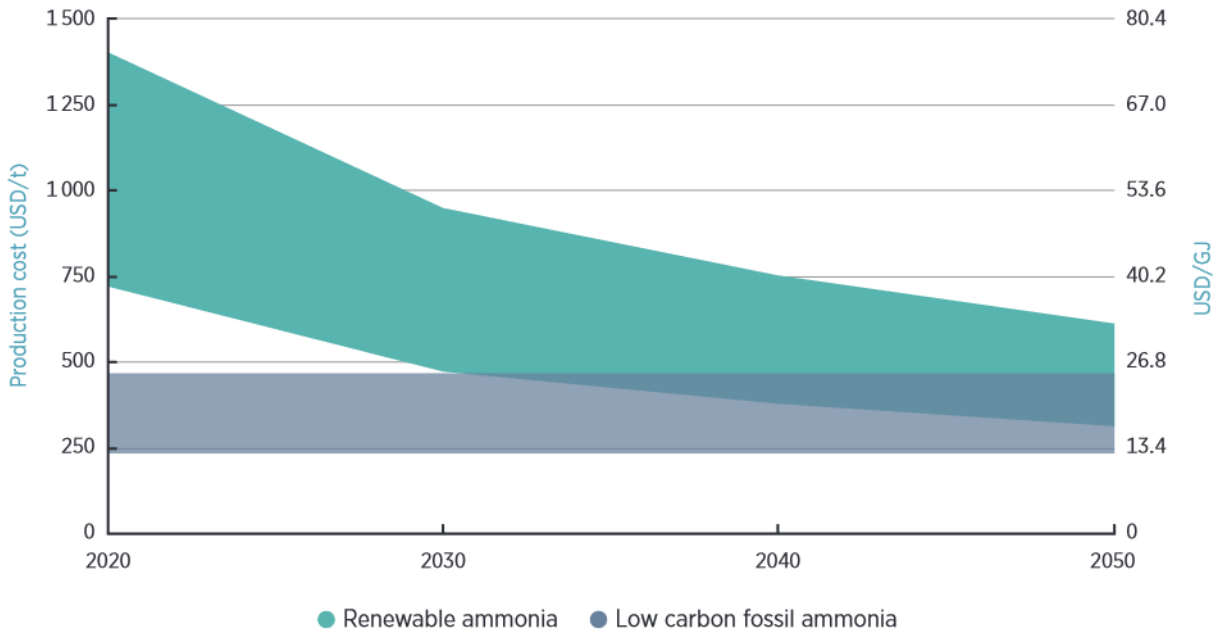

Figure 2.12: Current and predicted future costs of green ammonia, compared to low-carbon fossil ammonia[12]

- **Electricity Costs** Most of the reviewed equipment, besides fuel-powered ammonia cracker, is strongly dependent on continuous electricity supply. For example, the main source of total expenses for conventional purification unit, such as PSA are due to high electricity requirements (70-80% of total costs for PSA [76]). Also, the required product pressure for hydrogen network requires a lot of electricity. The costs of operating a compressor dominate over the capital costs, as hydrogen pressurization is highly energy-intensive. To double the pressure, electricity supply of 0.4-0.5 kWh/kg-H_2 is required for conventional mechanical compressors [77].

  The cost of electricity in the Netherlands is contingent upon the extent to which the country aims to achieve self-sufficiency in renewable power production. According to Netbeheer Nederland, if the Netherlands integrates into the broader European energy system and enhances its electricity imports from neighboring European countries, the anticipated cost of electricity is projected to approach 70 EUR per megawatt-hour (MWh) [78] by 2050. This scenario is predicted to result in cheaper cost of electricity than more self-reliant or fully international energy systems [78].

  The electricity price in Europe for industrial plants is expected to be influenced by factors such as energy demand, carbon prices, and renewable energy expansion. According to Energy Brainpool[79], rising CO_2 prices will contribute to higher power prices from 2030, but increased contributions from wind and photovoltaic power plants, coupled with adaptable electricity demand, will mitigate this effect. Consequently, actual electricity prices are projected to rise modestly, from 69 EUR/MWh to 78 EUR/MWh from 2030 to 2050 [79]. This aligns with predictions from TNO (Dutch organization for applied scientific research), forecasting a Dutch weighted average electricity price of 74 EUR/MWh by 2030 [80]. Similar projections are made for neighbouring Germany, where industrial customer electricity prices are expected to hover around 70 EUR/MWh from 2030 to 2050 [81], see Figure 2.13.

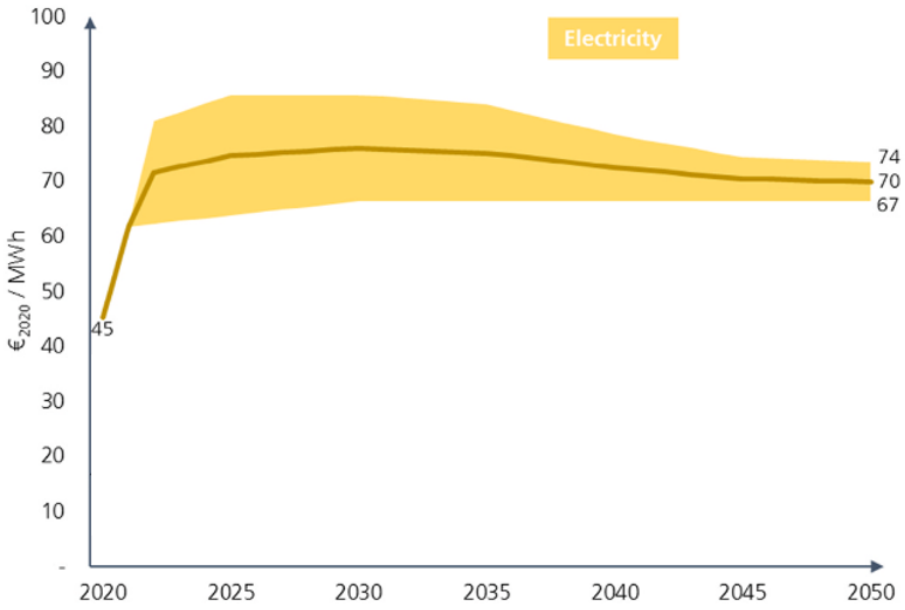

Figure 2.13: Predicted development of annual market prices for electricity and natural gas for energy-intensive industrial customers in Germany. Reprinted from (George G.,2022[81])

2.5.2. Comparison of Hydrogen Production Routes in the Netherlands

The cost of hydrogen production from imported green NH_3 is compared with alternative hydrogen production methods in the Dutch context (see Table 2.7). The figures for the levelized cost of hydrogen are taken from the TNO Supply Chain Model (2022)[82] and the report by Boston Consulting Group (2023) [83].

The projected costs for green and blue hydrogen production in the Netherlands are compared with the import of green hydrogen from countries with more favorable renewable energy conditions:

- Local production of green hydrogen is estimated to be in the range of €5.00-8.00/kg[83]. This higher cost is attributed to the elevated expenses associated with renewable electricity, as well as the supply chain challenges for renewable electricity and electrolyzers.
- The Levelized Cost of Hydrogen (LCOH) for the blue hydrogen route, involving hydrogen production from natural gas with carbon capture and storage (CCS), is projected to be between €1.90-3.00/kg. However, this value is heavily dependent on the natural gas market. In the event of a threefold increase in natural gas prices, the cost could exceed €5.00/kg[82].
- Given the current projections, where local green hydrogen production is not anticipated to be competitive with blue hydrogen, the importation of green hydrogen from regions with more cost-effective renewable energy sources emerges as an appealing alternative. Countries with favorable conditions for renewable energy, such as Australia, Chile, or Morocco, may produce it at a cost of €3.1-3.6/kg [84]. That hydrogen could be imported in liquefied form (LH2) or as a hydrogen carrier, such as ammonia or liquid organic hydrogen carriers (e.g., toluene). The LCOH estimates for these transportation routes are compared in Table 2.7. The projected cost for hydrogen import routes falls within the range of €6.00-9.00/kg, contingent on the selected route [82].

Table 2.7: The Comparison of the predicted LCOH values by 2030 by various sustainability-aimed hydrogen production routes in Central Europe (incl. Netherlands).

Hydrogen Production Route in Central Europe (incl. Netherlands)		LCOH Values in 2030 Reported	Commentary:
Domestic Green Hydrogen Production:		€5,00-8,00/kg [83]	- The cost of renewable electricity and is the largest contributing factor to the cost of green hydrogen.
Domestic Blue Hydrogen Production:		€1.9-3.0/kg [82]	- The production of blue hydrogen is heavily dependent on natural gas prices. - If naturar gas cost rises by 200% from 2023 value, the LCOH can rise above €5.00[82]
Imported Hydrogen Routes:	**Liquification (LH2)**	€ 5.8-7.4/kg[82]	- The cost is determined by the liquification process and expensive storage and transport due to boil-off and tank seepage[82].
	Hydrogen Carrier: LOHC (toluene)	€6.2-8.9/kg[82]	- The cost is determined by investment in LOHC hydrogenation and dehydrogenation. Large storage volume required due to low hydrogen denstity[82].
	Hydrogen Carrier: NH3	€6.8-9.3/kg [82]	- The major cost contributors are the costs of green NH3 synthesis, and decomposition and purification of imported NH3 back to hydrogen[82]. - **Determining the contribution to LCOH by ammonia decomposition is the aim of this thesis**.

3

Case Definition

In **Section 3.1** two formulated cases for large-scale ammonia decomposition process are described. **Section 3.2** describes the approach to feasibility evaluation and comparison of both cases.

3.1. Formulated Cases

After the review on available technologies and market perspectives, two cases are formulated for process simulation and techno-economical analysis of large-scale hydrogen production from ammonia cracking. Both of the formulated cases are represented by the simplified block diagrams in Figure 3.1. The subprocesses of the formulated cases are listed and described in Table 3.2.

- Case I represents a design for the near future (2030) and is based on conventional industrial process technologies. **Chapter 4** is dedicated to Case I process simulation
- Case II is formulated around the assumption that a highly promising emerging technology will be ready for commercial application by 2040. This emerging technology will be compared to base case scenario Case I. **Chapter 5** is dedicated to Case II process simulation.

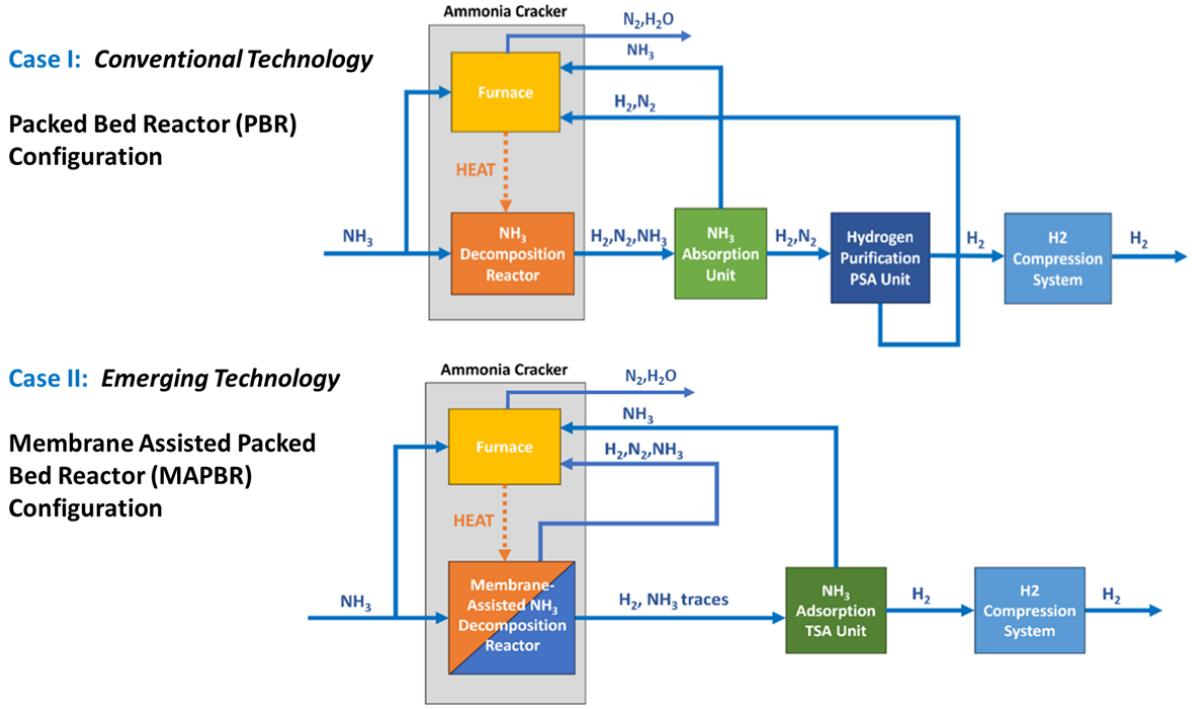

Figure 3.1: Block diagrams depicting the defined configuration cases of the ammonia cracking process.

Both of the process cases are to be designed to meet a hydrogen production target of 100 TPD (tons per day). This production scale is comparable to the largest domestic hydrogen production projects currently in development in the Netherlands (such as Shell Holland Hydrogen 1 project, which aims for 60 TPD production by the end of this decade [85]).

The green ammonia feedstock is assumed to arrive liquefied (at 1 bar, -34 °C) and diluted with 0,5mol% of water for prevention of stress corrosion cracking of the equipment material. The product requirement is defined by the Dutch Hydrogen Network specifications. Both the ammonia feedstock and product requirements are depicted in Table 3.1.

Ammonia-to-Hydrogen Process Condiotions:			
Product conditions:	Flow rate:	**100 TPD**	
	Temperature:	30 °C	
	Pressure:	50 bar	
	Molar composition:	**H2**	>98%
		N2	<2%
		H2O	<30 ppm
		NH3	<10 ppm
Feed conditions:	Flow rate:	**>567 TPD (from stoichiometry)**	
	Temperature:	-34 °C	
	Pressure:	1 bar	
	Molar composition:	**NH3**	99,50%
		H2O	0,50%

Table 3.1: Product requirements and the corresponding ammonia feedstock requirements

Table 3.2: Selected subprocess configurations for formulated ammonia cracking process plant scenarios.

Section	Case 1 (2030)	Case 2 (2040)
Ammonia Cracker:		
NH_3 Decomposition Reactor:	Conventional multi-tubular packed bed reactor. Ni/Al_2O_3 catalyst used as packed bed inside the tubes.	Membrane-assisted multitubular packed bed reactor. Ni/Al_2O_3 catalyst used as packed bed. Palladium-based membrane modules integrated inside the packed bed.
Heat Supply:	Supplied by burners, which combust ammonia from feed, ammonia recovery streams, and unrecovered hydrogen from PSA waste stream.	Supplied by burners, which combust ammonia from feed, ammonia adsorption unit stream, and unrecovered hydrogen from membrane module retentate.
NH3 Recovery:	Conventional absorber-stripper unit. Water used as a cheap and effective solvent. As water is already present in feed ammonia, no new impurities are introduced. Water can be removed by a downstream adsorption operation.	Temperature Swing Adsorption utilized for ammonia traces removal. Zeolite packing used as adsorbent. This method is preferred due to low concentration of ammonia traces expected in the product
Hydrogen Purification:	Pressure Swing Adsorption as a well-established technology for high throughputs, with low capital investment costs, able to reach high recovery (up to 90%) for required moderate purity (>98 mol% H_2, <2 mol% N_2).	Utilizes the membrane module for separating hydrogen from nitrogen and most of the ammonia due to high selectivity.
Compression:	Reciprocating compressors working in parallel. Capable to compress given product flow rates up to the required pressure.	Reciprocating compressors working in parallel. Capable to compress given product flow rates up to the required pressure.

3.2. Feasibility Evaluation Approach

The evaluation of feasibility of defined process configuration cases is split in technical and economical.

3.2.1. Technical Evaluation

- Both configurations are simulated and optimized using the chemical process simulation software Aspen Plus V12.
- The processes are simulated as continuous and steady state.
- Peng-Robinson EOS model is used to predict the thermodynamic properties of process streams. The Peng-Robinson model, developed for hydrocarbon behaviour prediction in industrial processes, is a widely used EOS due to its accurate prediction of thermodynamic properties of fluids, including ammonia [86].
- For Case I, the fired-heater based ammonia cracker unit configuration and energy requirement are optimized through Aspen Exchanger Design and Rating V12.
- For Case II, the membrane-assisted packed bed reactor is approximated by the performance reported from the literature.
- Both of the cases are then compared by their resulting product yield, product purity and required energy inputs.

3.2.2. Economic Evaluation

- The cost estimation of the formulated case processes is done according to the recommendations of the Advancement of Cost Estimation International (AACE International)[87]. For this research, each configuration was estimated up to the preliminary estimate class, known as Class 4. At this level of estimation quality, the accuracy is expected to be within +/-30% range.
- The costs of major equipment are determined by using the software Aspen Economic Analyser and cost scaling procedures from the literature.
- The main economic evaluation parameter of the process is the Levelized Cost of Hydrogen (LCOH) , explained in Figure 3.2, which is a fundamental calculation of production cost used in the preliminary assessment of hydrogen projects.

$$LCoH = \frac{net\ present\ value\ of\ total\ cost\ (CAPEX\ plus\ OPEX)\ over\ the\ lifetime\ of\ the\ plant}{net\ present\ value\ of\ total\ hydrogen\ production\ over\ the\ lifetime}$$

Figure 3.2: Levelized cost of hydrogen (LCOH) calculation [88]

- From the obtained LCOH, the required market price of the product is calculated from the net present value of the project.
- Both LCOH and market price are determined from the formulated economic analysis model, explained in **Chapter 6**.
- The obtained LCOH is broken down in major expenditure components and compared with predicted LCOH by alternative hydrogen production routes in the Netherlands.

4

Process Simulation - Case I: Conventional Technology

This chapter is dedicated to the designed process simulation of ammonia cracking plant by using conventional industrial process technologies. It is devided in following sections:

- **Section 4.1 - Model Construction** introduces the constructed process simulation.
- **Section 4.2 - Ammonia Cracker Modelling & Integration** provides the details on the ammonia cracker modelling and its integration in the process simulation.
- **Section 4.3 - Reaction Kinetics** focuses on the kinetic model of the utilized ammonia cracking catalyst and its validation procedure.
- **Section 4.4 - Hydrogen Purification** focuses on the purification systems of the process
- **Section 4.5 Product Compression** is dedicated to compression system.

4.1. Model Construction

The constructed process simulation is depicted by the Aspen Plus flowsheet in Figure 4.1. The hydrogen production is performed in multiple steps:

1. Liquified NH_3 stream arrives to the process and is split in two streams: NH_3 fuel stream towards the combustion reactor (FURNACE) and the process stream to the ammonia decomposition reactor (PBR).
2. The NH_3 process stream is evaporated by hot flue gas stream (FLUEGAS) in the heat exchanger (HEX-1) and is further preheated in second heat exchanger (HEX-2) by the hot reactor product stream (REACPROD).
3. The pre-heated NH_3 process gas stream (REACFEED) is partially converted to N_2 and H_2 in the plug flow reactor (PFR). The reaction heat for PFR is provided by released fuel combustion heat from FURNACE, modelled as stoichiometric reactor. The FURNACE heat duty is set to match the PFR heat requirement. The fuel is provided by fresh NH_3 stream (NH3FUEL) and H_2 purification waste streams (NH3REC, PSAWASTE).
4. The reactor product stream (REACPROD) is cooled by a series of two heat exchangers (HEX-2 and HEX-3) and a cooling unit (COOL-1).
5. The cooled product stream enters the absorber-stripper system to remove remaining NH_3, which is supplied to combustion unit(FURNACE).
6. The obtained product stream (ABSPROD) from the absorber goes to further purification in the PSA unit. The H_2 purification waste stream (PSAWASTE) is supplied as fuel for combustion (FURNACE).
7. Water from purified H_2 product (PSA-PROD) is removed by a downstream adsorption operation (DRYER).
8. The obtained pure H_2 is pressurized by two multi-stage compressors in parallel up to required pressure.

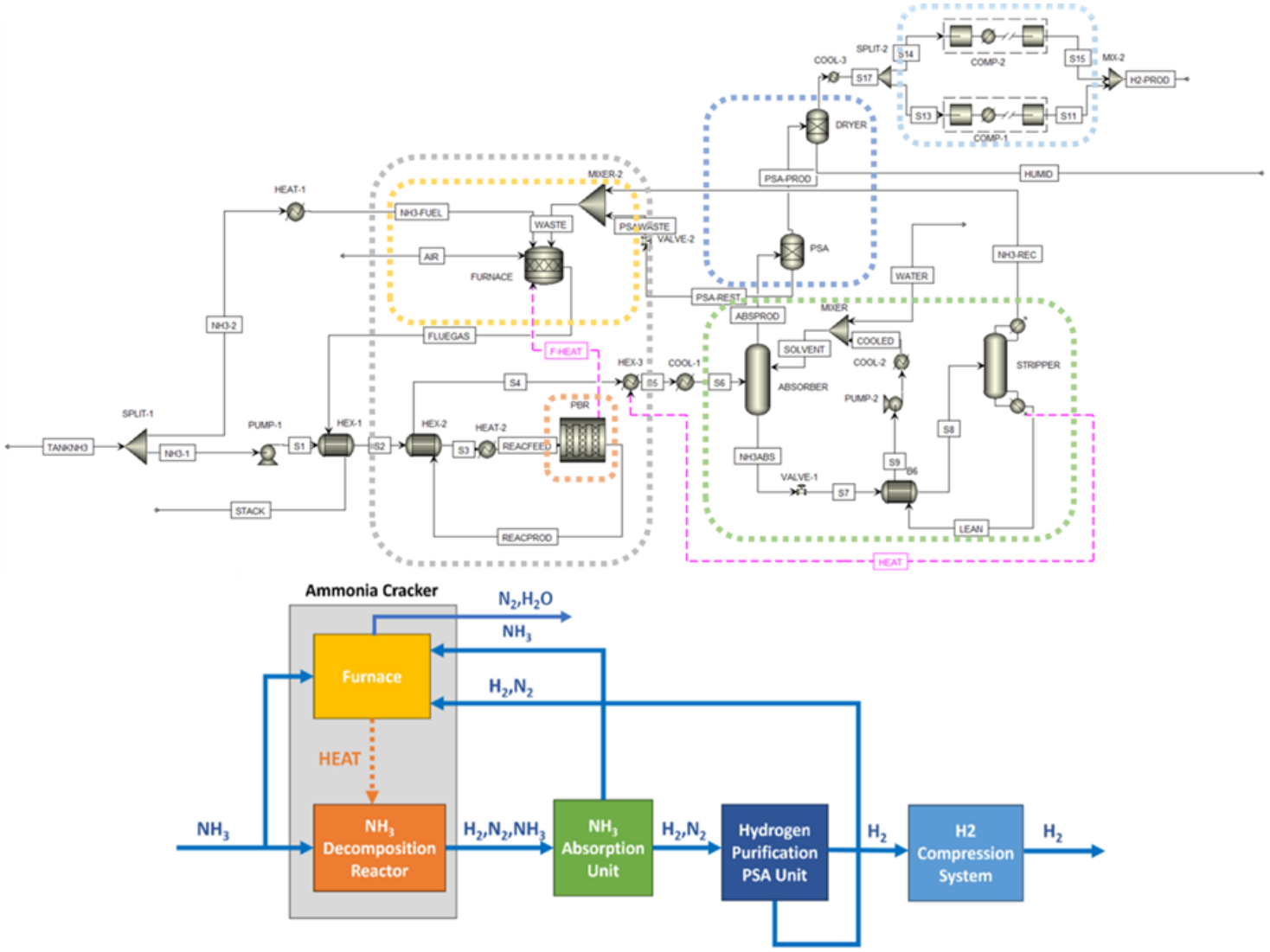

Figure 4.1: Process simulation flowsheet for Case I (Conventional Technology) from Aspen Plus. The function of each unit is depicted by frames and simplified block diagram.

4.2. Ammonia Cracker Modelling & Integration

The ammonia cracker configuration approximates the top-fired heater-reformer configuration. This configuration is commonly used in industry for similar endothermic processes, such as steam-methane reforming. In this configuration the multi-tubular ammonia cracking reactor is integrated into a fired heater. In the fired heater, the heat is produced by fuel combustion and is transferred to the reactor tubes and for preheating of other process streams.

The ammonia cracker is designed to ensure that the necessary heat for the endothermic ammonia decomposition reactor is provided solely by combustion of NH_3 feed stream and available H_2 purification waste stream. The waste stream includes unrecovered H_2 and unconverted NH_3. The design objective is to determine the minimum amount of fresh NH_3 feedstock required to meet the heat duty of the reactor.

The ammonia cracker design is done by a three-step cycle approach, in which two different process simulation tools are used, Aspen Plus and Aspen EDR (Exchanger Design and Rating). The ammonia cracker design approach is partially inspired by the method developed by (Makhloufi C., 2021)[13]. The design approach is visualized in Figure 4.2.

- **Step 1 - Reactor Modelling in Aspen Plus (Section 4.2.1):** The NH_3 decomposition is simulated by an isothermal plug flow reactor. The reactor product stream is then purified by H_2 purification system. The obtained reactor heat duty and available fuel from H_2 purification waste stream are exported to Aspen EDR.
- **Step 2 - Fired Heater Modelling in Aspen EDR (Subsection 4.2.2):** In Aspen EDR, the fired heater side of ammonia cracker is modeled from imported Aspen Plus data. From the obtained fired heater model, the heat flux profile along reactor tubing, required fresh NH_3 fuel and recoverable flue gas heat are exported for integration in Aspen Plus process simulation.
- **Step 3: Integration of Models (Subsection 4.2.3):** The process simulation in Aspen Plus is reconfigured to match the results obtained by Aspen EDR.
  - The heat flux profile from Aspen EDR is imported to the previously isothermal plug flow reactor, to determine the reactor process stream temperature and composition profiles.
  - The NH_3 feed stream is increased to provide required heat duty to the reactor and to match the exit furnace flue gas stream from the firebox.
  - The heat exchange unit, representing the fired heater convection bank, is scaled to match the recoverable flue gas heat obtained in Aspen EDR.
  - **The design of the ammonia cracker is accepted when the obtained NH_3 conversion matches the conversion of the isothermal PFR from Step 1.**

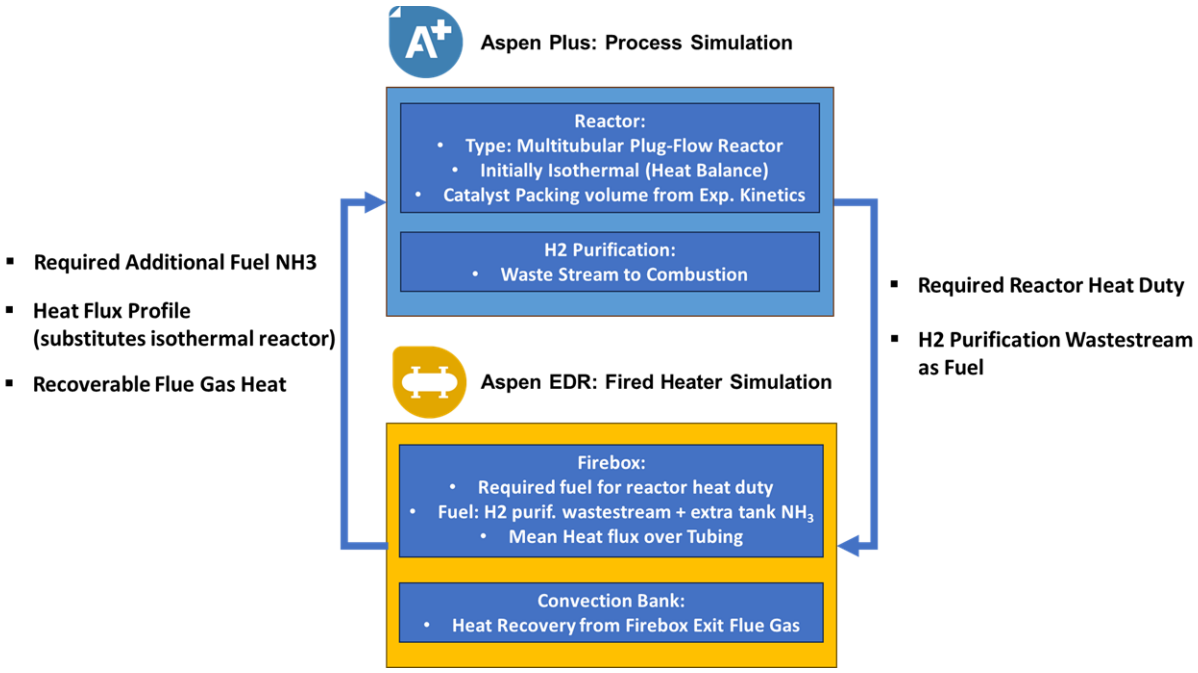

Figure 4.2: Ammonia cracker modelling and design approach for Case I - Conventional Technology.

4.2.1. Step 1: Reactor Modelling in Aspen Plus

Reactor Sizing

The NH_3 reactor is sized as a multi-tubular plug-flow reactor (PFR) with prescribed catalyst kinetics[89]. The following conditions were taken:

- To achieve a hydrogen product output of 100 tons per day (TPD), the NH_3 feed flow is set at 640 TPD. Stoichiometrically, 630 TPD of ammonia is required, assuming 90% H_2 recovery during H_2 purification.
- The PFR is initially modelled as isothermal.
- Sizing of the packed bed and determining the number of tubes are guided by the residence time derived from the Gas Hourly Space Velocity (GHSV) reported in the experimental setup of the catalyst kinetic model publication [89][90]. From the sizing procedure, the total catalyst packing volume is estimated at 14.5 m^3, which is distributed over 145 tubes. Refer to Appendix B.2 for a detailed procedure on packed bed sizing.
- The length and inner diameter of the tubes comply with the design standards for fired Heater - reformer (API 560) [91]. The length is set to 12 meters. The internal diameter is set to 4 inches.

The characteristics of the modelled multi-tubular reactor reactor and of the isothermal process stream are provided in the Table 4.1.

Table 4.1: Geometrical and operational characteristics of the reactor.

Reactor Characteristics		
Total packing volume	m^3	14.5
Number of reactor tubes	-	145
Tube length	m	12
D_{in} of the tube	in	4
GHSV	h^{-1}	12324
Reactor Process Stream Characteristics (at P = 10 bar, T = 689°C, F_{NH3} = 640 TPD)		
Stream velocity	m/s	2.71
residence time	sec	4.43

Operating Conditions

The isothermal reactor model is set at 689 °C. The operating pressure of the reactor is determined by the reactor kinetics model limitations and expected pressure drop, with inlet pressure at 11.3 bar and 1.5 bar pressure drop.

- The optimal operating temperature for the sized reactor is established based on the necessary extent of NH_3 conversion, ensuring a balance between the heat generated and recovered in the process. To pinpoint this optimal temperature, an idealized process model was simulated with the assumption that all of the heat generated by combustion of the H_2 purification waste stream can be fully recovered by the heat exchange network and NH_3 decomposition in the reactor. Details of this idealized process simulation are illustrated and explained in Appendix B.3.

  Through temperature sensitivity analysis, it was observed that the total generated heat and total recovered heat are in balance at a reactor temperature of 962 K (or 689 °C), see Figure 4.3. The reactor operation at this temperature region is therefore assumed to minimize the fresh NH_3 fuel requirement for the ammonia cracker.

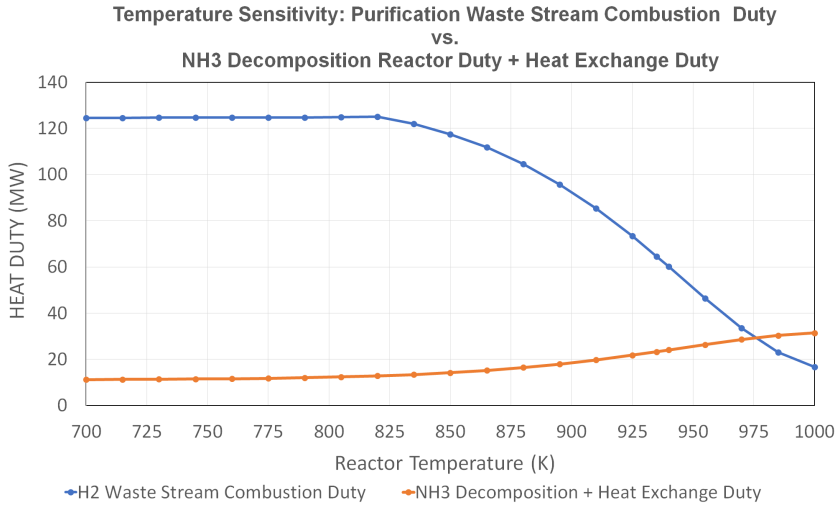

Figure 4.3: Temperature sensitivity plot for total duty of H_2 purification waste stream combustion and the sum of NH_3 decomposition and required heat exchange duties. The heat balance is pinpointed at T = 962 K (or 689°C).

- The utilization of an elevated pressure is anticipated to be advantageous as it would reduce the required downstream hydrogen compression. The targeted operating pressure is established to be in the range of 10 bar, as the reaction kinetics model is presumed to be unreliable beyond this value (see **Subsection 4.3.3** for a detailed evaluation of model performance at different pressures). The inlet pressure is specified at 11.3 bar, with an assumed pressure drop of 1.5 bar over the reactor tubes. This pressure drop value is assumed based on the characteristics of a catalyst-packed tubular reactor for steam methane reforming with similar tubing dimensions [92], considering that the dimensions of the loaded particles are not explicitly provided for the employed kinetics model.

Reactor Simulation Results

From the determined sizing of the reactor and the set operating conditions, the molar composition profile of the reactor process stream and the corresponding required reaction heat duty are determined.

- From the obtained composition profile (Figure 4.4), it is visible that the molar concentration of ammonia drops down to 4%. This concentration corresponds to conversion of 92 wt% of NH_3 supplied by the reactor feed stream. The converted percentage is determined from NH_3 concentrations of inlet and outlet streams of the isothermal reactor (refer to Appendix B.4).
- The heat duty for the PFR is determined to be 20,5 MW. This value is a summation of the required heat for NH_3 decomposition and sensible heat to increase the inlet stream temperature to the specified reactor temperature.

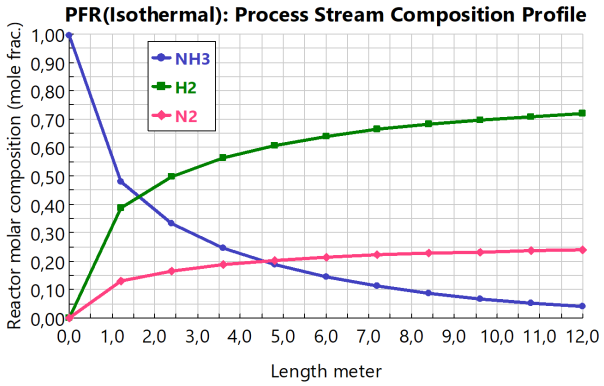

Figure 4.4: Process stream composition profile of the isothermal PFR (from Aspen Plus)

4.2.2. Step 2: Fired Heater Simulation in Aspen EDR

The schematic representation of the modeled fired heater is presented in Figure 4.5. The fired heater model is segmented into two main sections, namely the radiation and convection heat transfer zones, identified as the firebox and convection bank, respectively. In the firebox, the heat generated through fuel combustion in the top-fired burners is conveyed to the reactor tubing. Within these tubes, the process stream descends from top to bottom. The residual heat carried by the flue gas upon leaving the firebox from the top is then recuperated in the convection bank tubes. This recovered heat serves the purpose of evaporating and preheating the liquid ammonia feed.

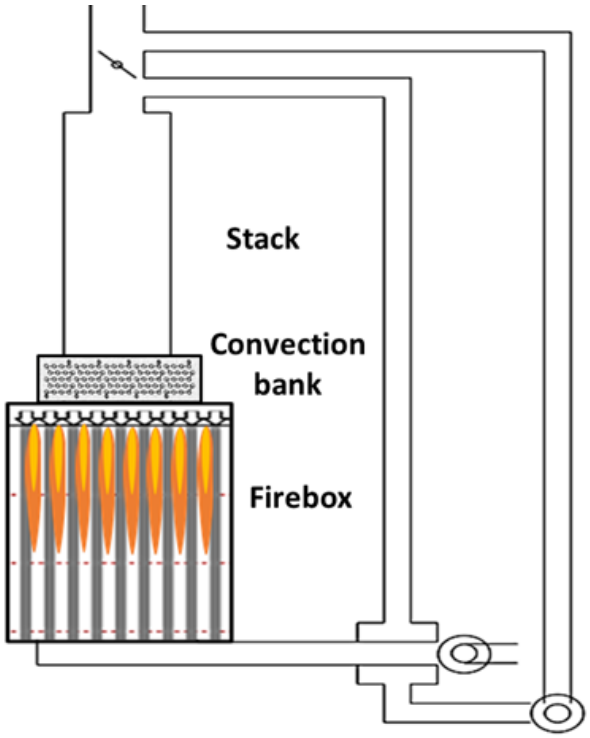

Figure 4.5: The simplified depiction of the fired heater model made in Aspen EDR.

Firebox Modelling

The following assumptions are taken during the firebox modelling:

- The base material for the firebox & reactor tubes is set to be from Stainless Steel 304, as resistant material to stress corrosion by present ammonia. This steel is normally considered for storage and handling of bulk ammonia [93].
- The firebox is sized to fit the reactor tubes determined by the reactor sizing in Aspen Plus. The tube pitch is set to 8 inch. The obtained firebox geometry is a rectangular casing of 12 m height, 8 meter length and 4 meter width.
- The thickness of the reactor tube walls is set to 15 cm, to fit the API 560 standard [91].
- Firebox is equiped with 36 natural draught, low NOx burners of 100 mm diameter (1 burner per 4 tubes [94]).
- The available fuel for the burners comprises of the H_2 purification waste stream and required fresh NH_3 fuel:
  - The waste stream quantity is fixed and determined by the H_2 purification system (refer to Section 4.4).
  - The quantity of NH_3 fuel is gradually increased until the firebox heat duty reaches the required heat duty for the reactor (20.5 MW).

- The air is supplied to ensure 10% excess air during combustion, which is assumed to reduce the NO_x formation [44]. It is assumed that the formed NO_X is converted to H_2O and N_2 by selective catalytic reduction unit(SCR)[46].
- As H_2 purification waste stream arrives with high N_2 concentration, it is assumed that fuel combustion is stable with given inert concentration.
- As Aspen EDR software does not consider the heat of reaction, the previously assumed constant temperature profile of the reactor process stream is ensured by increasing the mass flow rate of the reactor tubing process stream until a point is reached where the inlet and outlet temperature of the stream are nearly equal. This approach is undertaken to estimate the achievable heat flux to the reactor (see the prescribed process stream conditions is Appendix B.7).

Convection Bank Modelling
The extent of heat recuperation in the convection bank is limited to ensure realistic thermal efficiency of the fired heater (up to 90% efficiency [95]). The obtained information on recoverable flue gas heat is used for process simulation refining in Aspen Plus.

- The base material for convection bank is set to Stainless Steel 304 to prevent the tube walls from stress corrosion by ammonia stream [93].
- The convection tube bank geometry is set to 120 finned tubes. The tubes are 7 meters long with 4 inches in diameter.

Fired Heater Results
The designed fired heater model is visualized in Figure 4.6. The obtained values for fired heater performance parameters are listed in the Table 4.2. From fired heater simulation, the following results are obtained and integrated into Aspen Plus process simulation :

- **Heat Duty:** The heat transferred to the tubes in the firebox is equal to required reactor heat duty (20,5 MW). From fuel combustion 39.9 MW of heat is released. This corresponds to 51% of the thermal efficiency of the firebox.
- **Heat Flux Profile:** The avarage heat flux is 28,6 kW/m^2 (heat transferred over outer area of tubes). The heat flux profile over the reactor tube length (Figure 4.7) is then integrated into Aspen Plus process simulation.
- **Fresh NH3 Fuel** The fresh NH_3 fuel flow rate was gradually increased until heat transferred to firebox process stream reached 20,5 MW. The mass flow rate of NH_3 stream was determined to be at 68 TPD.
- **Combustion Fuel and Oxidant Composition** Mixing the H_2 purification wastestream with the fresh NH_3 feedstock to form the fuel blend yields a composition with a NH_3/H_2 ratio of 56%/44%. With a significant amount of nitrogen from the purification stream added to the fuel, there is an increase in the inert content introduced into the oxidant air stream, specifically raising the mole fraction of nitrogen. Consequently, the O_2/N_2 ratio is changed to 15%/85%. It is assumed that under the determined conditions, the burning of the fuel remains stable.
- **Flue Gas Heat Recuperation:** In convection bank, 14.9 MW of heat from the firebox exit flue gas is recovered by evaporating and preheating the ammonia process stream. This recuperation step brings the fired heater duty to 35.4 MW and elevates the total thermal efficiency of the fired heater to 89%.

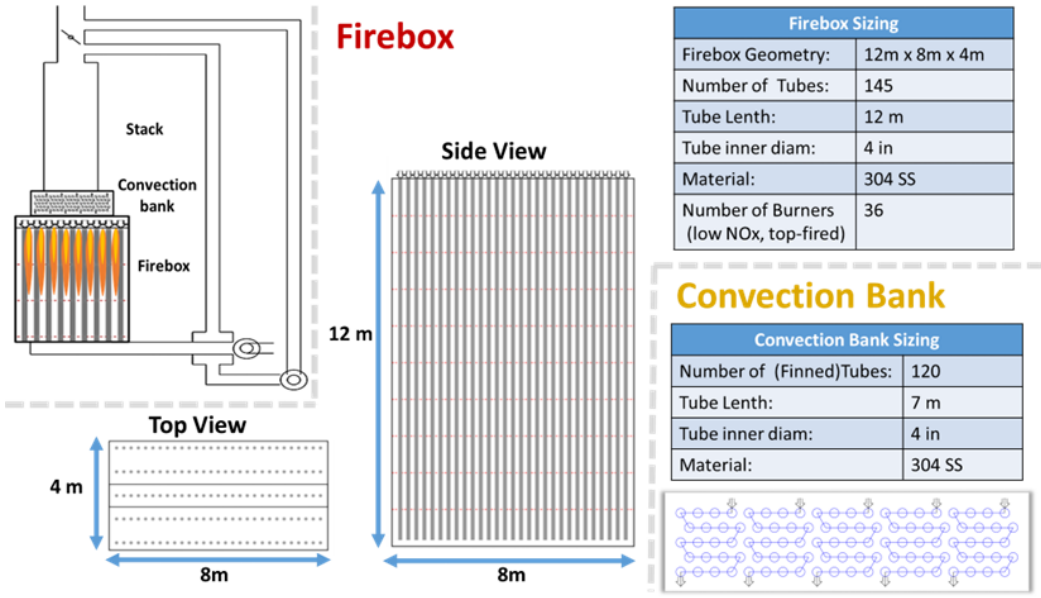

Figure 4.6: Main components of the ammonia cracker design defined in Aspen EDR.

Table 4.2: Results from the Fired Heater simulation by Aspen EDR

Fired Heater Duty	MW	35,4
Heat from combustion of fuel	MW	39,9
Firebox Heat Duty	MW	20,5
Thermal efficiency (%)		89%
Firebox thermal efficiency (%)		51%

NH3 Reactant Flowrate	TPD	640
Fresh NH3 Fuel Flowrate	TPD	68
% of Fresh NH3 supplied as Fuel	%	9,6
NH_3/H_2 molar ratio in fuel blend		56%/44%
O_2/N_2 mol. ratio in oxidant		15%/85%

Firebox well-stirred gas temperature	°C	939
Firebox flue gas exit temperature	°C	753
Stack flue gas outlet temperature	°C	132

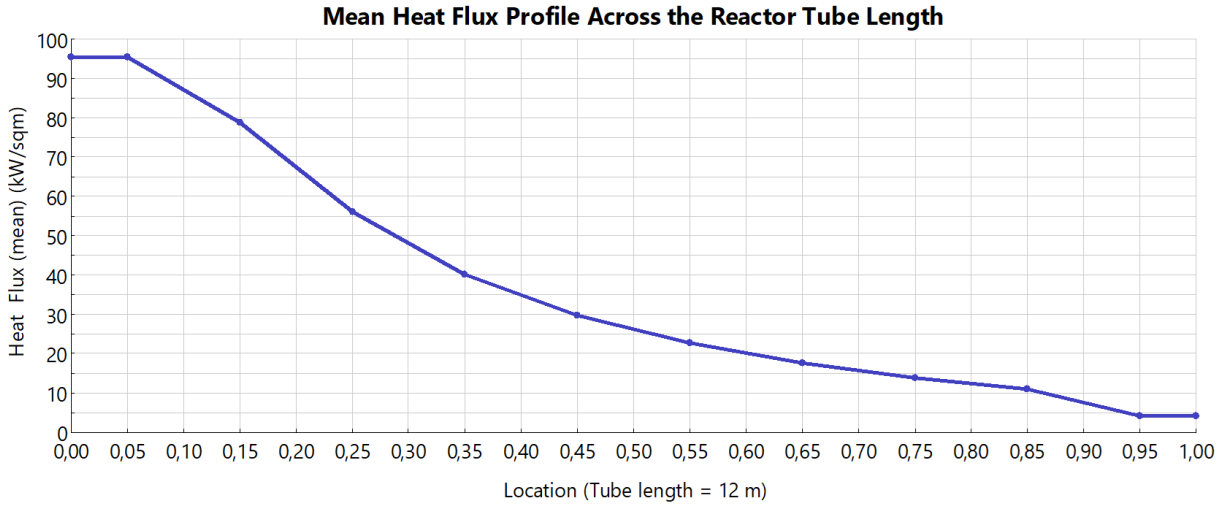

Figure 4.7: The Heat Flux profile to the reactor tubes, obtained from Aspen EDR V12

4.2.3. Step 3: Integration of Models

As final step of the ammonia cracker design, the results from Aspen EDR are integrated into the final process model in Aspen Plus:

- In Aspen Plus, the initially isothermal PFR reactor is substituted by the PFR reactor specified by the heat flux profile imported from Aspen EDR (Figure 4.7).From the imported heat flux profile, The process stream temperature profile along the reactor tube is determined in Aspen Plus (Figure 4.8)

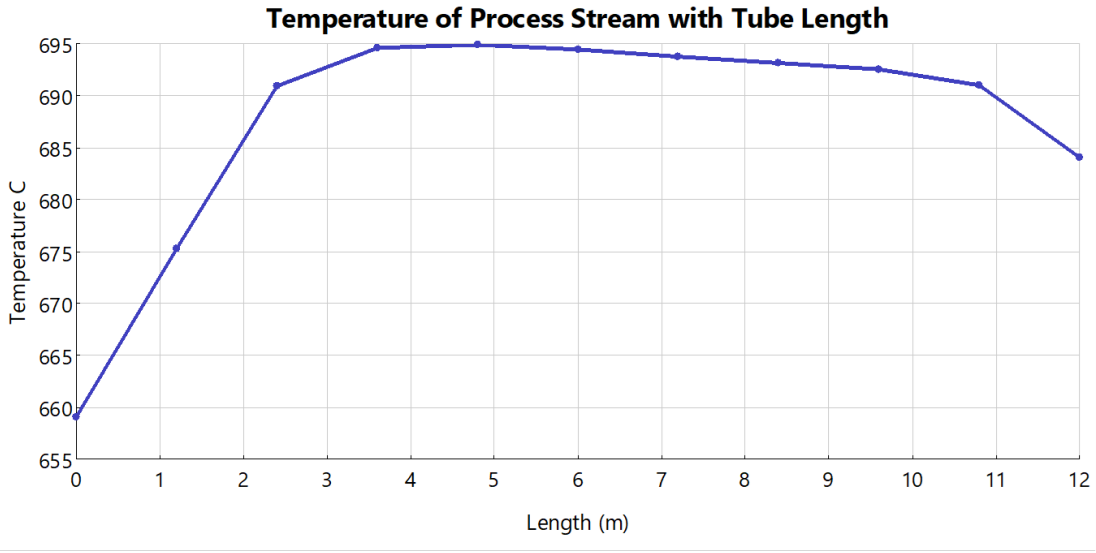

Figure 4.8: The temperature profile of the process stream, determined by the PFR specified by imported heat flux.

- Finally, the obtained process stream composition profile from PFR model with the external heat flux is compared with the result from isothermal PFR model in Step 1. See Figure 4.9 with both composition profiles side-by-side. It is visible that both of the models give the output streams with the same composition. Therefore, the integration of the fired heater model from Aspen EDR into the process simulation is completed and design is accepted.

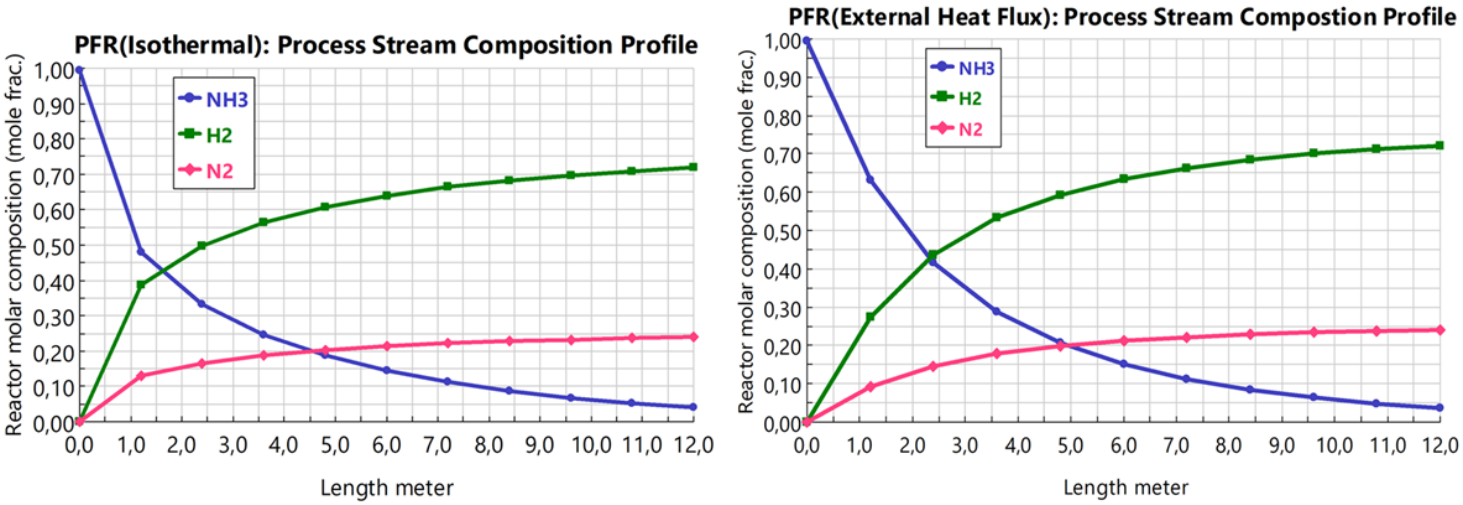

Figure 4.9: Left: Process stream composition profile in an isothermal PFR used for reactor sizing in Step 1. Right: Process stream composition profile in a PFR with a specified heat flux profile imported from the fired heater simulation in Step 3.

4.3. Reaction Kinetics

Ni/Al_2O_3-based catalyst is selected as preferred catalyst option for ammonia decomposition. The kinetic model of catalytic NH_3 decomposition is taken from the experimental research on the reaction kinetics of this catalyst type published by by Armenise. S. [89]. The catalyst bed is a crushed and sieved monolith structure covered with the Ni/Al_2O_3 coating. The details on the catalyst physical properties and experimental conditions during kinetics modelling are provided in Appendix B.1.

4.3.1. Catalyst Kinetics Model

The influence of the reverse reaction was identified to be virtually zero during the catalyst experiments, as the reaction remained very far from the equilibrium at the conditions of the experiments [89]. Therefore, the kinetic model was simplified to a simple powerlaw form without equilibrium correction. This is also known as Temkin-Pyzhev powerlaw equation. In the kinetics model, the ammonia decomposition rate per gram of catalyst ($-r_{NH_3}$) is expressed by the following formula:

$$(-r_{NH_3}) = k_0 exp(\frac{-E_{act}}{RT})(\frac{{p_{NH_3}}^{\alpha}}{{p_{H_2}}^{\beta}}) \tag{4.1}$$

with pre-exponential factor k_0 having a value of 4.859 x 10^8 $\frac{mol}{g_{cat}\ s\ atm^{\alpha+\beta}}$, activation energy E_{act} at 202,3 kJ $mol^{-}1$, and partial pressure exponents α and β of 0.73 and 0.64 respectively.

4.3.2. Catalyst Kinetics Validation

The validation of the catalyst kinetics model was done in Aspen Plus by the isothermal plug flow reactor model. The conditions for catalyst kinetics model validation were selected to be equivalent to the experimental conditions[89]:

- Reactor inlet stream is 100% NH_3 (NH_3/H_2 ratio of 1/0)
- Operating pressure = 1 bar
- Operating temperature range between 700 K and 1000 K
- GHSV (gas-hourly-space-velocity) = 12317 h^{-1}

Through sensitivity analysis the correlation of conversion percentage of feed NH_3 to operating reactor temperature was derived and compared to experiments [89]. The NH_3 conversion plots from the sensitivity analysis and from experimental results[89] are put side by side in Figure 4.10.

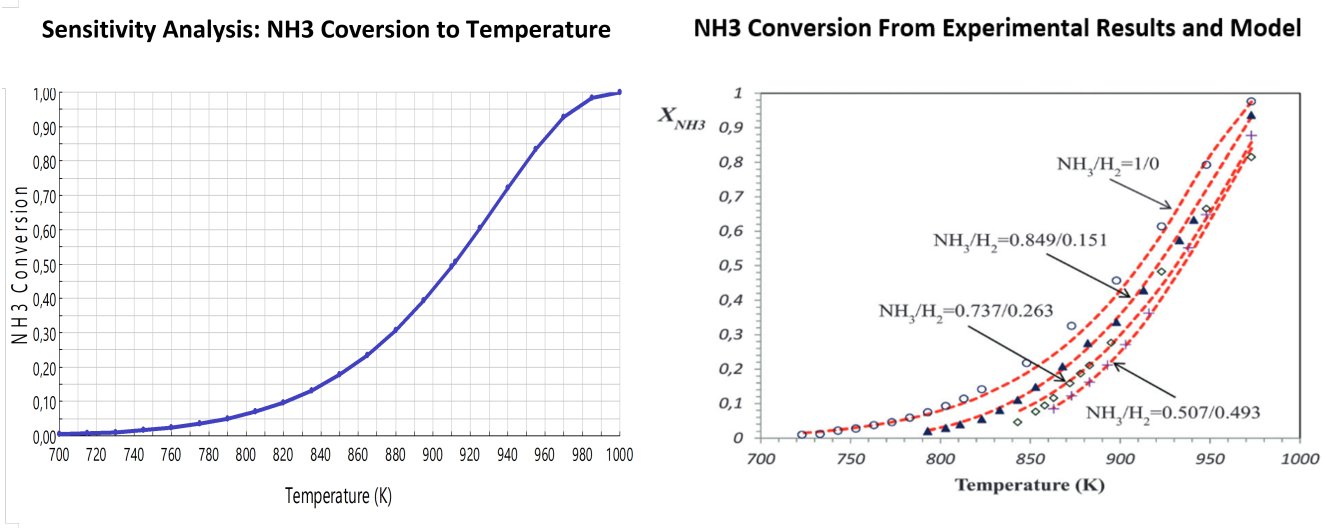

Figure 4.10: Properties of the Ni/Al_2O_3/monolith based packed bed, from experiments by Armenise.S. [89]

When comparing both cases on NH_3 conversion the similar trend is observed. In the region between 700 and 950 K, the observed deviation is below 1%. The highest deviation is observed at the last

experimental datapoint at 973K, where the sensitivity analysis predicts 93% conversion, whereas the experimental data indicates a value of around 97%.

The observed deviation can be attributed to the use of a different model to fit the experimental data[89]. While the Temkin-Pyzhev model (Eq. 4.1) was employed in the simulation, the conversion pattern from published experiments was plotted using the LHHW (Langmuir-Hinshelwood-Hougen-Watson) kinetic model. The latter offers more detailed kinetics by accounting for various stages of the catalytic reaction. However, it has to be noted that this approach could not be reproduced from published data (see Appendix figure C.12 for details). Hence, it is plausable that the employed power law model from the same publication [89] might have given less precise predictions of performance.

Nonetheless, the maximum deviation in converted percentage between performed simulation and the experiments is within 4%, which is taken as sufficiently accurate for this research.

4.3.3. Validity Limit of Kinetics Model for Varying Pressures and Space Velocities

The investigation into the validity limits of the applied kinetics model aims to assess its capability to predict NH_3 conversion under diverse pressure and gas-hourly-space-velocity (GHSV) conditions (as defined in Eq. 4.2). Of particular interest are elevated pressures, given the significance of downstream product pressurization requirements, and higher GHSV, which would offer increased reactor throughput.

However, it is essential to note that the kinetics model for ammonia decomposition using Ni/Al_2O_3 has been derived solely from experimental data collected at atmospheric pressure and a fixed GHSV. The validity of the model is tested by subjecting it to various pressures and GHSVs. Figure 4.11 provides a sensitivity analysis, illustrating the impact on NH_3 conversion percentage under different pressures and GHSVs. This analysis highlights an increase in NH_3 conversion with higher pressure and a reduction in conversion percentage at elevated flow rates, as indicated by GHSV in h^{-1}.

$$GHSV = \frac{Total\,Vol.\,Flow\,Rate\,to\,the\,Reactor\,(STP)}{volume\,of\,the\,catalyst} \tag{4.2}$$

The limitations of the kinetics model become evident when the gas hourly space velocity (GHSV) drops below 9000 h^{-1}, leading to predicted conversions that surpass the thermodynamic equilibrium curve. Consequently, the kinetic model is considered reliable only for GHSV values above 9000 h^{-1}. This constraint is justified by the model's reliance on ammonia decomposition experiments conducted at a GHSV of 12317 h^{-1}, where NH_3 conversion remains far from thermodynamic equilibrium[89]. Simultaneously, as GHSV increases, the conversion of ammonia decreases, attributed to the lower residence time of the reactant in the catalyst. To mitigate potential inaccuracies and to ensure an adequate NH_3 conversion, the GHSV value derived from the experiments[89] is utilized in the design of the reactor.

Furthermore, the model suggests a higher NH_3 conversion at elevated pressures. This can be rationalized by the expected prolonged contact time between the reactant and the catalyst, leading to increased NH_3 conversion, provided the system remains sufficiently distant from thermodynamic equilibrium. In order to uphold the accuracy of the model, a cautious approach is taken by setting the maximum operating pressure at approximately 10 bar.

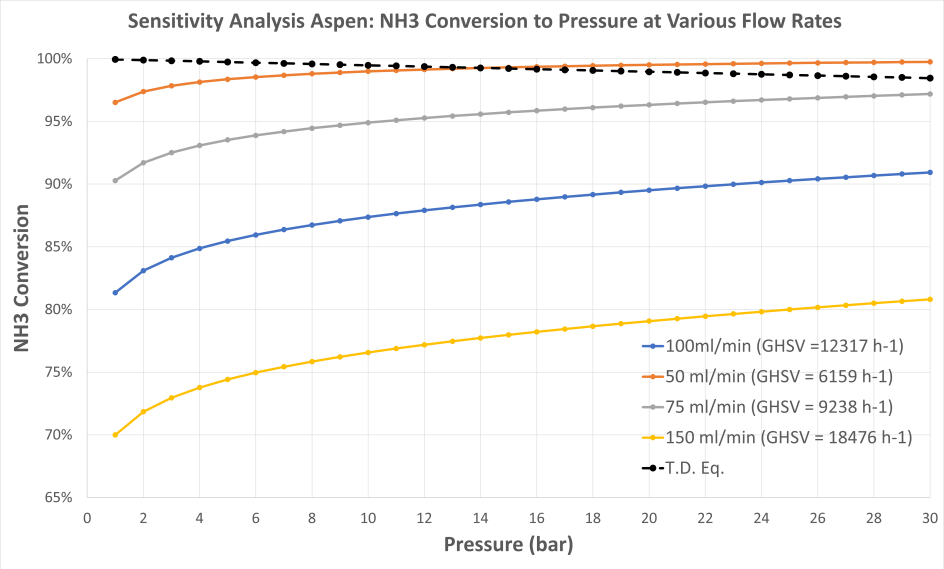

Figure 4.11: Sensitivity analysis of NH_3 Conversion extent to pressure and GHSV at fixed temperature (T = 680 °C), predicted by the used catalyst kinetics model [89]

4.4. Hydrogen Purification

The ammonia cracking reactor product stream is purified by the series of two processes:

1. **Ammonia Removal - Water Absorption (Subsection 4.4.1):** The unconverted ammonia from the cracker product is removed by the absorption-stripping system and is used as fuel to heat the ammonia cracker.
2. **Hydrogen Purification (Subsection 4.4.2):** Nitrogen is split from hydrogen product by Pressure Swing Adsorption. The refined product undergoes dehumidification through a subsequent adsorption operation.

4.4.1. Ammonia Removal - Water Absorption

Unconverted NH_3 is removed from reaction product by water absorption. Water is a common and cheap solvent for NH_3 absorption [52]. As the NH_3 arrives with 0.50 mol% of water, no new impurities are introduced to the product stream during absorption.

The ammonia removal and recovery system consists out of absorption tower, stripping tower (including condenser and reboiler), a heat exchanger in between and a recycle loop of the solvent. The integrated system is simulated in Aspen Plus V12. Both columns are simulated by RadFrac model, commonly used for preliminary design of separation towers [96]. The simulation flowsheet of the system is shown in Figure 4.12.

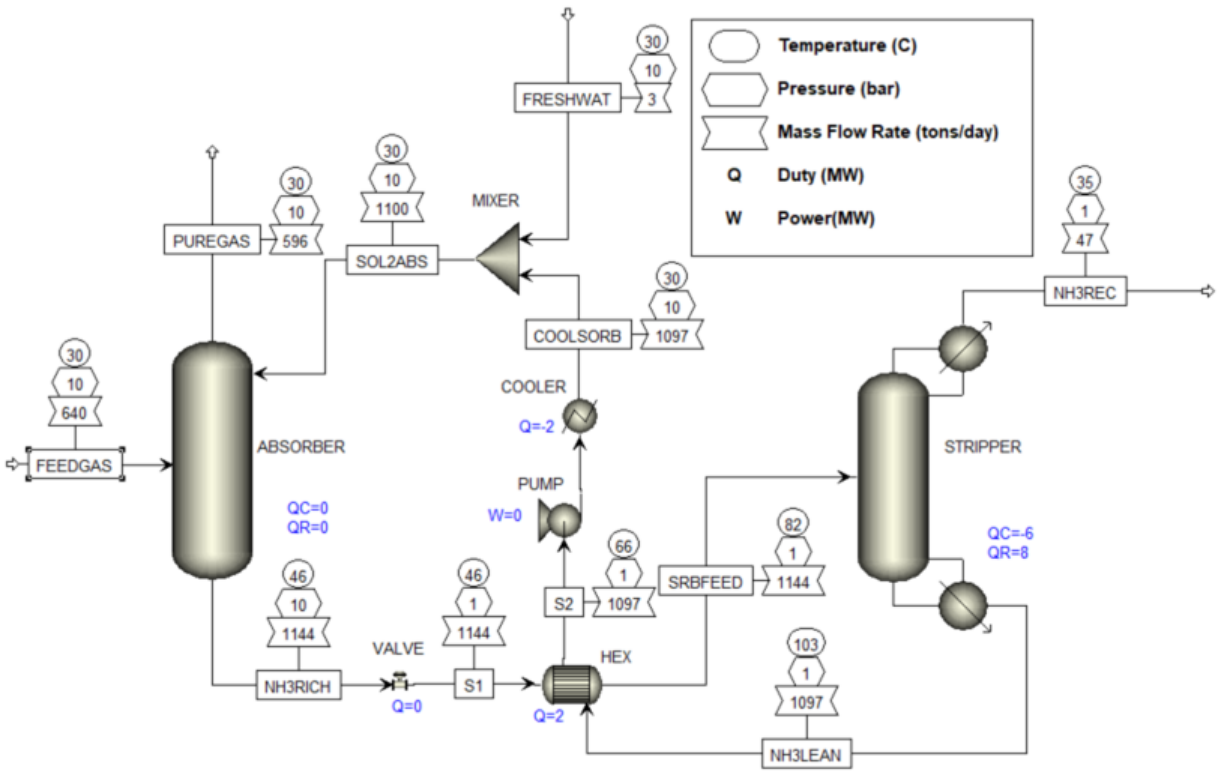

Figure 4.12: Process flowsheet of the designed ammonia absorption-stripping unit.

Ammonia absorption and recovery is performed in multiple steps:

1. The reactor product stream (FEEDGAS) enters the absorption column (ABSORBER).
2. Inside the ABSORBER, the NH_3 from reactor product is removed by the solvent stream (SOL2ABS) entering from the top. The purified product stream (PUREGAS) leaves from the top of the ABSORBER, while the NH_3-rich solvent stream (NH3RICH) leaves from the bottom of the tower. The temperature of the solvent is increased due to the exothermic nature of the absorption process.
3. The NH_3-rich solvent is depressurized through the valve and is preheated via heat exchanger (HEX) by a hot NH_3-lean solvent stream (NH3LEAN).
4. The obtained warm NH_3-rich solvent stream (SRBFEED) enters the stripping tower (STRIPPER).
5. Inside the STRIPPER, NH_3 is separated from the solvent through distillation process. The recovered NH_3 stream (NH3REC) leaves from the stripper top and is used as fuel for fired heater. The purified solvent stream (NH3LEAN) leaves the stripper from the bottom.
6. NH3LEAN stream is cooled by a heat exchanger (HEX) and is pressurized up to the set absorption pressure before its reintroduction to the ABSORBER.
7. To maintain the steady flow of the water solvent, fresh water stream (FRESHWAT) is added to the recovered solvent. The solvent mixture (SOL2ABS) is reintroduced to the absorber.

Absorption Tower

The absorption tower functions under the pressure and temperature conditions of the incoming feed stream.

- The feed stream is cooled down to the ambient temperature prior to entering the absorber, which is beneficial as water absorption is exothermal. It is visible by the increased bottoms temperature in Figure 4.12.
- The pressure at the top of the absorber is set at 9.8 bar, which is the same as the pressure of the streams, entering at the top of the column. The pressure drop over the column packing is set at 50 mbar as a recommended absorption step limit [97].
- The required flow rate of the solvent was derived from the sensitivity analysis of the concentration of NH_3 in the top product stream. The sensitivity plot in Figure 4.13 shows that the absorber reaches the desired mole fraction of ammonia at the flow rate of solvent at 1100 TPD.

The results of the absorber simulation are listed in Table 4.3. The details on the input and output streams are provided in the Appendix A.

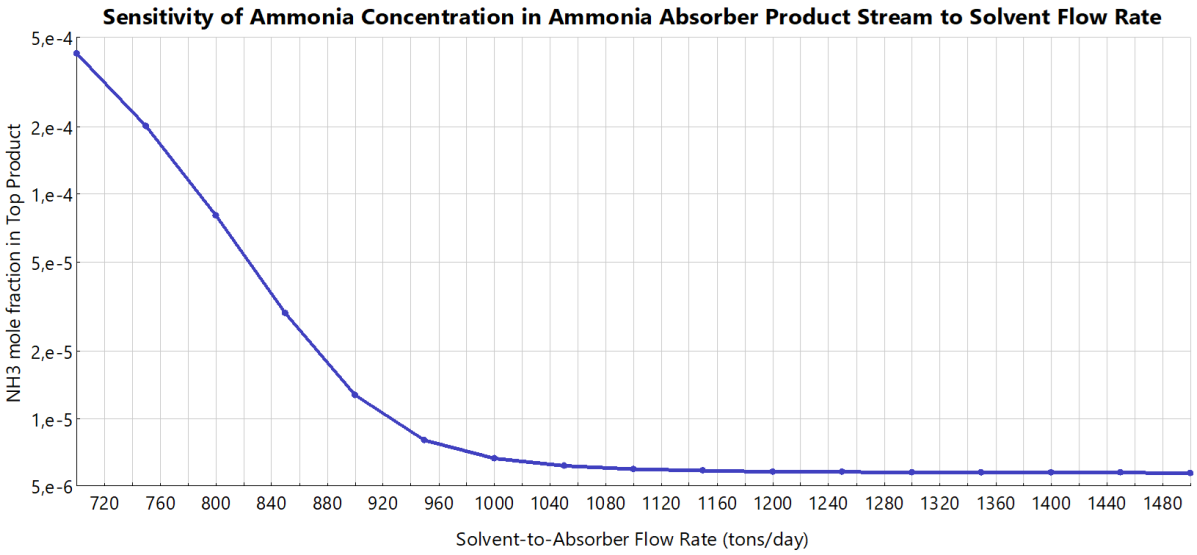

Figure 4.13: Sensitivity analysis of the obtained NH_3 mole fraction to varying solvent flowrate. P = 9.8 bar, T = 30 °C. The NH_3 mole fraction reaches desired value at 1100 TPD.

Table 4.3: Results from the absorption tower model

Design Parameter	Value	Unit	Comment:
Solvent (Water) Flow Rate	1100	TPD	- Determined by sensitivity analysis of NH_3 concentration in product (Figure4.13) - 1097 TPD of solvent recycled - 3 TPD of fresh water stream required
Number of stages	8	-	Determined iteratively as sufficient; 10 theoretical stages reported in Literature [97]
Mole frac. NH_3 in Top Product	6 ppm		Meets quality requirements

Stripping Tower
After being absorbed by the solvent, NH_3 has to be recovered from the mixture by the stripper column:

- Stripping Column is operated at atmospheric pressure. Pressure drop was taken as 50 mbar, same as the absorption column.
- NH_3 recovery and purity of the solvent are controlled by the condenser on top and the reboiler at the bottom.
- The stripping temperature and product purity are controlled by the bottoms controlling specifications, such as boilup ratio and bottoms rate.
- The lean solvent must be at least 99,99% pure to mitigate ammonia impurities at the column top. The conditions for the stripper column were selected to minimize the energy requirements to the reboiler and condenser.

The results of the absorber simulation are listed in Table 4.4. The details on the input and output streams are provided the Appendix A.

Table 4.4: Results from the stripping tower model

	Value	Unit	Comment:
Condenser Heat Duty	-6	MW	External cooling utilities required
Reboiler Heat Duty	8	MW	Can be provided by heat recovery from reactor product stream
Theoretical Stages	8	-	Assumed same as for absorber
Boilup Ratio	0.28	-	Determined by iteration
Bottoms Rate	1097	TPD	
Solvent (Bottoms) Purity %	99.99	%	High-purity solvent required
NH_3 % recovered	99.9	%	49 TPD of NH_3 recovered; Used as combustion fuel

Heat Exchange and Solvent Recycle
After designing the specifications for both columns separately, the solvent stream cycle must be closed and heat integration conducted:

- A pump is essential to increase the pressure for the outgoing NH_3 lean stream from the solvent, ensuring it enters the absorber at 9.8 bar pressure.
- A heat exchanger is configured to preheat the NH_3-rich solvent before entering the stripper, and simultaneously, to cool the NH_3-lean solvent prior to entering the absorber column.

4.4.2. Hydrogen Purification: Pressure Swing Adsorption

The purified gas from the water absorption step is further purified by two adsorption operations. H_2 is split from N_2 by pressure swing adsorption. Afterwards, the obtained hydrogen product is dried by removing the water traces by the adsorption operation.

Pressure Swing Adsorption

Pressure swing adsorption stands as a well-established technique for gas separation, frequently employed in the purification of hydrogen. This method follows a two-step cyclic process, wherein nitrogen from the process gas is adsorbed by the pressurized adsorption bed during the adsorption step. In the second step, the adsorption column undergoes depressurization to regenerate the adsorption packing. Zeolite structures, like 13X zeolites, are frequently applied in hydrogen purification [60].

Due to Aspen Plus limitations in simulating the pressure swing adsorption process, it is modeled in the form of a component separator with predetermined split fractions (see Table 4.5). These split fractions are established based on the following assumptions:

- **Product Purity Adjuctment**: To meet specified requirements, the product purity of H_2 is enhanced to 98%, while the concentration of N_2 is reduced to 2 mol%
- **Hydrogen Recovery**: A hydrogen recovery of 90% is assumed for purification, as it aligns with the moderate purity level required for hydrogen. This value is a reported upper limit of hydrogen recovery [60].
- **Adsorption Pressure**: Adsorption is presumed to occur at a pressure of 10 bar in the incoming feed stream, a condition supported by literature[59].

The composition and flowrate of the obtained purified product stream and purification waste stream are determined (listed in Table 4.6):

- The obtained NH_3,H_2 and N_2 concentration is sufficient to be admitted to Hydrogen Network. However, the concentration of water is too high and has to be removed by the downstream adsorption operation.
- The molar composition of the purification waste stream comprises 24 mol% H_2 and 76 mol% N_2. This waste stream contains 10.4 TPD of hydrogen supply, serving as the fuel stream for the fired heater. In the design of the fired heater, it was assumed that the combustion would remain stable despite the elevated amount of inert N_2 added to the oxidant by the H_2 waste stream.

Table 4.5: The defined split frations for the PSA product and waste streams.

Component	PSA-Product Split Fraction	PSA-Waste Split Fraction
NH3	1	0
H2	0,9	0,1
N2	0,0551	0,9449
H2O	1	0

Table 4.6: Results from the PSA component separator

PSA streams results			
		Product	PSA waste stream
Mole Fractions			
NH3		8,6 ppm	0
H2		97,5%	0,241
N2		1,99%	0,759
H2O		0,55%	0
Mass Flows	**tons/day**	**125,3**	**467,3**
NH3	**tons/day**	0,007	0
H2	tons/day	93,9	10,4
N2	tons/day	26,6	456,8
H2O	tons/day	4,7	0

Hydrogen Dryer

The final purification step for the produced hydrogen involves the removal of water traces to a level as low as 45 ppm. The hydrogen dryer is modelled as a component separator The residual water is effectively eliminated through the adsorption operation. The obtained dry H_2 product stream meets the Hydrogen Network purity specifications. This operation is modelled as a component separator, as was done with PSA unit (see Table 4.7 for taken split fractions). The product stream properties are listed in Table 4.8.

Key assumptions regarding this purification step are as follows:

- **Integration with PSA unit:** Commonly reported methods for hydrogen drying include temperature swing adsorption (TSA) [98] and pressure swing adsorption (PSA) [99]. Zeolites are common adsorbents used for hydrogen dehumidification [100]. It is assumed that the hydrogen drying packed bed can be integrated into a single system with the PSA unit, where the separation of hydrogen from nitrogen takes place.
- **Negligible Product Loss:** The product loss during drying step is assumed to be negligible. According to hydrogen dryer producers, the regeneration of the adsorption bed results in a maximum product loss of 1-2% [98].

Table 4.7: The defined split frations for the drying unit product and waste streams.

Component	Dry H2 Product Split Fraction	Dryer-Waste Split Fraction
NH3	1	0
H2	1	0
N2	1	0
H2O	0,00819	0,99181

Table 4.8: Properties of the H2 dryer product stream.

Drying Unit Product Stream Properties		
	Unit:	
Temperature	°C	30
Pressure	bar	9,79
Mole Fractions		
NH3		9 ppm
H2		98%
N2		2%
H2O		45 ppm
Mass Flows	tons/day	121
NH3	tons/day	0,007
H2	tons/day	95
N2	tons/day	27
H2O	tons/day	0,04

4.5. Compression System

In the simulation, the purified H_2 arrives to compression system at 10 bar. The compressor system pressurizes the produced hydrogen up to 50 bar pressure to be admitted to Hydrogen Network. The compression system consists out of two identical two-stage reciprocating compressor units in parallel. The compressors are modelled as positive displacement multistage compressors in Aspen Plus , see Figure 4.14.

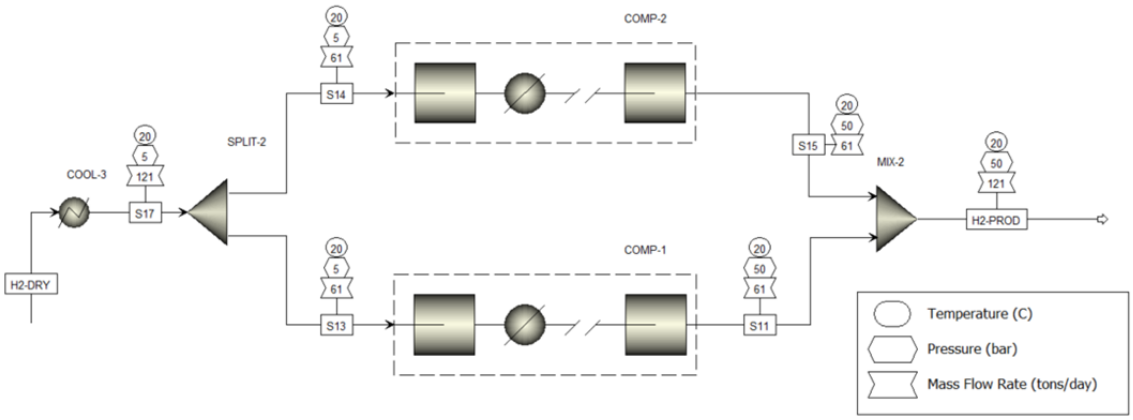

Figure 4.14: Compression system model.Two two-stage reciprocal compressors with intercooling for hydrogen compression up to 50 bar

The following assumptions were taken for the compression simulation:

- The compressors are suitable for given volumetric flowrate (20548 m^3/hr (STP) per compressor), as the maximum achievable flowrate for commercial compressor is reported at 34000 m^3/hr [68].
- The efficiency of each compressor unit is set at 72%.
- The maximum discharge temperature for the compressor gas is set to 130°C, as the (reciprocating) compressors suffer from thermal stress at temperatures above 150°C [101]. The product stream is

pre-cooled and intercooled between compression stages to maintain the outlet temperature limit for each compression stage.

- Note: It is expected that additional compression would be required for the H_2 compression system, which was not considered in Aspen Plus Simulation. The compression work is assumed to be equivalent to compression done by a single compressor unit, which is equivalent to compression of purified H_2 from 4,5 bar to 10 bar.

The obtained performance parameters for required compression stages and intercoolers per compression unit are given in Table 4.9 and Table 4.10, respectively. From the simulation, the total electricity requirement for compression is estimated at 3.2 MW. When considering the additional compression requirement for H_2 purification, the total electricity requirement is estimated at 5 MW.

Table 4.9: Results for a single reciprocating compression unit.

Stage	Outlet Temperature (C)	Outlet Pressure (bar)	Pressure Ratio	Indicated Power (MW)	Volume Flow (m3/hr)	Efficiency Used
1	131	22	2,2	0,81	2215	0,72
2	131	50	2,2	0,82	996	0,72

Table 4.10: The results for required intercoolers after each compression stage.

Stage	Temperature (C)	Pressure (bar)	Duty (MW)	Vapor fraction
1	20	22	-0,81	1
2	20	50	-0,81	1

5

Process Simulation - Case II: Emerging Technology

This chapter focuses on simulating the process design of an ammonia cracking plant using cutting-edge technologies that have the potential for widespread application on a large scale. The chosen emerging technology for this study is the membrane-assisted ammonia decomposition reactor. The membrane reactor is chosen as attractive process intensification technology due to synergy of ammonia decomposition and simultaneous hydrogen product purification. The constructed process is developed for further comparison with a conventional technology scenario (Case I).
The chapter is divided in following sections:

- **Section 5.1 - Model Construction** introduces the constructed process simulation.
- **Section 5.2 - Membrane-Assisted Ammonia Cracker Modelling** provides the details on the developed model for the membrane-assisted ammonia cracker simulation
- **Section 5.3 - Ammonia Traces Removal** focuses on the downstream purification process which removes remaining impurities from the membrane reactor product.
- **Section 5.4 - Product Compression** is dedicated to compression system.

5.1. Model Construction

The constructed process simulation is depicted by the Aspen Plus flowsheet in Figure 5.1. The hydrogen production is performed in multiple steps:

1. Liquified NH_3 stream arrives to the process and is split in two streams: NH_3 fuel stream towards the combustion reactor (FURNACE) and the process stream to the membrane assisted ammonia decomposition reactor.
2. The NH_3 process stream is evaporated by hot furnace flue gas stream (FLUEGAS) in the evaporator (EVAP-HEX) and is further preheated by two heat exchangers (HEX-1 and HEX-2), which transfer heat from hot membrane retentate (RET3EXIT) and membrane permeate (TOTAL-H2) streams, respectively. The heater (HEAT-2) adds the remaining heat to the process stream to meet the membrane-reactor temperature requirement.
3. Preheated NH_3 stream enters the membrane reactor. Membrane reactor is approximated by a cascade of Gibbs reactors and component separators. This approach is explained in detail in Section 5.2. The heat required for the Gibbs reactors (GIBBS1-GIBBS3) is supplied from fuel combustion by FURNACE. The permeated H_2 stream is cooled down to ambient temperature by the NH_3 process stream via HEX-2 and a cooler. The membrane retentate (RET3EXIT) is cooled down and is streamed to the FURNACE as combustible fuel.
4. TSA unit splits the remaining NH_3 traces from H_2 permeate stream. The removed NH_3 stream (DES-NH3) is directed to the furnace as combustion fuel.
5. Finally, the obtained pure hydrogen stream (H2CLEAN) is pressurized by parallel compressors up to required pressure.

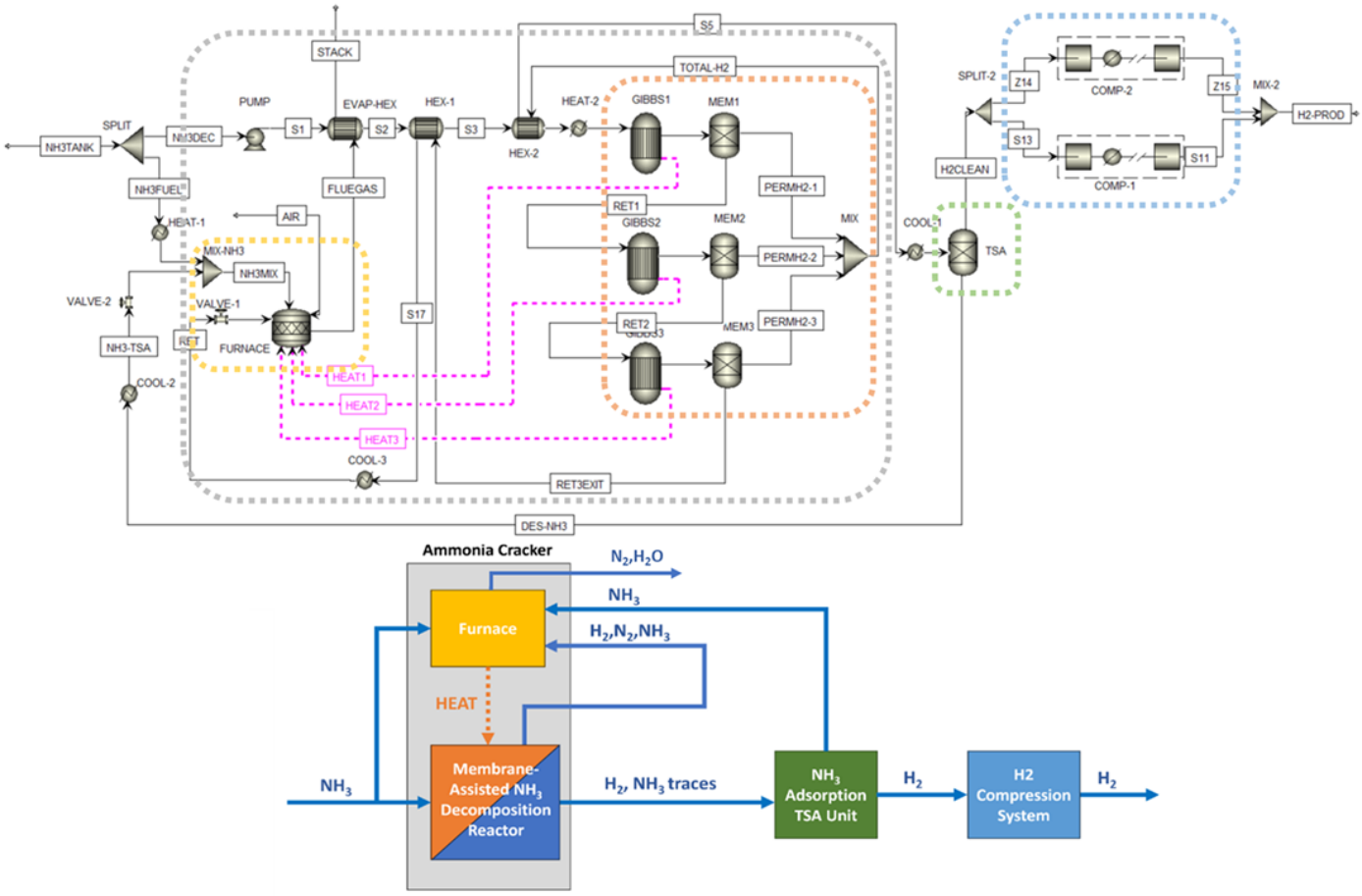

Figure 5.1: Process simulation flowsheet for Case II (Emerging Technology) from Aspen Plus. The function of each unit is depicted by frames and simplified block diagram.

5.2. Membrane-assisted Ammonia Cracker Modelling

In emerging technology case, the NH_3-to-H_2 production process is intensified by assisting the catalytic NH_3 decomposition reactor with the Pd-Ag membrane modules inside the reactor packing. The membrane-assisted packed bed reactor configuration creates synergy of NH3 decomposition and H_2 purification. NH_3 decomposition enhanced by the selective H_2 permeation through membrane. At the same time, highly pure hydrogen product is obtained in the permeate stream.

The ammonia cracker is designed to secure the necessary heat for the endothermic NH_3 decomposition reactor through the exclusive combustion of the fresh NH3 feed stream and the available waste stream from H_2 purification. The waste stream contains unrecovered H_2 and unconverted NH_3 from the membrane retentate. The primary goal of the design is to determine the quantity of the required fresh NH_3 feedstock.

The entire model of the ammonia cracker is done in Aspen Plus. The ammonia cracker model is divided in two parts:

- **Membrane-assisted Reactor Modelling (Section 5.2.1):** The synergetic decomposition-purification performance of the membrane reactor is simulated by a cascade of Gibbs reactors and component separators. The determined reactor heat duty and the available fuel from membrane retentate stream are used for modelling the combustion unit, which supplies heat to the reactor.
- **Combustion Unit Modelling (Section 5.2.2):** The combustion unit is modelled by a stoichiometric reactor with prescribed reactions for H_2 and N_2 combustion. Based on the reactor heat duty and available fuel from H_2 purification waste stream, the required additional fuel in form of fresh NH_3 feedstock is determined.

5.2.1. Membrane-assisted Reactor Modelling

As Aspen Plus does not have a separate model for membrane-assisted reactor simulation, the approach is developed which approximates the membrane reactor based on the assumptions taken from the published examples of the membrane-assisted reactor performance[40, 35, 66, 42].

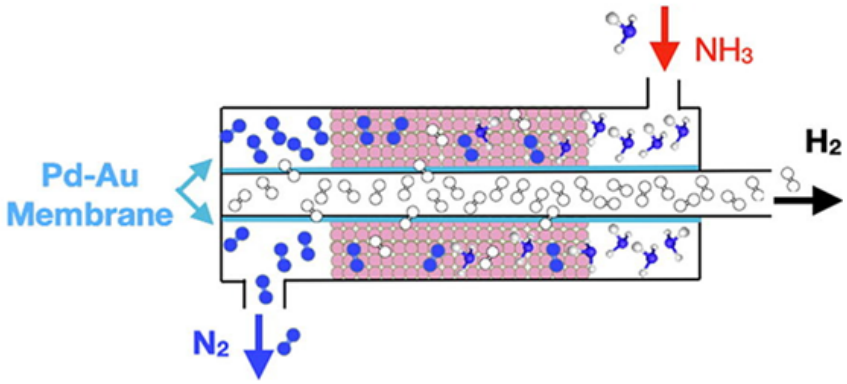

Figure 5.2: Working principle of the membrane assisted packed bed reactor[35]

Membrane Reactor Modelling Assumptions

The assumptions on the membrane module sizing and its performance are formulated based on the published performance from literature. The side-by-side comparison with the best performing experimental case, where the highest hydrogen permeation flux was obtained, is given in Appendix B.10:

- **Feed NH_3 Flow Rate**: The NH_3 feed flow rate is set to 640 TPD, which is the same as the one taken for the conventional case (Case I).
- **Membrane Pressure Ratio:**Hydrogen permeation hinges on the pressure differential (P_{H2}) between the feed (retentate) and permeate sides of the membrane. To facilitate this permeation, a retentate side-to-permeate side absolute pressure ratio of 7.5 is employed. This ratio proves sufficient to sustain hydrogen permeation [40][38]. According to the experiments by (Cerrillo J.,2022 [38]),this pressure ratio guarantees a 99% decomposition of NH_3 with a concurrent 90% recovery of the produced hydrogen in the permeate stream. The influence of the pressure ratio on NH_3 conversion and H_2 recovery is detailed in Appendix B.9.
- **H_2/N_2 Selectivity:** The H_2/N_2 selectivity is set to 300, as reported for relatively high permeation fluxes [40].
- **H_2/NH_3 Selectivity:** H_2/NH_3 selectivity is set to be the same, as it is reported to be of the same order of magnitude as H_2/N_2 selectivity [66].
- **H_2/H_2O Selectivity:** At given concentrations of H_2O in the process stream, it is assumed that no H_2O is permeated through membrane and no poisoning of palladium layer (such as PdO formation [102]) occurs.
- **Membrane Area:** The required membrane area was estimated at 763 m^2. The required amount of membrane area was determined based on the set process stream flow rate (640 TPD) and highest permeation flux reached by Pd-Ag membrane (13.5 ml $min^{-1}cm^{-2}$) reported from the literature for NH_3 decomposition with 90% H_2 recovery [40]. See side-by-side comparison of the experimental setup and the derived large-scale configuration in Appendix B.10.
- **Operating Temperature:** The operating temperature is limited to 500 °C as Pd-Ag membrane layer suffers from degradation due to interaction with the membrane support layer, leading to instability.
- **Catalyst Performance:** As the catalyst bed is in the same environment as the membrane, it is assumed that it is able to ensure sufficient NH_3 conversion at 500°C.
- **Thickness of the selective layer:**The thickness of selective layer of the membrane is minimized down to 1 μm due to economic considerations of minimization of precious palladium requirement [42] in the membrane. As the membrane selectivity reduces with thickness, the downstream removal

of slipped NH_3 traces is added (see Section 5.3 on NH_3 traces removal). This approach is chosen as downstream purification was estimated as economically favorable compared to increasing the membrane thickness to reach the required product specifications [42].

Table 5.1: Membrane Module Parameters used for the simulation

Membrane-Assisted Reactor	
Reactor Temperature :	500°C
Retentate Pressure:	15 bar; 30 bar; 60 bar
Permeate Pressure:	2 bar; 4 bar; 8 bar
Pressure Ratio Retentate-Permeate	7.5
Reactor Inlet Flow Rate	640 TPD
H2/N2 selectivity	300
H2/NH3 selectivity	300
H2 recovery	90%
Membrane area	763 m^2
Membrane thickness	1 µm

Model Configuration
The Aspen Plus model for the membrane-assisted reactor utilizes a cascade of three Gibbs reactors and three component separators to emulate the reaction and separation processes, see Figure 5.3. The Gibbs reactor model defines the thermodynamic equilibrium of the reaction mixture, while the separator model defines the separation of permeated hydrogen product from the retentate stream. This cascading strategy enables the design and optimization of the membrane reactor for nearly complete conversion, facilitated by the thermodynamic shift induced by selective hydrogen removal.

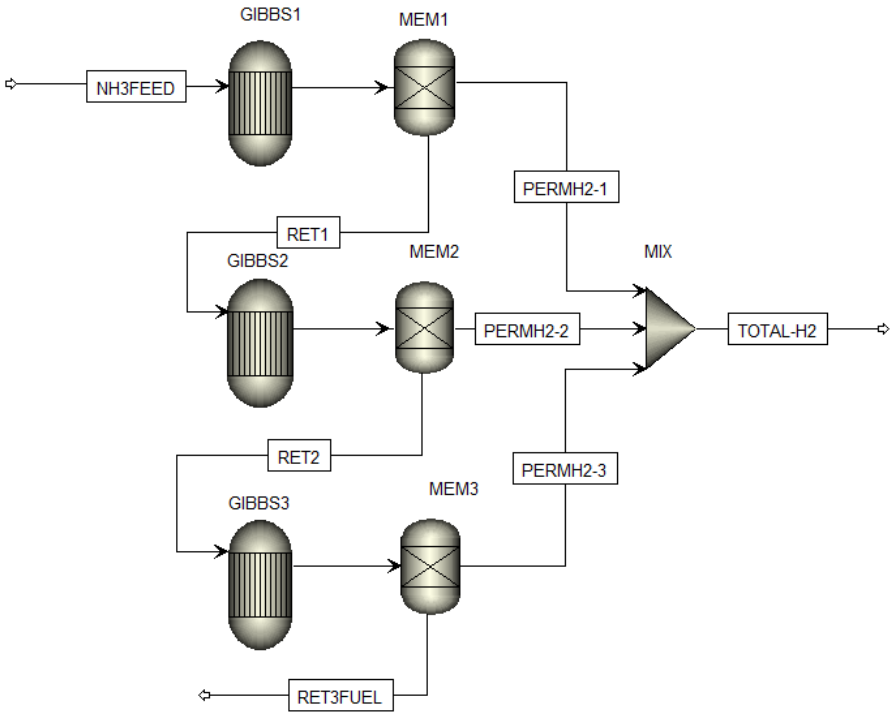

Figure 5.3: A cascade of three Gibbs reactors and three component separators emulates simultanious reaction and separation processes in the membrane assisted reactor.

In this iterative process, the reaction product from each Gibbs reactor, existing in thermodynamic

equilibrium, undergoes separation in the component separator using specified split fractions, based on previously mentioned assumptions. The resulting retentate stream is then directed to the subsequent Gibbs reactor for re-equilibration, contributing to additional hydrogen production.

- Each Gibbs reactor operates under identical temperature and pressure conditions:
  - The temperature is set at 500°C, adhering to the upper limit for Pd-Ag membrane stability. The heat to maintain the temperature is provided by the combustion unit, as depicted in Figure 5.1.
  - The pressure within the Gibbs reactor mirrors that of the feed (retentate) side of the membrane. Three distinct process models were developed to assess performance under increased retentate pressures, represented by Gibbs reactor pressures at 15 bar, 30 bar, and 60 bar. The comparative analysis of their performance is presented in the results section. For detailed examination in this chapter, the 30 bar configuration is considered as the base case.
  - The product streams obtained from the reactors at given operating conditions are directed to the component separators.
- The component separators divide the product stream from the Gibbs reactor based on assumed membrane module selectivity and hydrogen recovery in the permeate. Each separator employs the same specified component split fractions (see Table 5.2), determined by the aforementioned assumptions. The resulting streams represent H_2 permeate streams and membrane retentate streams.
  - The H_2 permeate streams are set to exit at permeate pressure according to a retentate-to-permeate pressure ratio of 7.5, as outlined in Table 5.1. These H_2 permeate streams from each separator are combined and directed to the product treatment section.
  - The retentate streams from first two separators, no longer in thermodynamic equilibrium, progress to the next Gibbs reactor for reequilibration, leading to additional hydrogen production as a consequence. The retentate stream from the last component separator is directed to combustion unit as fuel.

Table 5.2: The defined split frations for three component separators in the membrane reactor model, determined from taken assumptions of H_2/N_2 and H_2/NH_3 selectivities at 300 and 90% H_2 recovery.

Component	Permeate Stream Split Fraction	Retentate Stream Split Fraction
NH3	0,00183	0,99817
H2	0,55	0,45
N2	0,00183	0,99817

Simulation Results

The following results were obtained for the membrane reactor simulation, specified at 30 bar retentate pressure of the membrane:

- **NH3 Conversion:**The percentage of converted NH_3 was estimated at 98%, see Table 5.3. As the thermodynamic equilibrium at 500°C is 93%, the simulated thermodynamic shift increased the conversion level by additional 5%.
- **H_2 Product Recovery:** 90% of the produced H_2 was recovered in the permeate stream.
- **Heat duty:** The required heat supply, represented by heat duty of Gibbs reactors, is estimated at 23.9 MW. Most of the heat duty is required to the first Gibbs reactor (22.7 MW), as 95% of converted ammonia was converted by this block. The second and third Gibbs reactors require 0.7 MW and 0.5MW, respectively.
- **Output Streams**
  - Product Stream (Permeate): The stream properties and compositions are listed in Table 5.3. As all of the component separators have the same split ratio, most of the product is separated in the first component separator. The N_2 concentration of the permeate product stream is 0,2%,

which is 10 times less then the allowable maximum for the Hydrogen Network. However, NH_3 concentration of the membrane permeate is at 176 ppm, which exceeds the allowed maximum. To reduce the NH_3 concentration, the product stream is treated in the Temperature Swing Adsoption unit (refer to Subsection 5.3).

- Waste Stream (Retentate): The obtained retentate stream contains 11 TPD of unrecovered H_2 and 12 TPD of unconverted NH_3. This stream is directed to the combustion unit to generate heat required for the process. It is assumed that the combustion is stable with high concentration of N_2 inert introduced to the combustion unit.

Table 5.3: Properties of the membrane-assisted reactor retentate stream and permeate stream from Aspen Plus simulation.

	Units	Retentate Stream to Combustion	Separator 1 Permeate	Separator 2 Permeate	Separator 3 Permeate	Total Permeated Product
Temperature	C	500	500	500	500	500
Pressure	bar	30	4	4	4	4
Mole Fractions						
NH3		2,9%	166 ppm	189 ppm	190 ppm	176 ppm
H2		22,6%	99,9%	99,7%	99,5%	99,8%
N2		73,8%	0,1%	0,2%	0,5%	0,2%
H2O		0,8%	0	0	0	0
Mass Flows	**TPD**	**537,5**	**58,8**	**28,9**	**14,7**	**102,5**
NH3	TPD	12,1	0,08	0,04	0,02	0,15
H2	**TPD**	**11,3**	**57,9**	**28,0**	**13,8**	**99,6**
N2	TPD	510,8	0,9	0,9	0,9	2,8

5.2.2. Combustion Unit Modelling

The second component of the ammonia cracker involves the modeling of a fuel combustion unit responsible for providing heat to both the NH_3 decomposition reaction and the preheating of the NH_3 feedstock. This combustion unit is represented as a stoichiometric reactor (FURNACE) with predefined combustion reactions. The residual heat from the flue gas is then recovered for preheating the NH_3 feedstream through a heat exchanger (EVAP-HEX), as illustrated in Figure 5.1.

$$2\,NH_3(g) + 1,5\,O_2(g) \rightarrow 3\,H_2O(g) + N_2(g), \quad \Delta H_{reac} = -316\,kJ/mol \tag{5.1}$$

$$2\,H_2(g) + O_2(g) \rightarrow 2\,H_2O(g), \quad \Delta H_{reac} = -286\,kJ/mol \tag{5.2}$$

Combustion Unit Assumptions

The stoichiometric reactor utilizes the membrane retentate stream and the additional fresh NH_3 feed as fuel. The amount of NH_3 feedstock required is determined from following requirements:

- The combustion unit produces enough heat to be supplied to the Gibbs reactors.
- The flue gas heat from the combustion unit leaves through the stack at 150 °C after heat recuperation in a heat exchanger. This is the temperature similar to the more rigorous fired heater simulation result from conventional technology case, see Figure 4.2.
- As for conventional technology case, it is assumed that the combustion will be stable with the determined fuel blend composition and the inert concentration in the oxidant.

Result

From combustion unit simulation it was determined that 60 TPD of ammonia feed is required to ensure sufficient heat supply to the system at 30 bar retentate pressure. The total combustion heat transferred

to the process is estimated at 31 MW, with 24 MW transferred to the Gibbs reactors in the membrane assisted reactor model and 7 MW transferred in the heat exchanger for ammonia preheating.

Table 5.4: The results from the combustion unit simulation

Combustion Unit Heat Duty	31 MW
Heat to Reactor	24 MW
Heat Recuperated in HEX	7 MW
Fresh NH3 Fuel Feedstock	60 TPD
% of Fresh NH3 supplied as Fuel	8,5%
NH_3/H_2 mol. ratio in fuel blend	43%/57%
O_2/N_2 mol. ratio in oxidant	15%/85%

5.3. Ammonia Traces Removal - TSA

To reach the required purity, the remaining traces of ammonia in produced hydrogen stream are removed by the adsorption operation. The adsorption operation is selected instead of water absorption due to low concentration of ammonia remaining in the product stream (175 ppm), requiring a small adsorption packing and low energy inputs.

However, as ammonia strongly adsorbs to the zeolite, it cannot be released from adsorbent by pressure swings [103]. Therefore, the bed can only be regenerated by supplied heat. This process is ensured by the temperature swing adsorption (TSA) operation. A suitable adsorption packing for ammonia removal is zeolite 13x [42]. The required heat can be supplied by recuperation of heat from the hot output streams of the membrane reactor, as depicted in Figure 5.4.

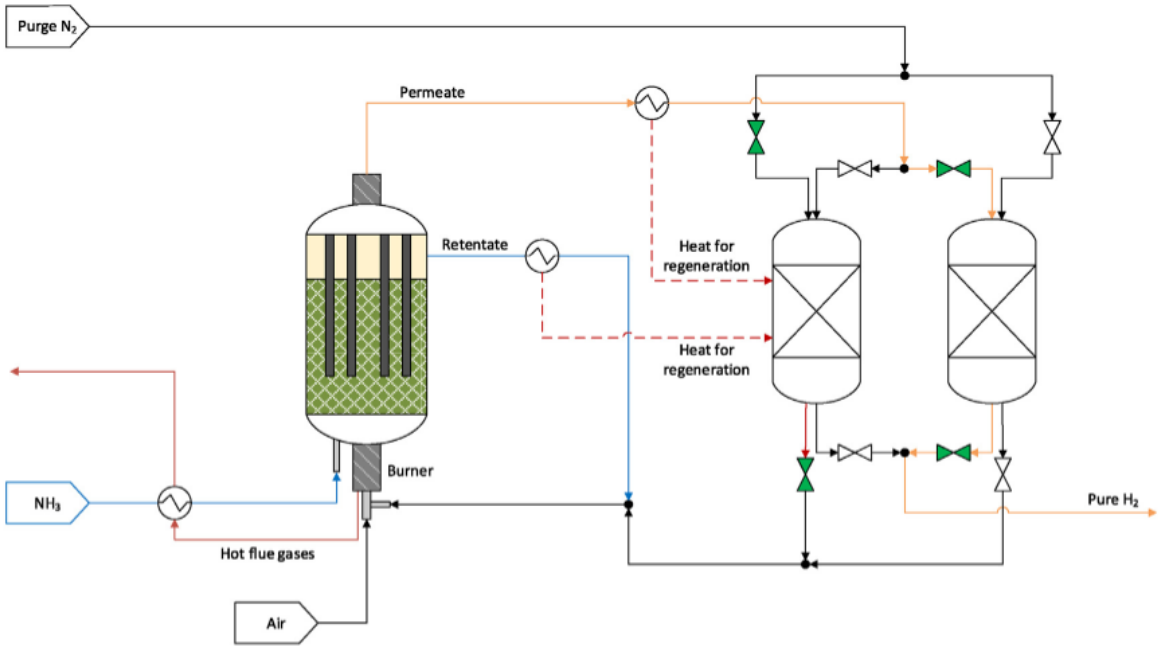

Figure 5.4: The heat for the regeneration of the zeolite 13x bed in the TSA unit can be provided by the hot output streams from the membrane reactor [37]. Picture by (Chechetto V., 2022)[37]

The TSA unit is simulated as a component separator, equivalently to the PSA unit in the conventional technology case. The component split fractions, listed in Table 5.5 are set to reduce the NH_3 concentration in the H_2 product from 175 ppm down to 10 ppm. It is assumed that no losses of H_2 will occur. The obtained product stream properties are given in Table 5.6.

Table 5.5: The defined split frations for the TSA unit product and waste streams.

Component	TSA-Product Stream Split Fractions	NH3 Traces Stream Split Fractions
NH3	0,057	0,943
H2	1	0
N2	1	0

Table 5.6: Properties of the purified H_2 product stream from TSA unit.

		TSA Product Stream
Temperature	C	500
Pressure	bar	4
Mole Fractions		
NH3		10 ppm
H2		99,8%
N2		0,2%
Mass Flows	**tonne/day**	**102,3**
H2	**tonne/day**	**100**

5.4. Hydrogen Compression

The compression system was modelled by equivalent approach to the Case I configuration. Please refer to Section 4.5 on the taken approach.

The required compression work depends on the obtained permeate pressure of the membrane permeate stream. The lower the pressure of the permeate stream, the more compression is required for the product to reach 50 bar. The required compression work for each case is listed in table below.

Table 5.7: The required work to compress the hydrogen product for analyzed cases of membrane retentate pressure.

Membrane retentate pressure	15 bar	30 bar	60 bar
Inlet stream pressure for compression system	2 bar	4 bar	8 bar
Required Compression Work (MW)	**9.1 MW**	**6.9 MW**	**5.1 MW**

6

Economic Model

The cost estimation of the simulated hydrogen production process cases is done according to the standard of the Advancement of Cost Estimation International (AACE International). For this research, each configuration was estimated up to the prelimentary estimate class, known as Class 4. At this level of estimation quality, the accuracy is expected to be within +/-30% range.

The fixed capital investment (FCI) and the required working capital for each project case are scaled from the purchased equipment cost according to the guidelines from Chemical Engineering Design: Principles, Practice and Economics of Plant and Process Design [104]. Also fixed yearly operating expenditure (OPEX), including labor costs, maintainance, overhead and taxes is estimated according to the guidelines from the same source [104].

6.1. Purchased Equipment Cost

- The cost of the process equipment, such as compressors, heat exchangers, columns, and pumps has been estimated by Aspen Economic Analyser V12 from the Aspen Plus V12 process simulation results.
- The cost estimation of ammonia cracker is given in **Subsection 6.1.1**.
- The cost estimation of membrane module is given in **Subsection 6.1.2**.

- The 2023 exchange rate of Euro to Dollar is 0.95.
- The basis of cost data for purchased equipment costs from Aspen Economic Analyzer is U.S. Gulf Coast, 2019. The cost escalation is taken into account by scaling the cost up to 2023 level by employing the Chemical Engineering Plant Cost Index (CEPCI). The CEPCI for 2023 is 803.

$$Cost_{2023} = Cost_{2019} \frac{CEPCI_{2023}}{CEPCI_{2019}} \tag{6.1}$$

- The equipment cost list for Case I (established technology) is put in Appendix C.1
- For Case II (membrane reactor technology), the equipment costs are estimated for different membrane module retentate pressures:15 bar, 30 bar and 60 bar. The equipment cost lists for taken configurations are put in Appendix C.2.

6.1.1. Ammonia Cracker

The cost of the ammonia cracker equipment, without catalyst, is approximated by the guideline for estimating the cost of the reformer furnace from Analysis,Synthesis and Design of Chemical Processes by Turton R. [105]. The equation for bare module (C_{BM}) cost of the ammonia cracker is given as:

$$C_{BM} = C_p^0 F_{BM} F_P \tag{6.2}$$

with C_p^0 as purchased cost of furnace ($CEPCI_{2001}$, at ambient opeerating pressure with carbon steel construction), F_{BM} as base metal factor and F_P as pressure factor. C_p^0 depends on the duty of the

ammonia cracker. F_P is calculated through formula[105]:

$$log_{10}F_P = 0.1405 - 0.2698log_{10}P + 0.1293(log_{10}P)^2 \tag{6.3}$$

The obtained factors and final cost of the ammonia cracker for Case I, considering CEPCI change and exchange rate, are given in Table 6.1.

Table 6.1: Ammonia cracker cost estimation result for Case I.

Factor	Value	Unit	Condition
C_p^0	3009000	$ (2001)	Q = 35.4 MW
F_P	1	-	P = 10 bar
F_{BM}	2.8	-	Stainless Steel

CEPCI 2001	397
CEPCI 2023	803
Euro-to-Dollar Exchange Rate	0.95

Final Cost Ammonia Cracker:	**€ 17.9 mln (2023)**

For Case II, the ammonia cracker costs are determined from the heat duty of the combustion unit and the membrane retentate pressure. Three retentate pressures are reviewed (15 bar, 30 bar and 60 bar). The obtained ammonia cracker equipment costs are listed below:

Table 6.2: Ammonia cracker cost estimation results for Case II.

Case II	Pressure of Membrane Module Retentate		
	15 bar	30 bar	60 bar
Final Ammonia Cracker Cost :	€ 15,3 mln	€ 15,5 mln	€ 18,6 mln

The economic model includes the cost of the selected catalyst packing(Ni/Al_2O_3/crushed monolith) at €400 per liter. This elevated value is presumed as the production cost is not reported, coupled with unknown durability and required frequency of catalyst packing refilling over a 15-year operational period.

6.1.2. Membrane Module Cost

The cost of the membrane module, integrated in the reactor, is determined by the thickness of membrane active layer and required area. Another factor taken into account is the durability extent of the membrane and its support layer. For this project, the durability of the membrane is taken as 5 years. The durability extent and corresponding module costs are taken from literature[43] and are listed in Table 6.3. The Table shows that recycling of the membrane components can achieve up to 52% savings on membrane module cost.

Table 6.3: The cost of the non-recyclable and recyclable membrane module (1μm Pd-layer) per square meter, considering the 15 years of plant life

Ceramic Membrane Module Cost at Different Recyclability Extent		
Plant Lifetime: 15 years (Membrane Module durability: 5 years)		
Membrane Module Cost Parameters	**Non-recyclable Membrane**	**Support + 90% Selective layer Recycling**
Ceramic Support [€/m2]	3550	1500
Selective Layer (1µm Pd) [€/m2]	2925	293
Production Cost [€/m2]	1625	2100
Total Cost [€/m2]	**8100**	**3893**

6.2. Capital Investment

- The fixed capital Investment (FCI) is determined by setting the installation factor from the total cost of equipment (TCE) to the direct and indirect costs of the project according to empirical chemical engineering guidelines [104]. The FCI consists out of inside battery limits (ISBL) and outside Battery Limits (ISBL).
- The ISBL installation factors are taken as the percentage of the determined equipment cost (TCE).
- The OSBL factors are taken as percentage of Determined ISBL.
- The required working capital is taken as 15% of the FCI.
- FCI and the working capital are forming the total capital investment (TCI)

Table 6.4: The installation factors used to derive the fixed capital investment (FCI) for the project.

DIRECT COST:	INSTALLATION FACTOR of TEC
Equipment Cost (TEC)	100%
Predominant Material: Stainless Steel	15%
Equipment Erection	30%
Piping	103%
Instrumentation and control	30%
Electrical	20%
Civil	30%
Structures &Buildings	20%
Lagging/Insulation/Paint	10%
TOTAL DIRECT COSTS (ISBL):	**358% of TEC**
INDIRECT COST:	**INSTALLATION FACTOR OF ISBL**
Offsites	40%
Design and Engineering	69%
Contingency	43%
TOTAL INDIRECT COSTS(OSBL):	**152% OF ISBL**
FIXED CAPITAL INVESTMENT (FCI):	**ISBL + OSBL**
WORKING CAPITAL:	**15% of FCI**
TOTAL CAPITAL INVESTMENT:	**FCI + WORKING CAPITAL**

6.3. Operating Costs

- The yearly operating expenditure consist out of fixed operating costs and variable operating costs.
- The fixed operating costs (Fix. OPEX) include labor, maintainance, plant overhead,tax,insurance and debit financing interest. The fixed operating costs are determined through Chemical Engineering Guidelines [104], see Table 6.5.

Table 6.5: Fixed operating costs contribution factors

FIXED OPEX COSTS		
Labor Costs:	Operating Labor +Supervision Cost +Direct Overhead	
Operating Labor		€ 900.000,00
Position:	**Number of daily shifts**	**Salary (€/year)**
Plant Operators (3 shifts, 5 operators per shift)	15	€ 60.000,00
Supervision Costs	25% of Oper. Lab	
Direct Overhead	45% of Op.Lab and Superv	
Maintainance	3% of ISBL	
Plant Overhead	65% of Labor and Maint	
Tax and Insurance	2% of FCI	
Interest of Debit Financing	6% of Working Capital	

- The variable operating costs (Var. OPEX) include the required process utilities. The main utilities used are NH_3 feed and electricity. The cost of ammonia in 2030 and 2040 is taken from the prognosis published by IRENA[12], considering the most optimistic estimates. The costs of European electricity for the same time frames are retrieved from published outlook by Energy Brainstorm [79]. Both of the costs are listed in Table 6.6.

Table 6.6: Major utility costs taken for economic analysis

Utility	Unit	Cost 2030 (€/unit)	Cost 2040 (€/unit)
Green Ammonia	**ton**	€ 452,32	€ 360,00
Electricity	**MWh**	€ 69,00	€ 73,00

6.4. Levelised Cost of Hydrogen & Market Price of Hydrogen

To calculate the LCOH and NPV, the following conditions are set for both project cases:

- Plant Lifetime (n): 15 years
- Plant Availability: 95%
- Interest Rate (i): 8%

6.4.1. LCOH

The levelized cost of hydrogen is calculated from the determined project costs and conditions:

$$LCOH = \frac{(TCI \times CCF) + OPEX_{fix} + (OPEX_{var} \times 95\%)}{Hourly\ H_2\ Production\ Capacity \times 8760 \times 95\%} \tag{6.4}$$

with $OPEX_{fix}$ as fixed operating costs, $OPEX_{var}$ as variable operating costs, CCF as Capital Charge Factor.

The Capital Charge Factor is calculated from the interest rate i and plant lifetime n:

$$CCF = \frac{i \times (1+i)^n}{(1+i)^n - 1} \tag{6.5}$$

6.4.2. Market Price

The market price required for the profitability of the process is determined by its net present value (NPV). NPV is the sum of the net cash flow (costs minus revenues) of the project over its lifetime. The minimum market price is set to ensure that NPV reaches zero in 10 years after project start up. The start-up schedule of the plant is given in Table 6.7.

Table 6.7: The Start-up Schedule for the Estimation of the Market Price of Produced Hydrogen

Year	Costs	Revenues
1st year	30% of FCI	0
2nd year	50% of FCI	0
3rd year	20% of FCI + Working Capital + Fix. OPEX + 30% of Var. OPEX	30% of Design Basis Revenue
4th year	Fix. OPEX + 70% of Var. OPEX	70% of Design Basis Revenue
5th year+	Fix. OPEX + Var. OPEX	100% of Design Basis Revenue
Target NPV in 10 years	0	

7

Results and Discussion

The Levelized Cost of Hydrogen for NH_3 decomposition is is determined and compared between the conventional technology process (Case I) using a multi-tubular packed bed reactor and the emerging technology process (Case II) employing a membrane-assisted reactor. The results are discussed in the following sections:

- **Section 7.1 - Technical comparison:** The constructed process configurations are compared on the obtained product purity, requirement of NH_3 feedstock and energy requirements.
- **Section 7.2 - LCOH Breakdown:**: The determined LCOH for both cases is broken down into its main cost contributors.
- **Section 7.3 - Purchased Equipment Costs:** The purchased equipment cost is broken down and compared for both cases.
- **Section 7.4 - Emerging Technology LCOH:** For Case II, the major membrane reactor parameters are analysed on their contribution to the Levelized Cost of Hydrogen (LCOH).
- **Section 7.5 - Sensitivity Analysis:** The sensitivity of LCOH to the major process parameters is determined and discussed.
- **Section 7.6 - Market Price for Project Profitability:** The required market price of produced hydrogen is identified for project profitability.
- **Section 7.7 - Comparison with alternative H_2 production routes:** The determined LCOH is compared with the alternative sustainable H_2 production routes in the Netherlands by 2030.
- **Section 7.8 - Model Limitations and Recommendations:** The limitations of the study are outlined together with provided recommendations for future research.

7.1. Technical Comparison

The conventional technology (multi-tubular packed bed reactor) case is compared to the determined optimal configuration in the emerging technology (membrane-assisted reactor) case (refer to Section 7.4) on required feedstock of ammonia:

- Both cases generate hydrogen with sufficient purity, as indicated in Table 7.1. In the conventional case, the purity meets the maximum allowable impurity concentration. Conversely, the emerging membrane reactor technology surpasses purity requirements, achieving a final product purity of 99.8% due to the high selectivity of the palladium membrane module for hydrogen over nitrogen.
- In the emerging technology scenario, a higher quantity of hydrogen is generated from the same amount of NH_3, reaching 79% of the stoichiometric maximum (refer to Table 7.1). In comparison, the conventional case achieves 76% of the stoichiometric maximum , due to higher NH_3 fuel requirement for heat generation.
- In Case I 10% of feed NH_3 is used for combustion, while for Case I only 8.6% is used.

Table 7.1: The obtained product quality for both cases compared to Hydrogen Network requirements. The NH3 utilization efficiency relative to Stoichiometry.

Component mole fraction:	Case I: Conventional Technology	Case II: Emerging Technology	Hydrogen Network Requirements
NH3	8 ppm	9 ppm	<10 ppm
H2	98%	99,80%	>98%
N2	2%	0,20%	<2%
H2O	45ppm	0	<45 ppm
Product H2-to-Feed NH3	**Case I: Conventional Technology**	**Case II: Emerging Technology**	**Theoretic Maximum (Stoichiometry)**
Mass Flow NH3 feed (TPD):	708 (16% Fuel/84% Reactant)	700 (8.6% Fuel/ 91.4% Reactant)	567 (100% Reactant)
Product H2 (TPD):	95	100	100
kg-H2/kg-NH3	0,13	0,14	0,18
kg-H2/kg-NH3 (relative to Stoichiometry)	**76%**	**79%**	**100%**

- The total heat duty of the combustion unit,supplying heat for NH3 decomposition and NH3 feed preheating, is estimated at 35.4 MW for Case I and 31 MW for Case II.
  - In Case I, the ammonia decomposition reactor's heat duty is calculated at 20.5 MW due to lower conversion in the conventional packed bed reactor. Conversely, the membrane-assisted reactor in Case II shows a higher estimated heat duty of 24 MW, attributed to nearly complete NH3 conversion.
  - In Case I, 15 MW of heat is recuperated in the convection section for ammonia preheating, while Case II recuperates 7 MW. The higher value in Case I results from the combustion flue gas being significantly hotter after transferring heat to the reactor compared to Case II, with temperatures at 750 and 450 degrees, respectively.
- Both configurations require electricity supply to the compressors to pressurize pure product. In Case I, additional compression is expected to ensure sufficient pressure in the H_2 purification system. Compared the compression work, the emerging technology is estimated to require 15% more electricity supply than conventional case, due to process stream entering the compression system at low pressure.
- For Case I, higher cooling duty is required compared to Case II as more excess heat is present in reactor product stream due to higher operating temperature in the reactor.
- In the simulated processes, heating utilities were necessary for preheating the NH_3 feedstock. However, the required heat for the NH_3 streams could be provided by exchanging heat with hot streams utilizing external cooling. This approach eliminates the need for steam in preheating and reduces the demand for cooling water in the overall cooling system.

Table 7.2: Energy Requirements for defined cases

Energy Requirements for 100 TPD-H2	Case I: Conventional Technology	Case II: Emerging Technology
Reactor Heat Duty (MW)	20.5	24
Compression Work(MW)	6	7
Total Cooling Duty (MW)	-12,7	-7,7
Total Heating Duty (MW)	1,16	2,18

7.2. LCOH: Breakdown in Expenditures

The levelized cost of hydrogen (LCOH) is determined based on estimated capital costs for the designed plant configurations and optimistic predictions for green NH_3 and electricity prices, as provided in Table 6.6.

For Case I, the LCOH is compared using predicted utility prices for 2030 and 2040. Additionally, the LCOH in 2040 for Case I is contrasted with the LCOH of Case II, presumed to have reached technological maturity by then. For Case II, the optimal scenario is considered, with a retentate pressure of 30 bar and maximum achievable recyclability of the membrane material.

In both cases, the LCOH is analyzed in terms of three main expenditure components: capital expenditures (CAPEX), fixed operating expenditures (Fixed OPEX), and variable operating expenditures (Variable OPEX).

- In 2030, the required utilities contribute to 67% of the total hydrogen cost, with ammonia constituting 65% of the LCOH and electricity contributing 2%. The contribution to the cost by the cooling utilities is below 0.5% and is considered negligible. For the case in 2040, the contribution of ammonia reduces to 59% due to the projected price reduction.
- When comparing the LCOH in 2040 for both configured cases, the LCOH distribution over major expenditure groups is nearly equivalent. The total LCOH for the emerging technology is only €0,38/kg less then for a conventional technology, which can be considered negligible for the taken cost estimation accuracy. Therefore, under taken optimistic assumptions regarding the robustness and scalability of the membrane-assisted reactor, the obtained lowest LCOH for Case II would only approach the conventional case value.

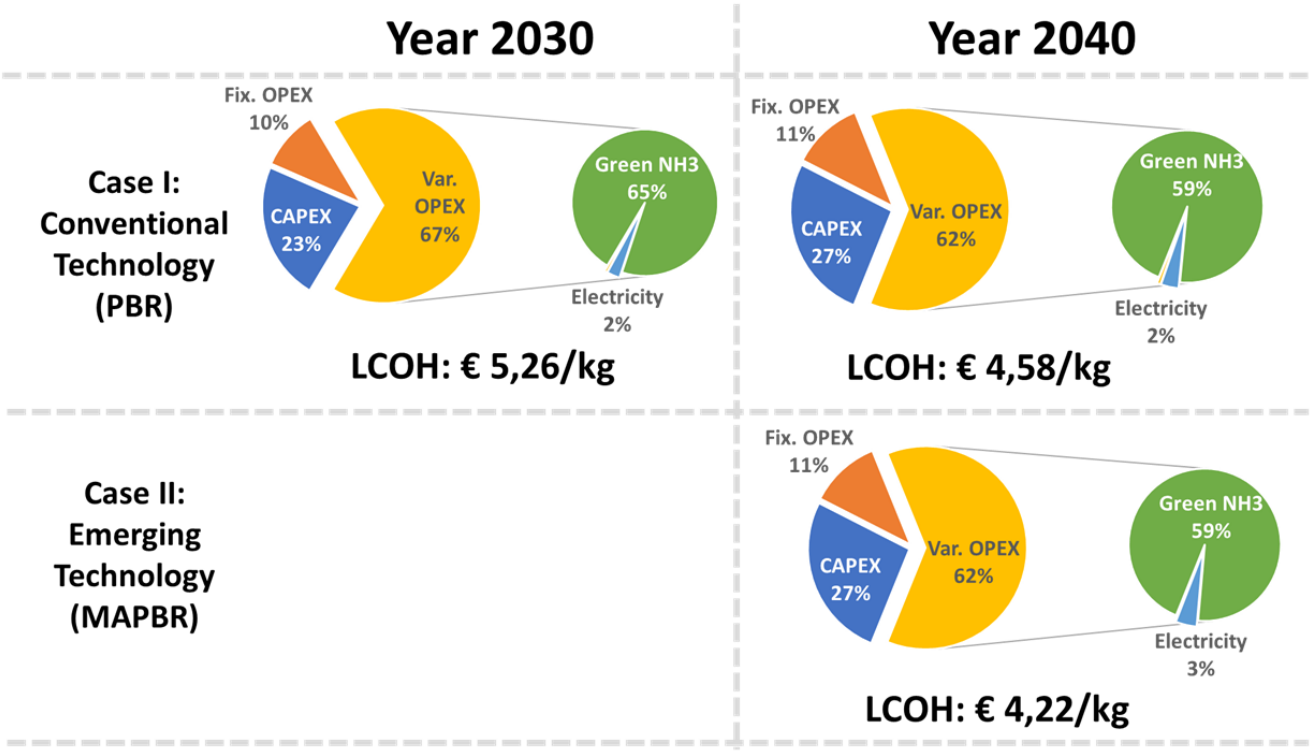

Figure 7.1: LCOH by Case 1 (PBR) and Case II (MAPBR) is broken down to the expenditure types in 2030 and 2040. It is visible that green ammonia feedstock is the main contributor to the LCOH.

7.3. Purchased Equipment Breakdown

In Figure 7.2, the total cost of purchased equipment is broken down in subgroups for each of the reviewed scenarios. The equipment cost is scaled to the production requirement of 100 TPD of hydrogen.

- Independent of selected technology, the main investment in equipment goes to the purchasing of the fired heater-reformer for ammonia cracking, which is determined by required heat duty and the operating pressure.
- The second main investment goes to the compression sub-process. It is visible in three reviewed configurations for emerging technology, that compression unit cost is strongly dependent on the operating pressures in the upstream due to additional compression work required.
- The hydrogen purification by PSA unit (together with pre-compression) requires less investment than the membrane module integration in case of no recycling option for the membrane material. In case if most of the membrane is recycled, the investment in membrane integration reduces by 50% and becomes lower than the cost of the PSA configuration.
- It is apparent that initially, raising the retentate pressure from 15 to 30 bar results in a decrease in the total equipment cost, attributed to a significant reduction in the necessary compression equipment. However, as the pressure is further increased to 60 bar, the savings in compression costs are outweighed by a more substantial rise in the ammonia cracker cost.

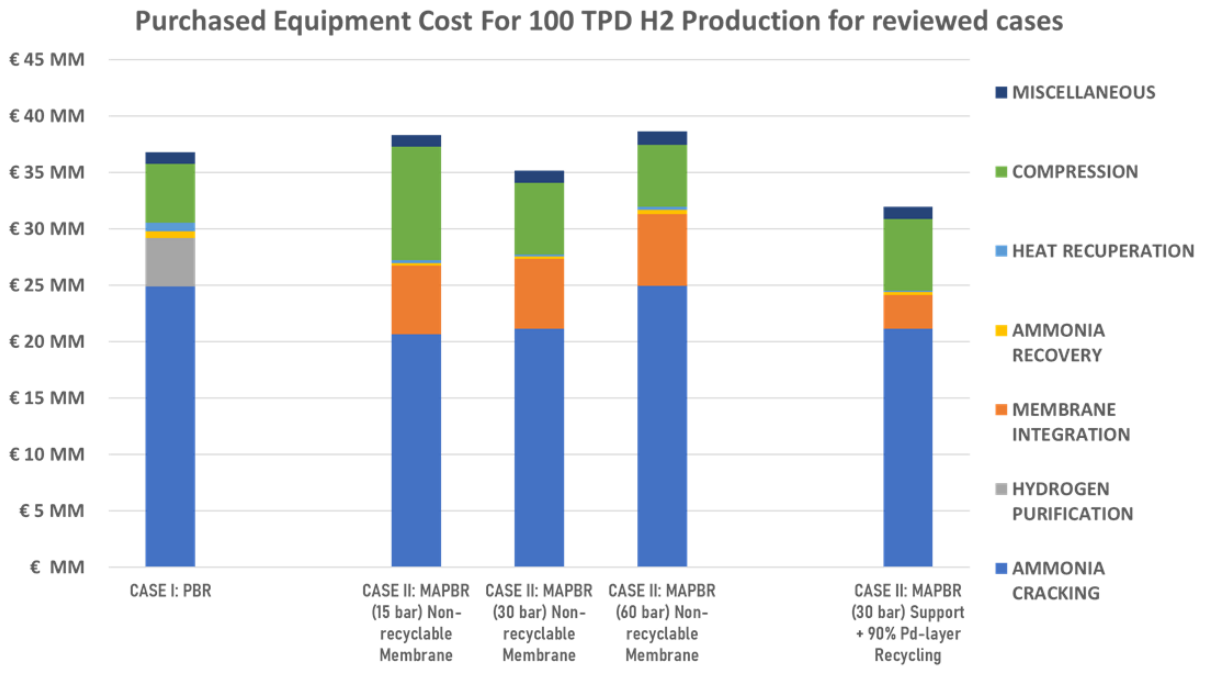

Figure 7.2: Purchased cost of equipment for modelled cases. 1) Case I: PBR; 2) Case II: Membrane-assisted PBR at 15 bar retentate pressure; 3) Case II: Membrane-assisted PBR at 30 bar retentate pressure; 4) Case II: Membrane-assisted PBR at 60 bar retentate pressure; 5) Case II: Membrane-assisted PBR at 30 bar retentate pressure and membrane material recycling

7.4. LCOH by Emerging Technology Configuration

The emerging technology case for ammonia decomposition utilizes the integration of the membrane separation module in the packed bed reactor. The two main performance defining parameters, membrane retentate pressure and membrane recycling extent, are analyzed on their impact on the obtained LCOH.

7.4.1. Membrane Recycling

The membrane module cost can decrease by 50% in case if membrane is recyclable (see Table 7.3). It is visible from the obtained LCOH, that the contribution of the membrane module cost on the total process is relatively low as the cost of the LCOH reduces only by 3%. Therefore, the membrane module cost does not play a defining role for LCOH.

Table 7.3: The equipments cost of the non-recyclable and recyclable membrane module and corresponding LCOH (for membrane retentate pressure at 30 bar)

	Non-recyclable Membrane	Support + 90% Selective layer Recycling
Total Cost of Membrane Module:	**€ 6.2 mln**	**€ 3.0 mln**
LCOH 2040 (30bar retentate)	**€ 4,36 /kg**	**€ 4,22/kg**

7.4.2. Retentate Pressure of the Membrane Module

The obtained results for different retentate pressures of the membrane module in 2040 are visualized in Figure 7.3. The recyclable membrane is taken for analysis. When increasing the pressure, the change in the LCOH is affected by changes in the following cost components:

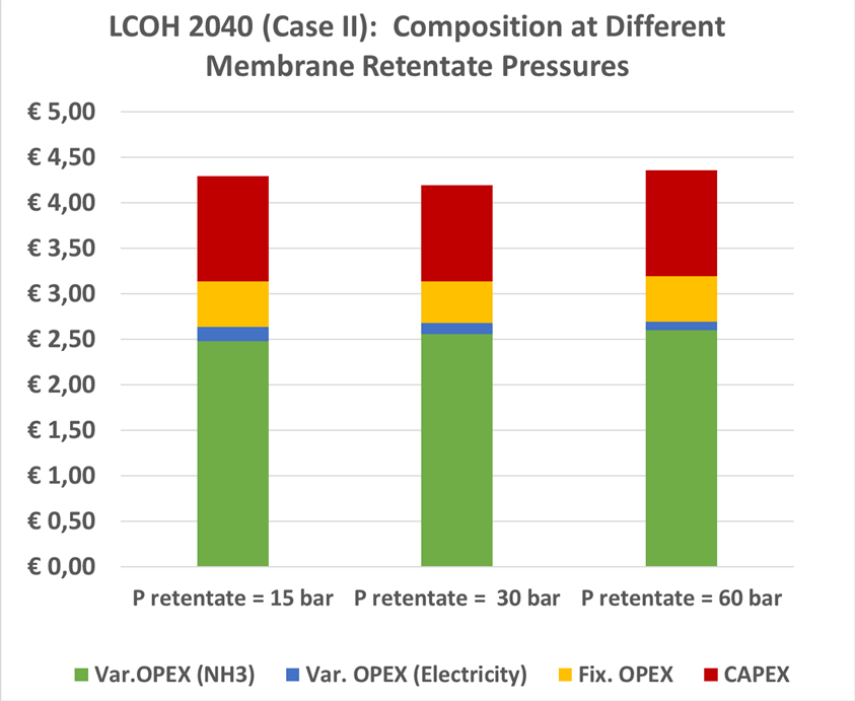

Figure 7.3: Obtained LCOH for different retentate pressure configurations and the corresponding contributions of the project expenditure types

- **CAPEX** is mainly affected by the change in ammonia cracker and compression system costs:
  - Ammonia Cracker: equipment cost increases with elevated pressure, as thicker walls are required for high pressure operation.
  - Compressor system: equipment cost decreases due to higher pressure achieved upstream.
- **Fixed OPEX** scales linearly with the obtained CAPEX in the created model.
- **Variable OPEX** is mainly affected by the change in required utilities quantity:
  - Electricity: the electricity supply requirement for product compression reduces with higher pressures upstream of the compression section.

- Ammonia Feedstock: The thermodynamic ammonia conversion reduces for the same membrane module at elevated pressures, leading to more ammonia supply required to produce the same amount of hydrogen.
- Other utilities, required for heaters and coolers in the process have shown to be negligible to the final LCOH.

The graphical representation in Figure 7.3 clearly indicates that the optimal membrane retentate pressure falls within the 30 bar operating range. This is evident from the observation of the lowest LCOH recorded at €4.29/kg in the year 2040.

7.5. Sensitivity Analysis on Major Cost Parameters

The obtained LCOH has been analysed on its sensitivity to the costs of the major process parameters. For established technology case in 2030 the impact of changing CAPEX costs, electricity costs and green ammonia costs on the LCOH is analysed (see Figure 7.4).

- As was shown previously in the LCOH expenditures breakdown, the LCOH shows the strongest dependence to the cost of green ammonia feedstock. In Case I, when reducing the base case ammonia cost (€452/ton in 2030 from optimistic prediction by IRENA[12]) by 50%, the LCOH drops from €5,26/kg down to €3.56/kg, leading to 32% reduction.
- In case of reducing the base case electricity cost (€69/MWh) by 50%, the LCOH drops only by 1%. This result correlates well with the results of LCOH breakdown into major expenditure groups in Figure 7.1.
- In case of reducing the CAPEX by 50% , the LCOH drops by around 16% to the value of €4,43/kg.

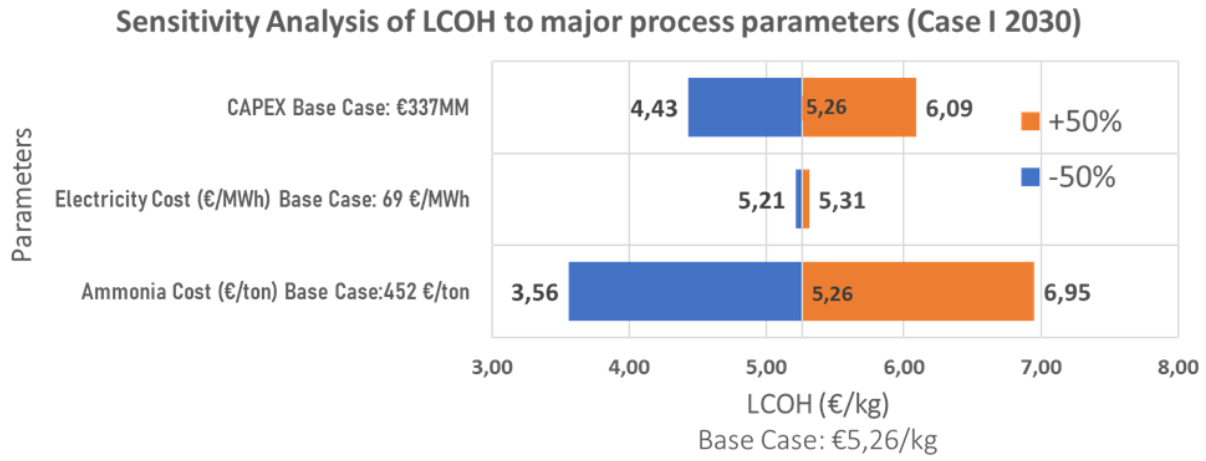

Figure 7.4: LCOH (Case I, 2030) sensitivity to changes in CAPEX, electricity costs and ammonia costs

The sensitivity analysis was also performed for the parameters, only applicable to the membrane-assisted ammonia decomposition reactor from Case II (emerging technology case). Figure 7.5 depicts the LCOH sensitivity to membrane cost and the retentate pressure. The results indicate that the improvements in the membrane-assisted parameters do not reduce the production cost significantly.

- As the membrane cost drops by 50% towards the near-complete recycling of membrane from the base case value of 8100€/m^2(non-recyclable membrane module), the LCOH reduces by 3%.
- In case if the retentate pressure (base case of 30 bar) is reduced by a half, the LCOH incrases by 4.5%. The LCOH also increases by 2% in case if the pressure is increased by 100% to 60 bar. This indicates that the optimum retentate pressure for the membrane-reactor operation has to be in the region of 30 bar due to the optimum trade-off of the capital and operating expenditures at this configuration, as was also determined in Section 7.4.2.

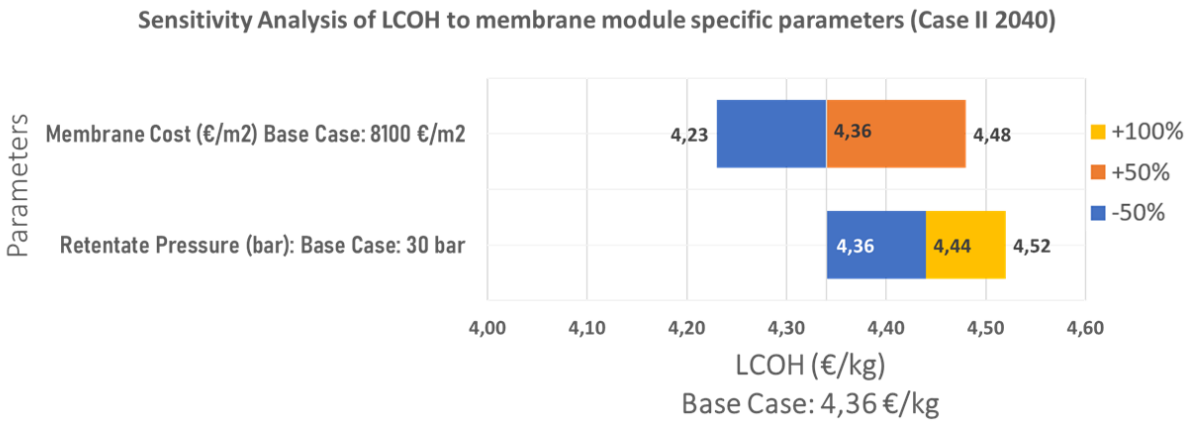

Figure 7.5: LCOH (Case II, 2040) sensitivity to changes in membrane production cost and different membrane retentate pressures

The total sensitivity analysis highlights that the cost of hydrogen production through ammonia cracking is primarily influenced by the price of ammonia, exerting twice the impact on the final LCOH cost in comparison to capital expenditures. The cost of electricity barely has any impact on LCOH, changing it by 1% with 50% price reduction. The analysis suggests that, under the given assumptions of robust membrane durability, the change in membrane reactor parameters do not lead to a significant reduction in production costs.

7.6. Market Price for Project Profitability

The market price of produced hydrogen is determined by approaching the net present value of the project to zero in 10 years from the project start-up,following the formulated schedule in table 6.7. The determined product prices for the Case I configuration and the determined best scenario for Case II configuration are listed in Table 7.4.

Table 7.4: The required market price of produced hydrogen for NPV = 0 in 10 years after the project start-up for both formulated cases.

	Year	LCOH (€/kg)	Market Price (€/kg) (for NPV = 0 in 10 years from project start-up)
Case I (Conventional Technology)	2030	5,26	6,17
	2040	4,58	5,48
Case II (Emerging Technology)	2040	4,22	5,01

7.7. LCOH Comparison with Alternative H_2 Production Routes

For year 2030, the obtained LCOH from conventional technology configuration (Case I) is compared with the alternative H_2 production routes in the Netherlands. In Figure 7.6 the determined LCOH is compared with the predicted LCOH figures for alternative sustainable hydrogen production routes.

As LCOH strongly depends on ammonia cost, the predicted LCOH region was plotted by taking the predicted green ammonia costs by IRENA[12]. Based on IRENA predictions, the cost of NH_3 would lay within €450-900/ton. The corresponding LCOH obtained based on this uncertainty would lay within €5,30- 8,60/kg.

- The obtained result lays within the same region as the local green hydrogen production in Central Europe, from the latest (2023) prediction by Boston Consulting Group[83], which ranges between €5,00- 8,00/kg. Therefore, H_2 production from imported NH_3 can be competitive with the domestic green hydrogen production.
- The cost of local blue hydrogen will lay within €2- 3/kg, according to TNO (independent research organization in the Netherlands)[80]. However, as blue hydrogen is strongly dependent on natural gas prices, the cost of blue hydrogen can reach €5,00/kg in case of tripling price of natural gas. In that case, hydrogen production by NH_3 import could become a competitive alternative in case if NH_3 price drops down to most optimistic cost predicitions.
- When compared with alternative H_2 import routes, the LCOH falls withing the same price region with $LH_2$and LOHC import routes. Also, the determined LCOH from this research shows a more optimistic outlook on LCOH by green NH_3 import, then was previously reported by TNO to lay withing €6,90-9,30. Based on the obtained figures, in case of most optimistic predictions in market expansion and production cost reduction for green NH_3, the import of H_2 in form of NH_3 as carrier has potential to become the cheapest import solution.

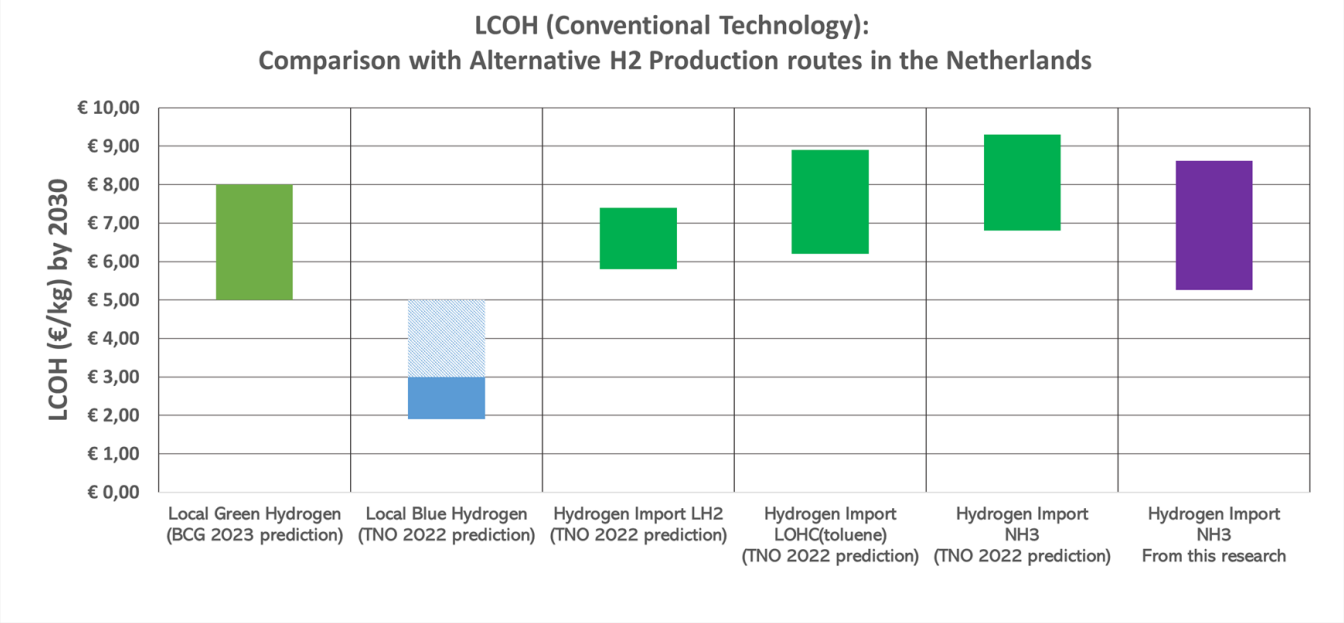

Figure 7.6: Determined LCOH prediction for hydrogen production from NH_3 decomposition, compared with the alternative sustainability-aimed H_2 production routes in the Netherlands, from the predictions by TNO[80] and Boston Consulting Group[83]

7.8. Model Limitations and Recommendations

The research focuses on assessing the technical and economic feasibility of the imported green ammonia decomposition process for industrial-grade hydrogen production, specifically for the Dutch hydrogen pipeline. The predicted costs of arriving green ammonia feedstock are taken from published predictions, while the production and transportation aspects of green ammonia are excluded from the research scope. However, it is acknowledged that the Levelized Cost of Hydrogen (LCOH) is contingent on market developments and technological advancements, particularly in green hydrogen electrolysis, a key component of green ammonia production. It is recommended for future research to encompass the entire value chain of hydrogen importation using green NH_3 as a hydrogen carrier.

The continuous green NH_3 supply to the process is assumed, while ammonia production from green hydrogen relies on intermittent renewable electricity from wind and solar sources. The variability in the renewable energy supply may impact the continuity of green ammonia supply, consequently affecting hydrogen production. Therefore, the intermittency of green NH_3 supply should be assessed in detail and incorporated in the LCOH.

In the defined process configurations, purification waste streams and fresh NH_3 are utilized as fuel to provide the necessary heat for the ammonia cracker. In the created model, the stable burning is assumed for the determined fuel blend. It was assumed that the NH_3-to-H_2 ratios in the blend and the concentration of inert nitrogen added with the purification waste stream can facilitate stable burning. Future research is required to explore various NH_3/H_2/N_2 concentrations in the fuel blend to assess combustion performance and optimize the fuel burner design. Additionally, research on NO_x production and capture, dependent on fuel composition, is crucial for minimizing environmental impacts.

While a non-noble nickel-based catalyst was employed for process modeling, a noticeable gap in research became apparent concerning the performance of non-noble catalysts in ammonia decomposition. While operating the NH_3 decomposition reactor at elevated pressures is attractive to minimize the downstream compression, the non-noble catalysts have currently only been analyzed on lab scale at atmospheric pressures. Therefore, the research is required on non-noble catalysts and their performance at different operating conditions.

In addressing emerging technology, the specifications for membrane module size and costs were assumed based on the published performance of lab-scale membrane modules. The assumed durability of the membranes was set at 5 years, yet no durability tests have been conducted beyond 1000 hours. Additionally, it was presupposed that the membranes can endure specified pressure ratios over the long term. Therefore, the evaluation tests on long-term robustness of the Pd-Ag membrane are required.

Furthermore, the calculation of required membrane area relies on lab-scale experimental data under idealized conditions that ensured optimal membrane performance. However, the translation of these findings to large-scale applications remains uncertain, particularly regarding heat and mass transfer dynamics.

Moreover, the imposed temperature limitation on the membrane, not exceeding 500°C, highlights a potential constraint for reactor heating. Future research should concentrate on achieving homogeneous heating of the membrane to ensure reactor temperatures stay within the prescribed limit.

8

Conclusion

This report examines the technical and economic feasibility of establishing a hydrogen production plant in the Netherlands by 2030, utilizing the decomposition of imported green ammonia with a capacity of 100 Tons Per Day (TPD). The research covers the entire hydrogen production chain, from ammonia arrival to the final delivery of industrial-grade hydrogen. Two distinct cases were examined: the established technology case was formulated for 2030, utilizing a multi-tubular packed bed reactor, and the emerging technology case anticipated to mature by 2040, employing a membrane-assisted membrane reactor technology.

Detailed design considerations were applied to configure the ammonia cracker for large-scale production demands. In both cases, the ammonia cracker is heated through the combustion of carbon-free fuel, consisting of waste streams from hydrogen purification and additional fresh NH_3 feedstock. In the conventional case, a thorough ammonia cracker design was executed through combining two modelling tools, with the detailed sizing and optimization of the internals and determining the fresh ammonia fuel requirements. On the other hand, for the emerging membrane reactor technology case, a simplified process simulation was performed by considering the performance data reported in the literature. Following the assessment of the performance of both ammonia cracker configurations, the corresponding downstream product purification and compression systems were incorporated into the overall production process.

A key finding was the pivotal role of the market cost of green ammonia as the defining parameter for the Levelized Cost of Hydrogen (LCOH). In the case of utilizing existing technologies, optimistic forecasts of green ammonia cost at €450/kg by 2030 result in a Levelized Cost of Hydrogen (LCOH) amounting to €5.26/kg, with green ammonia cost constituting 65% of the total LCOH cost. The determined LCOH figure is similar to optimistic projections for domestic green hydrogen production via electrolysis. Furthermore, it was established that the import of green hydrogen in the form of green ammonia might emerge as the most cost-effective import option by 2030 if the optimistic cost projections for green ammonia materialize.

Looking ahead to 2040, if green ammonia cost continues to decrease down to €360/kg, the green ammonia feedstock would constitute 59% of the LCOH for both existing and emerging technology cases, as both configurations require nearly equivalent amount of ammonia to produce the same quantity of hydrogen. The LCOH produced with existing technologies would then reduce to €4.56/kg. It was also determined that emerging membrane assisted reactor technology could further lower the LCOH to €4.22/kg by 2040, provided membrane technology reaches a level of maturity and durability suitable for large-scale applications. However, within the uncertainty range of the economic model, the projected savings are considered negligible. Additionally, the assumed robustness and scalability of the membrane reactor currently exceed its present stage of development, as the technology has not progressed beyond the experimental scale.

In summary, this study provides a valuable insight on the technical and economic perspectives of the ammonia cracking in the hydrogen import value chain. It is predicted that the large-scale ammonia-to-hydrogen plant is technologically feasible with already established technologies, showing its potential to become a competitive alternative for the local hydrogen production in the Netherlands by 2030. It emerges to be a viable route for importing green hydrogen to accelerate the sustainability transition of the Dutch industrial sector, provided that future technological advancements in electrolyzer technologies and green ammonia market expansion reduce the high cost of green ammonia by the time the Dutch hydrogen pipeline becomes fully operational.

References

[1] Carl Friedrich Schleussner et al. “Science and policy characteristics of the Paris Agreement temperature goal”. In: *Nature Climate Change* 6.9 (2016), pp. 827–835. DOI: 10.1038/nclimate3096.

[2] “The Future of Hydrogen”. In: *The Future of Hydrogen* June (2019). DOI: 10.1787/1e0514c4-en.

[3] The Port of Rotterdam. *Study shows shipping green hydrogen from Iceland to Rotterdam to be realistic before 2030*. https://www.portofrotterdam.com/en/news-and-press-releases/study-shows-shipping-green-hydrogen-from-iceland-to-rotterdam-to-be. 15 June 2021.

[4] Proton Ventures. *Morocco, Netherlands to partner on boost to green hydrogen production*. https://protonventures.com/news/morocco-netherlands-to-partner-on-boost-to-green-hydrogen-production/. 10 June 2022.

[5] Port of Rotterdam. *The Netherlands and Germany enhance their hydrogen import partnership with Australia*. https://www.portofrotterdam.com/en/news-and-press-releases/the-netherlands-and-germany-enhance-their-hydrogen-import-partnership-with. 15 February 2023.

[6] Joint Statement. *Joint statement of Chile and The Netherlands on collaboration in the field of green hydrogen import and export*. https://www.government.nl/documents/diplomatic-statements/2021/07/01/joint-statement-of-chile-and-the-netherlands-on-collaboration-in-the-field-of-green-hydrogen-import-and-export. Diplomatic Statement: 01-07-2021.

[7] Mohammad Reza Tahan. “Recent advances in hydrogen compressors for use in large-scale renewable energy integration”. In: *International Journal of Hydrogen Energy* 47.83 (Oct. 2022), pp. 35275–35292. DOI: 10.1016/J.IJHYDENE.2022.08.128.

[8] Department of Energy. *Liquid Hydrogen Delivery*. Nov. 2023. URL: https://www.energy.gov/eere/fuelcells/liquid-hydrogen-delivery.

[9] M. Niermann et al. “Liquid Organic Hydrogen Carriers and alternatives for international transport of renewable hydrogen”. In: *Renewable and Sustainable Energy Reviews* 135 (Jan. 2021), p. 110171. DOI: 10.1016/J.RSER.2020.110171.

[10] Dionissios D. Papadias et al. “Hydrogen carriers: Production, transmission, decomposition, and storage”. In: *International Journal of Hydrogen Energy* 46.47 (July 2021), pp. 24169–24189. DOI: 10.1016/J.IJHYDENE.2021.05.002.

[11] Muhammad Aziz et al. “Ammonia as effective hydrogen storage: A review on production, storage and utilization”. In: *Energies* 13.12 (2020), pp. 1–25. DOI: 10.3390/en13123062.

[12] IRENA (International Renewable Energy Agency). *Innovation Outlook: Renewable Ammonia*. 2022. URL: https://www.irena.org/publications/2022/May/Innovation-Outlook-Renewable-Ammonia.

[13] Camel Makhloufi et al. “Large-scale decomposition of green ammonia for pure hydrogen production”. In: *International Journal of Hydrogen Energy* 46.70 (2021), pp. 34777–34787. DOI: 10.1016/j.ijhydene.2021.07.188. URL: https://doi.org/10.1016/j.ijhydene.2021.07.188.

[14] Krystina E. Lamb et al. “Ammonia for hydrogen storage; A review of catalytic ammonia decomposition and hydrogen separation and purification”. In: *International Journal of Hydrogen Energy* 44.7 (2019), pp. 3580–3593. DOI: 10.1016/j.ijhydene.2018.12.024. URL: https://doi.org/10.1016/j.ijhydene.2018.12.024.

[15] HYNETWORK Services. *Hydrogen Network Netherlands*. https://www.hynetwork.nl/en/about-hynetwork-services/hydrogen-network-netherlands. Accessed: 2023-03-15.

[16] Gasunie. *Waterstofnetwerk Nederland*. Nov. 2023. URL: https://www.gasunie.nl/projecten/waterstofnetwerk-nederland.

[17] HYNETWORK Services. *Quality specification for hydrogen*. https://www.hynetwork.nl/en/news/quality-specification-for-hydrogen. 15 October 2021.

[18] A. S. Chellappa et al. "Ammonia decomposition kinetics over Ni-Pt/Al2O3 for PEM fuel cell applications". In: *Applied Catalysis A: General* 227.1-2 (Mar. 2002), pp. 231–240. DOI: 10.1016/S0926-860X(01)00941-3.

[19] *Ammonia Cracker Manufacturer, Gujarat, India*. https://www.adonequipments.com/product/ammonia-cracker/. Accessed: October 12, 2023. 2023.

[20] Ammonia Energy Association. *High Flow Ammonia Cracking between 400-600°C*. https://www.ammoniaenergy.org/paper/high-flow-ammonia-cracking-between-400-600c/. 2023.

[21] Yousefi Rizi Hossein Ali et al. "Green Hydrogen Production Technologies from Ammonia Cracking". In: *Energies* 15.21 (2022), p. 8246. DOI: 10.3390/en15218246.

[22] Opeyemi A. Ojelade et al. "Ammonia decomposition for hydrogen production: a thermodynamic study". In: *Chemical Papers* 75.1 (2021), pp. 57–65. DOI: 10.1007/s11696-020-01278-z. URL: https://doi.org/10.1007/s11696-020-01278-z.

[23] Big Chemical Encyclopedia. *Modelling Reactions on Nonuniform (Nonideal Surfaces)*. https://chempedia.info/page/030214054220191124168161034167165138168116214237/. Accessed: 21-03-2023.

[24] Duiker: Combustion Engineers. *Brochure: AMMONIA TO HYDROGEN CONVERTER*. https://duiker.com/news-and-press-releases/. Accessed: 12-04-2023.

[25] Yao Ahoutou et al. "Electrochemical Cells and Storage Technologies to Increase Renewable Energy Share in Cold Climate Conditionsmdash;A Critical Assessment". In: *Energies* 15.4 (2022). DOI: 10.3390/en15041579. URL: https://www.mdpi.com/1996-1073/15/4/1579.

[26] Phillimon Modisha et al. "Electrocatalytic Process for Ammonia Electrolysis : A Remediation Technique with Hydrogen Co-Generation". In: 11 (2016), pp. 6627–6635. DOI: 10.20964/2016.08.54.

[27] Hayato Yuzawa et al. "Reaction Mechanism of Ammonia Decomposition to Nitrogen and Hydrogen over Metal Loaded Titanium Oxide Photocatalyst". In: *The Journal of Physical Chemistry C* 116.6 (2012), pp. 4126–4136. DOI: 10.1021/jp209795t. eprint: https://doi.org/10.1021/jp209795t. URL: https://doi.org/10.1021/jp209795t.

[28] Ilaria Lucentini et al. "Review of the Decomposition of Ammonia to Generate Hydrogen". In: *Industrial and Engineering Chemistry Research* 60.51 (2021), pp. 18560–18611. DOI: 10.1021/acs.iecr.1c00843.

[29] Žiga Ponikvar et al. "Electrification of Catalytic Ammonia Production and Decomposition Reactions: From Resistance, Induction, and Dielectric Reactor Heating to Electrolysis". In: *ACS Applied Energy Materials* 2022 (2021), p. 5472. DOI: 10.1021/ACSAEM.1C03045/ASSET/IMAGES/LARGE/AE1C03045{_}0007.JPEG. URL: https://pubs.acs.org/doi/full/10.1021/acsaem.1c03045.

[30] S. F. Yin et al. "A mini-review on ammonia decomposition catalysts for on-site generation of hydrogen for fuel cell applications". In: *Applied Catalysis A: General* 277.1-2 (Dec. 2004), pp. 1–9. DOI: 10.1016/J.APCATA.2004.09.020.

[31] J. C. Ganley et al. "A priori catalytic activity correlations: The difficult case of hydrogen production from ammonia". In: *Catalysis Letters* 96.3-4 (2004), pp. 117–122. DOI: 10.1023/B:CATL.0000030108.50691.d4.

[32] Mohammad Yusuf et al. "12 - Challenges and remediation for global warming to achieve sustainable development". In: *Artificial Intelligence for Renewable Energy Systems*. Ed. by Ashutosh Kumar Dubey et al. Woodhead Publishing Series in Energy. Woodhead Publishing, 2022, pp. 243–257. DOI: https://doi.org/10.1016/B978-0-323-90396-7.00017-1. URL: https://www.sciencedirect.com/science/article/pii/B9780323903967000171.

[33] U.S. Department of Energy. *Hydrogen Production: Natural Gas Reforming*. https://www.energy.gov/eere/fuelcells/hydrogen-production-natural-gas-reforming. Accessed: 27-03-2023.

[34] Valeria Tacchino et al. “Multi-scale model of a top-fired steam methane reforming reactor and validation with industrial experimental data”. In: *Chemical Engineering Journal* 428 (2022), p. 131492. DOI: https://doi.org/10.1016/j.cej.2021.131492. URL: https://www.sciencedirect.com/science/article/pii/S1385894721030734.

[35] Jose L. Cerrillo et al. “High purity, self-sustained, pressurized hydrogen production from ammonia in a catalytic membrane reactor”. In: *Chemical Engineering Journal* 431.October 2021 (2022). DOI: 10.1016/j.cej.2021.134310.

[36] Scott Battersby et al. “An analysis of the Peclet and Damkohler numbers for dehydrogenation reactions using molecular sieve silica (MSS) membrane reactors”. In: *Catalysis Today* 116.1 (2006). Special Issue on the Heterogeneous Catalysis Session of the InternationalConference on Surfaces, Coatings and Nanostructured Materials(nanoSMat2005), pp. 12–17. DOI: https://doi.org/10.1016/j.cattod.2006.04.004. URL: https://www.sciencedirect.com/science/article/pii/S092058610600188X.

[37] Valentina Cechetto et al. “Ultra-pure hydrogen production via ammonia decomposition in a catalytic membrane reactor”. In: *International Journal of Hydrogen Energy* 47.49 (2022), pp. 21220–21230. DOI: 10.1016/j.ijhydene.2022.04.240. URL: https://doi.org/10.1016/j.ijhydene.2022.04.240.

[38] Jose L. Cerrillo et al. “High purity, self-sustained, pressurized hydrogen production from ammonia in a catalytic membrane reactor”. In: *Chemical Engineering Journal* 431 (Mar. 2022), p. 134310. DOI: 10.1016/J.CEJ.2021.134310.

[39] Zhenyu Zhang et al. “Efficient Ammonia Decomposition in a Catalytic Membrane Reactor to Enable Hydrogen Storage and Utilization”. In: *ACS Sustainable Chemistry and Engineering* 7.6 (2019), pp. 5975–5985. DOI: 10.1021/acssuschemeng.8b06065.

[40] Tae Woo Kim et al. “Highly selective Pd composite membrane on porous metal support for high-purity hydrogen production through effective ammonia decomposition”. In: *Energy* 260.May (2022), p. 125209. DOI: 10.1016/j.energy.2022.125209. URL: https://doi.org/10.1016/j.energy.2022.125209.

[41] Jon Melendez et al. “Effect of Au addition on hydrogen permeation and the resistance to H2S on Pd-Ag alloy membranes”. In: *Journal of Membrane Science* 542 (2017), pp. 329–341. DOI: https://doi.org/10.1016/j.memsci.2017.08.029. URL: https://www.sciencedirect.com/science/article/pii/S0376738817306294.

[42] Valentina Cechetto et al. “Advances and Perspectives of H2 Production from NH3 Decomposition in Membrane Reactors”. In: *Energy & Fuels* 37.15 (2023), pp. 10775–10798. DOI: 10.1021/acs.energyfuels.3c00760. eprint: https://doi.org/10.1021/acs.energyfuels.3c00760. URL: https://doi.org/10.1021/acs.energyfuels.3c00760.

[43] Luigi Toro et al. “Regeneration of Exhausted Palladium-Based Membranes: Recycling Process and Economics”. In: *Membranes* 12.7 (2022). DOI: 10.3390/membranes12070723. URL: https://www.mdpi.com/2077-0375/12/7/723.

[44] Hideaki Kobayashi et al. “Science and technology of ammonia combustion”. In: *Proceedings of the Combustion Institute* 37.1 (Jan. 2019), pp. 109–133. DOI: 10.1016/J.PROCI.2018.09.029.

[45] Pio Forzatti. “Present status and perspectives in de-NOx SCR catalysis”. In: *Applied Catalysis A: General* 222.1-2 (Dec. 2001), pp. 221–236. DOI: 10.1016/S0926-860X(01)00832-8.

[46] Jeremy Whorton. *Reducing NH3 Slip in Selective Catalytic Reduction (SCR)*. https://www.thermofisher.com/blog/identifying-threats/reducing-nh3-slip-in-selective-catalytic-reduction-scr/. 16-07-2023.

[47] Gani Issayev et al. “Ignition delay time and laminar flame speed measurements of ammonia blended with dimethyl ether: A promising low carbon fuel blend”. In: *Renewable Energy* 181 (Jan. 2022), pp. 1353–1370. DOI: 10.1016/J.RENENE.2021.09.117.

[48] Syed Mashruk et al. “Nitrogen oxide emissions analyses in ammonia/hydrogen/air premixed swirling flames”. In: *Energy* 260 (2022), p. 125183. DOI: https://doi.org/10.1016/j.energy.2022.125183. URL: https://www.sciencedirect.com/science/article/pii/S0360544222020746.

[49] Carlos Gervasio Rodríguez et al. “Possibilities of Ammonia as Both Fuel and NOx Reductant in Marine Engines: A Numerical Study”. In: *Journal of Marine Science and Engineering* 10.1 (2022). DOI: 10.3390/jmse10010043.

[50] M. E.H. Tijani et al. “Review of Electric Cracking of Hydrocarbons”. In: *ACS Sustainable Chemistry and Engineering* 10.49 (2022), pp. 16070–16089. DOI: 10.1021/acssuschemeng.2c03427.

[51] Vemuri Balakotaiah et al. “Modular reactors with electrical resistance heating for hydrocarbon cracking and other endothermic reactions”. In: *AIChE Journal* 68.2 (2022). DOI: 10.1002/aic.17542.

[52] R. Kumar et al. “Absorption of Ammonia in a Packed Tower”. In: *Industrial & Engineering Chemistry Process Design and Development* 14.2 (1975). Accessed: November 12, 2023, pp. 168–174. DOI: 10.1021/ie50376a012. eprint: https://doi.org/10.1021/ie50376a012. URL: https://doi.org/10.1021/ie50376a012.

[53] RVT Process Equipment. *Ammonia Recovery from Wastewater and Biogas Plants*. RVT Process Equipment. 2023. URL: https://www.rvtpe.com/fileadmin/documents/print_and_publications/rvt_Ammonia_recovery_WEB_20220809.pdf.

[54] Department of Labor. *Strengthening Community Colleges Training Grants (Second Round) FOA-ETA-22-02 Frequently Asked Questions (FAQs)*. Mar. 2022. URL: https://www.dol.gov/sites/dolgov/files/ETA/grants/pdfs/Frequently%20Asked%20Questions.pdf.

[55] NiGen. *What Is a Desiccant Air Dryer – How Desiccant Dryers Work*. NiGen. 2023. URL: https://nigen.com/how-desiccant-air-dryer-work-what-is-regenerative-desiccant-dryer/.

[56] Collin Smith et al. “Rates of Ammonia Absorption and Release in Calcium Chloride”. In: *ACS Sustainable Chemistry & Engineering* 6.9 (2018), pp. 11827–11835. DOI: 10.1021/acssuschemeng.8b02108. eprint: https://doi.org/10.1021/acssuschemeng.8b02108. URL: https://doi.org/10.1021/acssuschemeng.8b02108.

[57] Matthew J. Kale et al. “Optimizing Ammonia Separation via Reactive Absorption for Sustainable Ammonia Synthesis”. In: *ACS Applied Energy Materials* 3.3 (Mar. 2020), pp. 2576–2584. DOI: 10.1021/ACSAEM.9B02278/ASSET/IMAGES/LARGE/AE9B02278{_}0007.JPEG. URL: https://pubs.acs.org/doi/full/10.1021/acsaem.9b02278.

[58] Rok Sitar et al. “Compact ammonia reforming at low temperature using catalytic membrane reactors”. In: *Journal of Membrane Science* 644 (2022), p. 120147. DOI: https://doi.org/10.1016/j.memsci.2021.120147. URL: https://www.sciencedirect.com/science/article/pii/S0376738821010875.

[59] XEBEC. *Pressure Swing Adsorption (PSA) Systems for Ultra-Pure Hydrogen and Other Industry Gas Purification*. https://xebecinc.com/wp-content/uploads/2021/06/Xebec-Hydrogen-Brochure.pdf. Accessed: 03-04-2023.

[60] Mauro Luberti et al. “Review of Polybed pressure swing adsorption for hydrogen purification”. In: *International Journal of Hydrogen Energy* 47.20 (Mar. 2022), pp. 10911–10933. DOI: 10.1016/J.IJHYDENE.2022.01.147.

[61] María Yáñez et al. “PSA purification of waste hydrogen from ammonia plants to fuel cell grade”. In: *Separation and Purification Technology* 240.July 2019 (2020), p. 116334. DOI: 10.1016/j.seppur.2019.116334. URL: https://doi.org/10.1016/j.seppur.2019.116334.

[62] Muhammad Amin et al. “Issues and challenges in hydrogen separation technologies”. In: *Energy Reports* 9 (2023), pp. 894–911. DOI: 10.1016/j.egyr.2022.12.014. URL: https://doi.org/10.1016/j.egyr.2022.12.014.

[63] *Cryogenic Process of Air Separation – IspatGuru*. URL: https://www.ispatguru.com/cryogenic-process-of-air-separation/.

[64] Majid Aasadnia et al. “A novel integrated structure for hydrogen purification using the cryogenic method”. In: *Journal of Cleaner Production* 278 (Jan. 2021), p. 123872. DOI: 10.1016/J.JCLEPRO.2020.123872.

[65] Ahmad Naquash et al. “Hydrogen Purification through a Membranendash;Cryogenic Integrated Process: A 3 Ersquo;s (Energy, Exergy, and Economic) Assessment”. In: *Gases* 3.3 (2023), pp. 92–105. DOI: 10.3390/gases3030006. URL: https://www.mdpi.com/2673-5628/3/3/6.

[66] Ji Jiang et al. “Novel hollow fiber membrane reactor for high purity H2 generation from thermal catalytic NH3 decomposition”. In: *Journal of Membrane Science* 629 (2021), p. 119281. DOI: https://doi.org/10.1016/j.memsci.2021.119281. URL: https://www.sciencedirect.com/science/article/pii/S0376738821002301.

[67] G. Sdanghi et al. “Review of the current technologies and performances of hydrogen compression for stationary and automotive applications”. In: *Renewable and Sustainable Energy Reviews* 102 (Mar. 2019), pp. 150–170. DOI: 10.1016/J.RSER.2018.11.028.

[68] Howden. *Hydrogen and process gases compression for refineries secondary units, chemical and petrochemical processes, complemented by renewable energy applications and environmental solutions*. 2023. URL: https://www.energyconnects.com/media/mdon22jz/howden-1-28-10-2022_21-06-18.pdf.

[69] J. Tuhovcak et al. “Comparison of heat transfer models for reciprocating compressor”. In: *Applied Thermal Engineering* 103 (June 2016), pp. 607–615. DOI: 10.1016/J.APPLTHERMALENG.2016.04.120.

[70] Maha Rhandi et al. “Electrochemical hydrogen compression and purification versus competing technologies: Part I. Pros and cons”. In: *Chinese Journal of Catalysis* 41.5 (May 2020), pp. 756–769. DOI: 10.1016/S1872-2067(19)63404-2.

[71] Maria Nordio et al. “Experimental and modelling study of an electrochemical hydrogen compressor”. In: *Chemical Engineering Journal* 369 (Aug. 2019), pp. 432–442. DOI: 10.1016/J.CEJ.2019.03.106.

[72] European Commission. *Development of centrifugal hydrogen compressor technology | Programme | H2020 | CORDIS | European Commission*. Mar. 2015. URL: https://cordis.europa.eu/programme/id/H2020_FCH-02.6-2014.

[73] Keefe Borden. “Howden to provide compressors for Europe’s largest renewable hydrogen plant”. In: *CompressorTech2* (Jan. 2023). URL: https://www.compressortech2.com/news/howden-to-provide-compressors-for-europe-s-largest-renewable-hydrogen-plant/8026236.article.

[74] *Green Ammonia Market Size, Trends, Growth, Report 2030*. URL: https://www.precedenceresearch.com/green-ammonia-market.

[75] *Green Ammonia – An Alternative Fuel - FutureBridge*. URL: https://www.futurebridge.com/industry/perspectives-energy/green-ammonia-an-alternative-fuel/.

[76] Norbert Kohlheb et al. “Environmental-Economic Assessment of the Pressure Swing Adsorption Biogas Upgrading Technology”. In: *Bioenergy Research* 14.3 (Sept. 2021), pp. 901–909. DOI: 10.1007/S12155-020-10205-9/FIGURES/5. URL: https://link.springer.com/article/10.1007/s12155-020-10205-9.

[77] Joshua Eichman et al. *Hydrogen Station Compression, Storage, and Dispensing Technical Status and Costs*. Tech. rep. National Renewable Energy Lab.(NREL), Golden, CO (United States), 2014.

[78] Netbeheer Nederland. *Summary of the Dutch electricity and gas distribution networks 2020*. 2020. URL: https://www.netbeheernederland.nl/_upload/files/NetbeheerNL_Rapport-Samenvatting-ENG_A4_FC.pdf.

[79] Energy Brainpool. *EU Energy Outlook 2050: How will the European electricity market develop over the next 30 years?* https://blog.energybrainpool.com/en/eu-energy-outlook-2050-how-will-the-european-electricity-market-develop-over-the-next-30-years/. Accessed: 05-10-2023.

[80] Jos Sijm et al. *The role of demand response in the power system of the Netherlands, 2030-2050*. Technical Report P10131. Ministry of Economics and Climate Policy of the Netherlands, May 2022, p. 155.

[81] Jan Frederick George et al. “Is blue hydrogen a bridging technology? - The limits of a CO2 price and the role of state-induced price components for green hydrogen production in Germany”. In: *Energy Policy* 167 (2022), p. 113072. DOI: https://doi.org/10.1016/j.enpol.2022.113072. URL: https://www.sciencedirect.com/science/article/pii/S030142152200297X.

[82] Energy.nl. *Ontwikkeling kosten groene en blauwe waterstof*. Sept. 2023. URL: https://energy.nl/publications/productiekosten-waterstof/.

[83] Boston Consulting Group. *Turning the European Green Hydrogen Dream into Reality: A Call to Action*. https://media-publications.bcg.com/Turning-the-European-Green-H2-Dream-into-Reality.pdf. Oct. 2023.

[84] Reuters. *Imported hydrogen can beat EU production costs by 2030 - study*. https://www.reuters.com/business/energy/imported-hydrogen-can-beat-eu-production-costs-by-2030-study-2023-01-24/. Jan. 2023.

[85] Shell. *Holland Hydrogen 1*. Oct. 2023. URL: https://www.shell.nl/energy-and-innovation/waterstof/welkom-waterstof/_jcr_content/par/toptasks.stream/1680267350018/0a5bcc38e8969b5b30bc923805b910b1722d63fc/ShellHydrogen1_MCW_v3.pdf.

[86] Hellovaia. *Peng Robinson Equation of State*. Oct. 2023. URL: https://www.hellovaia.com/explanations/engineering/engineering-thermodynamics/peng-robinson-equation-of-state/.

[87] AACE International. *AACE International Recommended Practices Cost Estimate Classification System – As Applied in Engineering Procurement, and Construction for the Process Industries*. Feb. 2005. URL: https://www.costengineering.eu/Downloads/articles/AACE_CLASSIFICATION_SYSTEM.pdf.

[88] Topsoe. *Blue Hydrogen - Levelized cost*. Nov. 2023. URL: https://www.topsoe.com/blue-hydrogen/levelized-cost.

[89] S. Armenise et al. “A Langmuir–Hinshelwood approach to the kinetic modelling of catalytic ammonia decomposition in an integral reactor”. In: *Phys. Chem. Chem. Phys.* 15 (29 2013), pp. 12104–12117. DOI: 10.1039/C3CP50715G. URL: http://dx.doi.org/10.1039/C3CP50715G.

[90] Carlos Plana et al. “Ni on alumina-coated cordierite monoliths for in situ generation of CO-free H2 from ammonia”. In: *Journal of Catalysis* 275.2 (2010), pp. 228–235. DOI: https://doi.org/10.1016/j.jcat.2010.07.026. URL: https://www.sciencedirect.com/science/article/pii/S0021951710002629.

[91] Esteem Projects. *Procedure for Fired Heater Design*. https://www.esteemprojects.com/library/guidelines-for-fired-heater-design/index.html. Accessed: October 23, 2023. 2023.

[92] Nenad Zečević et al. “Integrated Method of Monitoring and Optimization of Steam Methane Reformer Process”. In: *Processes* 8.4 (2020). DOI: 10.3390/pr8040408. URL: https://www.mdpi.com/2227-9717/8/4/408.

[93] British Stainless Steel Association. “Selection of stainless steels for handling ammonia (NH3)”. In: *BSSA* (2016). URL: https://bssa.org.uk/bssa_articles/selection-of-stainless-steels-for-handling-ammonia-nh3/.

[94] Anh Tran et al. “CFD modeling of a industrial-scale steam methane reforming furnace”. In: *Chemical Engineering Science* 171 (2017), pp. 576–598. DOI: https://doi.org/10.1016/j.ces.2017.06.001. URL: https://www.sciencedirect.com/science/article/pii/S0009250917303901.

[95] Furnace Improvements Services. *How to Boost the Performance of Fired Heaters*. https://static1.squarespace.com/static/5659c9cde4b05079e4b0c3d9/t/572b2877e3214012ea2b8e81/1462446304313/How+to+Boost+the+Performance+of+Fired+Heater.pdf. Nov. 2023.

[96] Kamal I. M. Al-Malah. *Aspen Plus: Chemical Engineering Applications*. 2nd. Wiley, 2022. URL: https://www.wiley.com/en-dk/Aspen+Plus:+Chemical+Engineering+Applications,+2nd+Edition-p-9781119868699.

[97] S. K. Saha et al. “Ammonia Absorption Refrigeration System: A Review”. In: *International Journal of Emerging Technology and Advanced Engineering* 4 (12 2014), pp. 875–880. URL: https://pdf.sciencedirectassets.com/277910/1-s2.0-S1876610214X00214/1-s2.0-S187661021401875X/main.pdf.

[98] *Compressed Hydrogen Dryers - H2 Dryers*. Webpage. URL: https://www.omega-air.si/products/compressed-gas-dryers/compressed-hydrogen-dryers (visited on 11/12/2023).

[99] *Psa Hydrogen Dryers Manufacturer Company Ahmedabad, India*. Webpage. URL: https://www.atmospower.in/hydrogen/ (visited on 11/12/2023).

[100] Anil Kumar et al. “In Silico Screening of Zeolites for High-Pressure Hydrogen Drying”. In: *The Journal of Physical Chemistry C* 125.4 (2021), pp. 2363–2375. DOI: 10.1021/acs.jpcc.0c10538. eprint: https://doi.org/10.1021/acs.jpcc.0c10538. URL: https://doi.org/10.1021/acs.jpcc.0c10538.

[101] Gunjan. “Reciprocating Compressor Discharge Temperature”. In: *Cheresources* (Nov. 2023). URL: https://www.cheresources.com/invision/topic/3772-reciprocating-compressor-discharge-temperature/.

[102] Kourosh Kian et al. “Performance of Pd-Based Membranes and Effects of Various Gas Mixtures on H2 Permeation”. In: *Environments* 5.12 (2018). DOI: 10.3390/environments5120128. URL: https://www.mdpi.com/2076-3298/5/12/128.

[103] Yuki Kudoh et al. *Life Cycle Carbon Dioxide Emissions from Ammonia-Based Power Generation Technology*. 2023, pp. 655–665. DOI: 10.1007/978-981-19-4767-4{_}46.

[104] Gavin P Towler et al. *Chemical Engineering Design: Principles, Practice and Economics of Plant and Process Design*. 2nd. Elsevier, 2013.

[105] Richard Turton et al. *Analysis, Synthesis, and Design of Chemical Processes*. Prentice Hall, 2009.

[106] Nobuko Hanada et al. “Hydrogen generation by electrolysis of liquid ammonia”. In: *Chemical Communications* 46.41 (2010). DOI: 10.1039/c0cc01982h.

[107] Dae Kwang Lim et al. “Solid Acid Electrochemical Cell for the Production of Hydrogen from Ammonia”. In: *Joule* 4.11 (2020), pp. 2338–2347. DOI: 10.1016/j.joule.2020.10.006. URL: https://doi.org/10.1016/j.joule.2020.10.006.

[108] Kazutaka Obata et al. “Photocatalytic decomposition of NH3 over TiO2 catalysts doped with Fe”. In: *Applied Catalysis B: Environmental* 160-161.1 (Nov. 2014), pp. 200–203. DOI: 10.1016/J.APCATB.2014.05.033.

[109] T. E. Bell et al. “H2 Production via Ammonia Decomposition Using Non-Noble Metal Catalysts: A Review”. In: *Topics in Catalysis* 59.15-16 (2016), pp. 1438–1457. DOI: 10.1007/s11244-016-0653-4.

[110] Ilaria Lucentini et al. “Catalytic ammonia decomposition over Ni-Ru supported on CeO2 for hydrogen production: Effect of metal loading and kinetic analysis”. In: *Applied Catalysis B: Environmental* 286 (June 2021), p. 119896. DOI: 10.1016/J.APCATB.2021.119896.

[111] Shulan Zhou et al. “First-Principles Insights into Ammonia Decomposition Catalyzed by Ru Clusters Anchored on Carbon Nanotubes: Size Dependence and Interfacial Effects”. In: *The Journal of Physical Chemistry C* 122.16 (2018), pp. 9091–9100. DOI: 10.1021/acs.jpcc.8b01965. eprint: https://doi.org/10.1021/acs.jpcc.8b01965. URL: https://doi.org/10.1021/acs.jpcc.8b01965.

[112] Johnson Matthey. *Steam reforming catalysts*. https://matthey.com/products-and-markets/chemicals/steam-methane-reforming. Accessed: 24-03-2023.

[113] Thien An Le et al. “A review on the recent developments of ruthenium and nickel catalysts for COx-free H2 generation by ammonia decomposition”. In: *Korean Journal of Chemical Engineering* 38.6 (2021), pp. 1087–1103. DOI: 10.1007/s11814-021-0767-7.

[114] Weiqing Zheng et al. “Effects of CeO 2 addition on Ni / Al 2 O 3 catalysts for the reaction of ammonia decomposition to hydrogen”. In: 80 (2008), pp. 98–105. DOI: 10.1016/j.apcatb.2007.11.008.

[115] Thomas J. Wood et al. “Assessing Potential Supports for Lithium Amide-imide Ammonia Decomposition Catalysts”. In: *ACS Applied Energy Materials* 1.6 (2018), pp. 2657–2663. DOI: 10.1021/acsaem.8b00351. eprint: https://doi.org/10.1021/acsaem.8b00351. URL: https://doi.org/10.1021/acsaem.8b00351.

[116] Joshua W. Makepeace et al. “Ammonia decomposition catalysis using non-stoichiometric lithium imide”. In: *Chemical Science* 6.7 (2015), pp. 3805–3815. DOI: 10.1039/c5sc00205b. URL: http://dx.doi.org/10.1039/C5SC00205B.

[117] Kanthal. *FIBROTHAL® HEATING MODULES AND INSULATION SYSTEMS: Product Overview*. https://www.kanthal.com/en/products/furnace-products/heating-modules/fibrothal-heating-modules/. Accessed: 19-03-2023.

[118] Zhemin Du et al. “A review of hydrogen purification technologies for fuel cell vehicles”. In: *Catalysts* 11.3 (2021), pp. 1–19. DOI: 10.3390/catal11030393.

[119] Cynthia Chin et al. “The Production of Industrial-Grade Oxygen from Air by Pressure Swing Adsorption”. In: *International Journal of Chemical Engineering* 2023 (2023). DOI: 10.1155/2023/2308227.

[120] Jun Zhang et al. “Alkali and alkaline-earth cation exchanged chabazite zeolites for adsorption based CO 2 capture”. In: 111 (2008), pp. 478–487. DOI: 10.1016/j.micromeso.2007.08.022.

[121] Takayoshi Adachi. “Production of High-Purity Hydrogen Through Ammonia Decomposition and Gas Removal”. In: *CO2 Free Ammonia as an Energy Carrier: Japan’s Insights*. Ed. by Ken-ichi Aika et al. Singapore: Springer Nature Singapore, 2023, pp. 391–400. DOI: 10.1007/978-981-19-4767-4_25. URL: https://doi.org/10.1007/978-981-19-4767-4_25.

[122] Jalon Zeolite. *What’s the difference: molecular sieve 3a 4a 5a 13x*. https://www.jalonzeolite.com/whats-different-molecular-sieve-3a-4a-5a-13x/. Accessed: 03-04-2023.

[123] Neha Pal et al. “Advances in materials process and separation mechanism of the membrane towards hydrogen separation”. In: *International Journal of Hydrogen Energy* 46.53 (Aug. 2021), pp. 27062–27087. DOI: 10.1016/J.IJHYDENE.2021.05.175.

[124] Lloyd M. Robeson. “The upper bound revisited”. In: *Journal of Membrane Science* 320.1-2 (July 2008), pp. 390–400. DOI: 10.1016/J.MEMSCI.2008.04.030.

[125] D. Sanz-Villanueva et al. “On the long-term stability of Pd-membranes with TiO2 intermediate layers for H2 purification”. In: *International Journal of Hydrogen Energy* 47.21 (Mar. 2022), pp. 11402–11416. DOI: 10.1016/J.IJHYDENE.2021.12.005.

[126] Ahmad Naquash et al. “Separation and purification of syngas-derived hydrogen: A comparative evaluation of membrane- and cryogenic-assisted approaches”. In: *Chemosphere* 313.November

2022 (2023), p. 137420. DOI: 10.1016/j.chemosphere.2022.137420. URL: https://doi.org/10.1016/j.chemosphere.2022.137420.

[127] S. Giddey et al. “Ammonia as a Renewable Energy Transportation Media”. In: *ACS Sustainable Chemistry and Engineering* 5.11 (Nov. 2017), pp. 10231–10239. DOI: 10.1021/ACSSUSCHEMENG.7B02219/ASSET/IMAGES/LARGE/SC-2017-02219T{_}0007.JPEG. URL: https://pubs.acs.org/doi/full/10.1021/acssuschemeng.7b02219.

[128] ARIEL: World Standard Compressors. *Downstream and Refinery*. https://www.arielcorp.com/compressors/compressor-applications/downstream-and-refinery.html. Accessed: 05-04-2023.

[129] Hooshang Heshmat et al. “On the Design of a Multi-Megawatt Oil-Free Centrifugal Compressor for Hydrogen Gas Transportation and Delivery: Operation Beyond Supercritical Speeds”. In: Jan. 2010. DOI: 10.1115/IMECE2010-40575.

[130] A.S Chellappa et al. “Ammonia decomposition kinetics over Ni-Pt/Al2O3 for PEM fuel cell applications”. In: *Applied Catalysis A: General* 227.1 (2002), pp. 231–240. DOI: https://doi.org/10.1016/S0926-860X(01)00941-3. URL: https://www.sciencedirect.com/science/article/pii/S0926860X01009413.

[131] Jian Zhang et al. “Kinetic study of NH3 decomposition over Ni nanoparticles: The role of La promoter, structure sensitivity and compensation effect”. In: *Applied Catalysis A: General* 296.2 (2005), pp. 257–267. DOI: https://doi.org/10.1016/j.apcata.2005.08.046. URL: https://www.sciencedirect.com/science/article/pii/S0926860X05006538.

A

Literature

A.1. Alternative Technologies to Ammonia Cracking

(Thermo-)Electrochemical Decomposition

The alternative method to decompose ammonia is through the electrolysis route. It can be performed in two ways, through direct liquid ammonia electrolysis, and through alkaline ammonia electrolysis. The direct liquid ammonia electrolysis uses Pt electrodes in ammonia liquid with amide present as a supporting electrolyte (see figure A.1)[106]. Though according to [26], a high potential of 2V was required for electrolysis, the experimental voltage above 1V is too high for practical use.

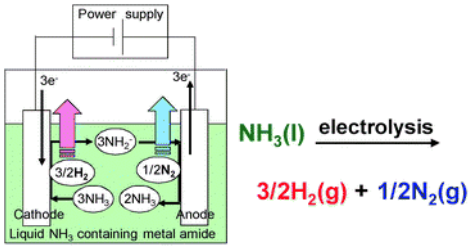

Figure A.1: The working principle of direct ammonia electrolysis for hydrogen generation[106]

In case of alkaline electrolysis, the potassium hydroxide is traditionally used as electrolyte, with cathodes and anodes from Pt-Ir alloy electrocatalyst[26]. At the anode side (Eq.(A.1)) the ammonia reacts with the hydrogxyl ion from the electrolyte (OH^-) to form nitrogen an water. At the cathode side (Eq.(A.2)) the formed water is dissociated to hydrogen and hydroxyl ions. In the net reaction (Eq.(A.3)) the ammonia in the solution is converted to nitrogen and hydrogen gasses.

$$2NH_3(aq) + 6OH^-(aq) \rightarrow N_2(g) + 6H_2O(l) + 6e^- \tag{A.1}$$

$$6H_2O(l) + 6e^- \rightarrow H_2(g) + 6OH^-(aq) \tag{A.2}$$

$$2NH_3(aq) \rightarrow N_2(g) + H_2(g) \tag{A.3}$$

It has been indicated that elevated temperatures are essential for ammonia electro-oxidation (Eq. A.1) and hydrogen production. At elevated temperatures the conductivity of the electrolyte (KOH) is increasing, leading to current density increase and enhanced ammonia electro-oxidation (see figure A.2a).

By increase in NH_3 concentration more NH_3 is adsorbed to the electrode, increasing the current density, causing enhanced ammonia electro-oxidation(see figure A.2b). However, at high concentrations of ammonia the electrodes get saturated and available cites of the electrode get blocked by intermediates, such as NH and NH_2, limiting further current density increase.[26]

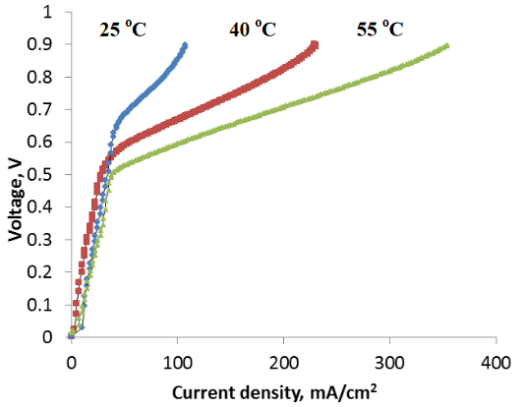

(a) Effect of temperature on current density

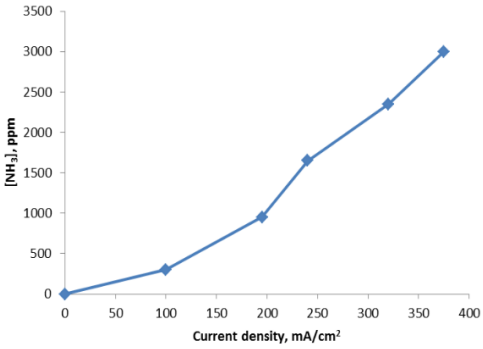

(b) Effect of NH_3 concentration on current density at $55°C$ and 0.9V

Figure A.2: Current density increase (a) with increase in temperature and (b) with increase in NH_3 concentration

In practice only low concentrations of ammonia can be used ($\leq$3000ppm), as the electrodes are prone to damage at higher concentrations [26]. The technology is therefore more suitable for purification of water from ammonia, and not for large-scale hydrogen production. The highest hydrogen production rate of 25L/h was achieved at constant current density of 250mA/cm^2, 2000 ppm of NH_3 in 5M KOH at 55°C, with corresponding power and energy requirement of 43 W and 1.6Wh/L-H_2 respectively [26]. The theoretic voltage for the reaction is 1.23V, but due to slow kinetics of the process, higher temperatures are required and therefore higher electric potential is needed. Therefore, alkaline ammonia electrolysis shows poor energy efficiency due to high operating potentials required and suffers from its electro-catalyst deactivation[26].

There is a hybrid method developed, which combines electrochemical conversion and thermal ammonia decomposition [107]. It consists out of a multilayered structure, The thermal cracking layer is made from the state-of-the-art Ru/CNT catalyst (catalysts are reviewed in chapter 2.1.3), which is followed by the electrochemical solid-state proton conductor layer for hydrogen removal, leading to ammonia-free hydrogen product. The process is performed at low voltage of 0.4V and is capable to produce hydrogen at rates comparable to thermal decomposition at 350-500°C range. The schematic of the designed cell is given in figure A.3. However, this technology is remaining at lab scale with ammonia flow rates of 30 mL/minute [107] and its large-scale potential remains undiscovered.

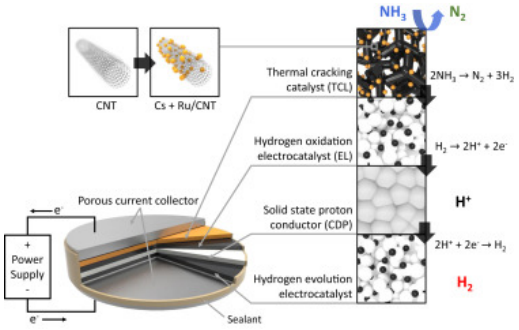

Figure A.3: The layered structure of the Hybrid Thermal-Electrochemical Cell[107]

Photocatalytic Decomposition

Ammonia can be decomposed by the metal-loaded photocatalyst in the reactor. The photocatalyst can be activated at room temperature and atmospheric pressure by using light radiation, such as electron beams, microwaves, solar energy, radio frequencies and more. Metal oxides are frequently researched photocatalysts. Under radiation by sufficient activation energy (hv), ammonia is converted to hydrogen and

nitrogen due to the photocalytic effect of oxidation and reduction of ammonia. See the graphic working principle of the catalyst on the figure A.4, for an example of the Platinum-supported TiO_2 catalyst[27], which decomposes aqueous NH_3 to hydrogen and nitrogen under solar irradiation.

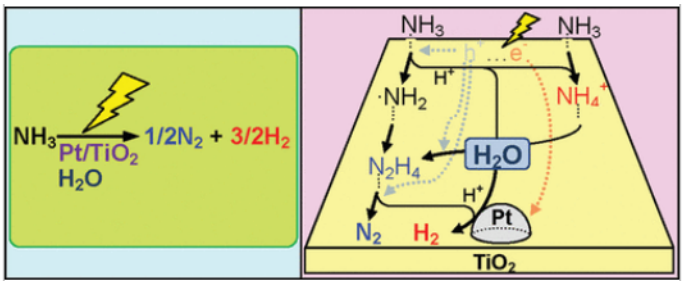

Figure A.4: Working principle of the photocatalyst[27]

The hydrogen production through TiO_2 photocatalyst, however, shows low efficiency due to its large bandgap located mainly at the UV region of solar radiation, rendering it impractical. However, it was also indicated, that when $TiO2$ is doped with Fe, the photocatalyst can also utilize visible light wavelengths to producer hydrogen from the aqueous NH_3 decomposition [108].

However, the experiments [108][27] on photocatalytic decomposition operate at labaratory scale with low feed rates of ammonia (1mL/min [27]), focused on ammonia removal from waste water (at concentrations of 0.59 mol $NH_3/L_{solution}$). Therefore, the current development of this technology is mainly focused on water purification. For this technology the reached H_2 production rates are in order of μmol/min and the potential for large-scale hydrogen production remains unknown.

A.2. Ammonia Cracking Catalyst Working Principle

The catalyst enhances the ammonia decomposition kinetics in three steps. First, the ammonia is getting adsorbed to active sites on the catalyst, which is a metallic chemical element. When adsorbed, the dehydrogenation of ammonia takes place, where the scission of N-H bonds takes place, and hydrogen is released, see figure 2.3 . Finally, nitrogen is desorbed from the catalyst. Depending on the type of catalyst, the N-H bonds cleavage becomes a limiting factor for the kinetics. Also, when operating at lower temperatures, the desorption of nitrogen and the dehydrogenation inhibition due to H_2 presence becomes a limiting step for the decomposition[109][110].

Catalyst Performance Parameters

It is important to note, that the best catalyst for ammonia synthesis is not necessarily the best ammonia decomposition catalyst [29]. The catalyst efficiency is defined by the following factors: the choice of the active metal component, the implemented catalyst supports and the use of promoters[30]:

- **the active metal component** is responsible for the catalytic conversion of the molecule. The support structures are employed to enhance the dispersion of the catalyst and to increase the catalyst surface area. From the research by (S. F. Yin et al., 2004) [31], the activity of the active metal components varies in the order Ru > Ni > Rh > Co > Ir > Fe,Pt > Cr > Pd > Cu,Te, with ruthenium showing unrivaled performance. The active metal components can be divided in noble and non-noble, which are reviewed in the end of this subsection.
- The **support structures** are employed to enhance the dispersion of the catalyst and to increase the catalyst surface area. The support has to be stable at the process temperatures and must have high specific surface area. The supports are commonly made from carbon structures or oxides. The catalytic activity of supports (with ruthenium as active metal component) is rated in following order: CNTs > MgO > TiO_2 > Al_2O_3 > ZrO_2 > AC(activated carbon) [28]. The state-of-the-art support is the catalytic nanotube(CNT), which improves the catalytic activity due to its high electronic conductivity, what facilitates the N_2 desorption enhancement due to a greater transfer of electrons. However, oxides are most commonly used in industry due to a lower cost and higher stability.

- The small particles of the active metal component tend to sinter during thermal treatment, what reduces the availability of active sites of the catalyst. The **promoters**, made from alkali, alkaline earth, or rare earth metal ions, can serve as intermediate agents to reduce the sintering, which improves the rate of conversion. The promotional effect is highly dependent on the selected active metal component. For example, the promotion by $K+$ ions from KOH on ruthenium is much stronger, than for a non-noble metal such as iron or nickel [30].

A.3. Catalyst Types

Noble Metal Catalysts Out all of the metals in the periodic table, ruthenium is unrivaled as ammonia decomposition catalyst, which has both the lowest temperature activity and highest hydrogen production rates (per mol of metal), as shown in figure A.5 [109]. Out of all state-of-the-art catalysts, the Ru/CNT is considered the most efficient. In this catalyst, carbon nanotubes (CNT), which are highly conductive, are used as support for the ruthenium particles (see figure A.6 for the molecular structure). The activity of Ru/CNT at 430 °C is 6353 $\text{mol}_{H_2}\text{mol}_{Ru}^{-1}\text{h}^{-1}$ with 7wt% Ru/gCNT. It has been also indicated that the activity of this catalyst can be further improved upto 7870 $\text{mol}_{H_2}\text{mol}_{Ru}^{-1}\text{h}^{-1}$ by the addition of an electron donating promoter (such as cesium) . The combination of CNT supports with cesium promoter enabled the decomposition of ammonia at low temperatures as 180°C.

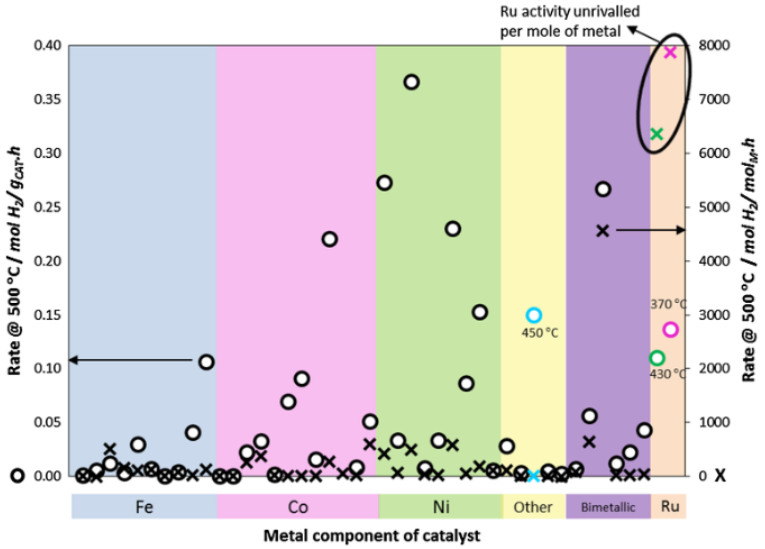

Figure A.5: The activity rate for the reviewed catalysts. Cross marks indicate the catalyst activity per mol of active metal component [109]. Ruthenium strongly outperforms other metals in terms of activity.

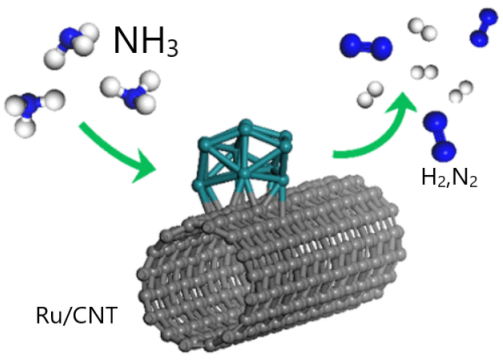

Figure A.6: Ru/CNT catalyst: ruthenium cluster sited on the carbon nanotube support[111]

However, both the high cost and scarcity of ruthenium and cesium (see figure A.7 for global production of various chemical elements) limit the economic feasibility of large-scale production of hydrogen from ammonia [109]. Therefore, catalysts made from the more common metals are urgently needed.

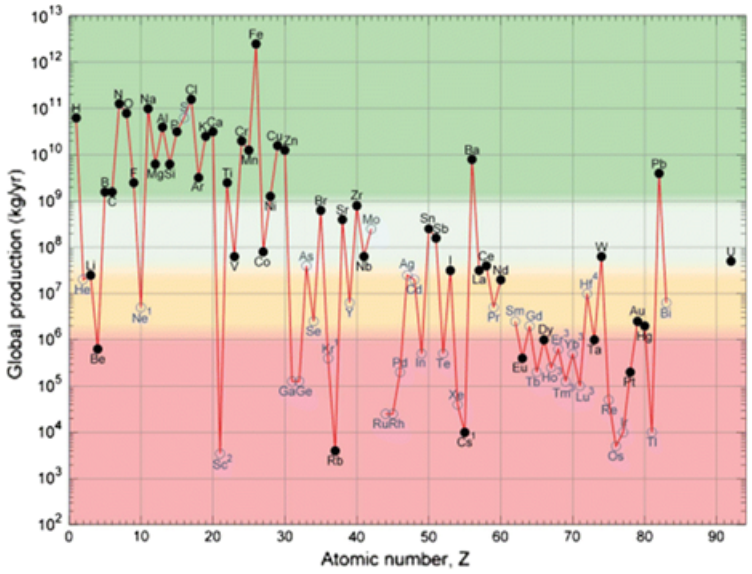

Figure A.7: Global yearly production of different chemical elements[109]. Ruthenium is among the most scarce chemical elements.

Non-noble Metal Catalysts Due to the high costs and scarcity of the noble metals, the costs of the Ru-based catalysts are a barrier for large-scale application. Therefore, a lot of research is shifted to non-noble metal based catalysts. The metals which receive the most attention are iron(Fe), cobalt(Co) and nickel(Ni). However, for these non-noble metals the desorption of N_2 is a barrier for the kinetics, which can only be overcome by operating at high temperatures[31]. Nickel is the most researched transitional metal catalyst, which is frequently employed in the industrial processes, such as steam methane reforming [112]. Besides, nickel-based catalyst is reported is the best performing out of non-noble metals [113], and can reach relatively high conversion rates when combined with supports and promoters. Also, Ni does not suffer from a water inhibition effect, as opposed to Fe /Fe-Co catalysts, which is an issue as commercial grade ammonia contains 0.2-0.5 wt% water. For example, when combined with alumina support (Ni/Al_2O_3) is reaching the conversion of 496 $mol_{H_2} mol_{Ni}^{-1} h^{-1}$ at 500°C [114].

Alkali metal amides/imides as New Catalysts Recently it was also found that alkali (and alkaline earth) metal amides and imides are catalytically active in relation to NH_3 decomposition. The examples are sodium amide, lithium amide-imide, lithium calcium imide, and calcium imide [115]. However, while having similar activity to ruthenium, most of these compounds turn to liquid at temperatures above 400°C, causing catalyst loss.
The only amide which remains solid is lithium amide-imide ($Li_{2x}NH_{1+x}$). The issue with this catalyst is its incompatibility with traditional catalyst support structures, due to the reactivity with the catalyst. One of the non-reactive supports is Magnesium-oxide. It has been shown that lithium amide-imide can even outperform Ru/CNT catalyst at 450°C when compared with conversion rates per gram of catalyst, though the conversion per mole of metal is significantly lower (see figure A.5).
However, the remaining issue with the amides/imides occurs in the practical setting of ammonia decomposition, as the imported ammonia will contain traces of water. The reaction of light metal amides with water to form hydroxides forms a barrier to durability of these catalyst compounds [116]. It was shown on lab scale in controlled environment, that for refrigerant-grade ammonia (99.8% purity) the catalyst activity reduces from 99.3% to 97.5% after 250 hours[116].

A.4. Membrane Reactor Types: Catalytic Packed bed (PBMR) and Catatic (CMR) Membrane Reactors

There are two main types of membrane reactors for hydrogen production from ammonia cracking, PBMR (packed bed membrane reactor) and CMR (catalytic membrane reactor). In PBMR configuration, the catalyst pellets are packed within the tubular reactor and are surrounded by a tubular hydrogen permeable membrane.

However, the effectiveness of PBMR is limited by the diffusion through pellet structure reducing the effectiveness of the catalyst in the bed and by the diffusion of converted hydrogen through the bed and membrane support, causing significant pressure drop on the retentate side. In CMR, the catalyst is incorporated in the separation membrane structure, eliminating poor dispersion, pressure drop and channeling issues, improving the hydrogen flux[39]. Also, CMR configuration reduces the required catalyst loading, which is especially beneficial when using noble metal catalyst . Besides, there is a lack of evidence of long-term stability of CMR technology, as the current research is still remaining on laboratory-scale and is only on its road towards commercialization [40].

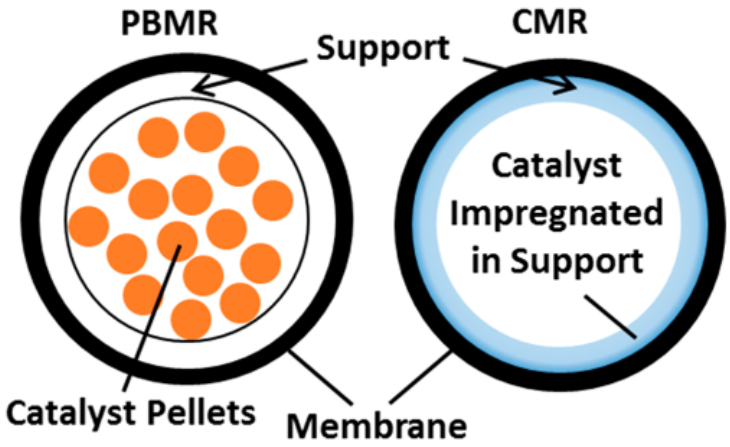

Figure A.8: Packed Bed Membrane Reactor internals (left) and Catalytic Membrane Reactor internals (right)

In the research, conducted by [35], the efficient ammonia decomposition is demonstrated in the catalytic membrane reactor, which uses a cobalt-based catalyst together with a PdAu membrane to produce PEM-cell grade purity hydrogen. The reactor has yielded very pure (>99.97% H_2) hydrogen product with the recovery of >90%. During the reactor testing, the robustness and durability were demonstrated for more than 1000 hours of total working time, during which the membrane stability remained unchanged.

A.5. Electrically Heated Reactor

In [50], the applications of electrical furnaces for endothermic reactors is reviewed. Various types of electric heating methods are reviewed, such as resistance (Ohmic) heating, arc/plasma heating, electromagnetic heating, shock wave heating and more.

In [51], various configurations of modular electric heating reactors are reviewed. Compared to traditional gas powered furnaces with 50% thermal efficiency, the resistance heaters are showing 90% thermal efficiency. Besides, the resistance heating eliminates the temperature gradient along the reactor, compared to gas furnace. Another advantage is that the start-up/shut-down of the electrified reactor is in order of seconds, compared to several hours duration for traditional fossil fuel reactors. The modularity, easy scale-up and flexibility are also the advantages of this technology.

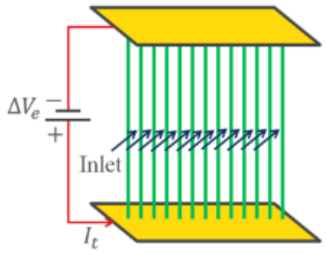

Figure A.9: Electrical resistence heating for endothermal reactions: Parallel Wire configuration[51]

The resistance heater works by passing current through the electrical resistance, what leads to the increase in temperature. From the lab scale research, it was indicated that the temperatures up to 3000°C are reachable. The state-of-the art commercial resistance heaters could provide 70kW/m^2 to maintain the furnace at 900°C [117]. Another advantage of the electric resistance heating is the simplicity of retrofitting, which would come handy when the electricity prices will be at able to compete with the gas prices. In the industry there are currently no industrial cases known where the resistance heating is used for large-scale endothermic reactors. However, small ammonia crackers are sometimes electrically heated, e.g. the ones used in the metallurgy industry.

Currently, as electricity costs are higher than for gas for the same amount of energy, the electrical heating in not applied on large scale due to higher operational costs compared to conventional cracking. The shift towards electricity would be possible with introducing higher taxation on CO_2 emissions and increasing availability of the renewable electricity. Besides, the electric heating is less attractive for the purpose of ammonia cracking by 2030, as it goes against the motivation of importing hydrogen due to cheaper and more abundant renewable electricity sources abroad.

A. Commentary on Reviewed Heat Supply Strategies

The review on ammonia-hydrogen fuel blends shows high promises and shows comparable performance to the conventional methane burning. Also, the solutions to the drawbacks of the ammonia burning, such as NO_X capture, flame stabilization and radiation heat enhancement have a sufficient level of maturity. Meanwhile, the application of electric heating has never been realised on the large scale due to absent infrastructure and high fluctuations in renewable electricity generation, what makes it a big barrier for large-scale ammonia cracking reactor, which requires continuous and stable heat supply. Therefore, the ammonia-hydrogen fueled heating is percieved as a more rational choice for ammonia cracking heat supply.

A.6. Hydrogen Separation Technologies: Detailed Review

There are various hydrogen purification methods currently existing (see figure A.10). The separation can be physical, such as by adsorption, low temperature separation or by membrane separation. For the purpose of large scale production, the physical separation methods are mainly considered and are reviewed in the following sections.

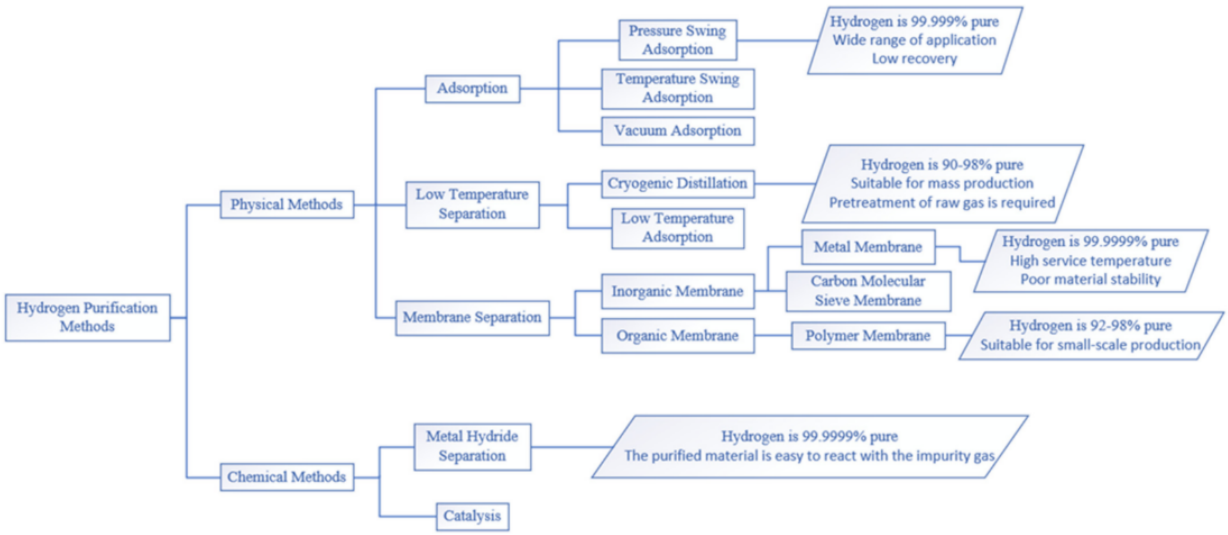

Figure A.10: Hydrogen Purification Technologies Classification[118]

A. Adsorption

In adsorption process, the separation of gasses occurs by preferential adhesion to the adsorbent material. As the adsorption packing material reaches the maximum saturation of adsorbed gas, the adsorption column has to go through regeneration process to separate the adsorbed impurity and remove it from the column. In practical operation the separated components are recovered by changing pressure or temperature conditions:

- In **Pressure swing adsorption (PSA)** a set of adsorbent-packed columns operate simultaneously in an adsorption-regeneration cycle, such that each bed undergoes the same sequence of steps, but at different times.
- In **Temperature swing adsorption (PSA)** column adsorption occurs at low temperatures, while adsorbent is regenerated by applying heat. TSA process consumes more energy than that of PSA, due to additional costs of heating and cooling [62]. Heating and cooling also require longer cycle times. TSA is therefore used for components which can not separate from the adsorbent by pressure decrease.

PSA is the most common commercial process for hydrogen separation, responsible for 85% of global hydrogen production. It is a common technology due to its attractive characteristics, such as low capital investment costs and low energy requirements for required recovery and purity. The performance of the PSA unit is determined by the adsorbent packing, operating pressures and the temperatures. Besides, different impurities possess different adsorption characteristics, requiring different operating conditions.

Working Principle and Optimization

Hydrogen is always an effluent of H_2 PSA, as it is difficult to adsorb due to its nonpolarity and high volatility, while other impurities are adsorbed easier. The tail gas from desorption is enriched with impurities and a portion of hydrogen is retained in adsorbent packing. The conventional 2-column 4-step PSA Skarstrom cycle (see figure A.11)[119] consists of:

- **Adsorption (AD)**: At highest pressure, the impurities from the feed stream are adsorbed to the bed, while hydrogen is withdrawn as the product.
- **Counter-current blowdown (BD)**: The adsorption bed is countercurrently depressurized to the lowest pressure in the cycle. Outgoing stream with a portion of desorbed impurities is extracted at the feed.
- **Counter-current purge (AD)**: At the lowest pressure in the cycle, the adsorption bed is purged by counter-current H_2-rich stream from another adsorption bed, removing the remaining impurities

- **Concurrent pressurization (AD)** The column is then pressurized by feed flow up to the maximum pressure, and the cycle repeats itself.

However, due to huge product losses of this simple cycle (<25% recovery), the process has been optimized by additional/alternative steps such as **pressure equilization** or **counter-current product pressurization** in the column to increase recovery and energy consumption[119].

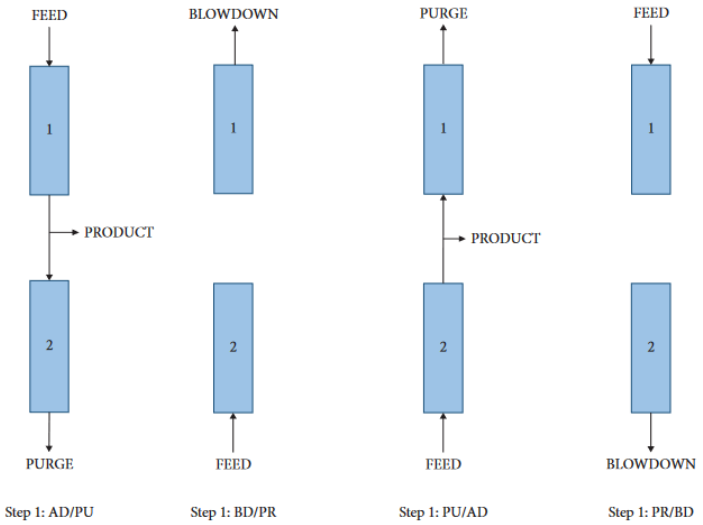

Figure A.11: The basic PSA process by Skarstrom[119]

As the adsorption column gets larger, the influence of heat due to adsorption/desorption influences the thermodynamics in the column. Therefore, the separation performance of PSA is reducing with the scale up. One way of increasing recovery and throughputs is by employing a poly-bed system (more than 4 beds), which incorporates at least three pressure equilization (PE) steps and has at least two beds receiving the feed gas at the same time. The increase in number of beds and PE steps increases the recovery of hydrogen up to above 90% at ultra-high purities (99.99+%) with high throughputs (>280000 m^3/h)[60].The new PSA units, significantly modified by additional steps such as pressure equalization are able to produce H_2 with purities between 98% and +99.99%, with 70–90% H2 recovery in large units with more than 12 columns and adsorption pressures above 20 bar [61]. Conventionally, the PSA units operate at 10-40 bar pressures [59]. High adsorption pressure increases partial pressure of H_2 and is beneficial for as it reduces downstream compression costs of hydrogen product.

Adsorbent Selection

The traditional PSA adsorbent materials are zeolite molecular sieves, activated carbon, activated alumina, and silica gel. Activated carbon has low affinity to inert gasses such as N_2 and is therefore not preferred for ammonia cracker downstream purification [62], and is more suitable for CO_2 and CH_4 adsorption [60]. Meanwhile, zeolites have strong attraction to both N_2 and NH_3, and very low attraction to hydrogen, what makes them unrivaled to other traditional adsorbents [60] [62]. The most popular zeolite for nitrogen adsorption are 5A (5A stands pore size in angstroms) and 13X zeolite molecular sieves, which are frequently used in oxygen purification. Also 5A zeolite is common in H_2 PSA for steam reformer syngas treatment, where it removes N_2 and CO[60].

It was previously demonstrated that cation exchange of zeolites can alter the N_2 adsorption properties of zeolites [120]. The recently developed X-type zeolites, cation-exchanged with calcium or lithium, are able to adsorb large amounts of nitrogen [121]. They are currently used in oxygen PSA and are also applicable for hydrogen purification purposes.The state-of-the-art commericial X-type zeolite LiLSX developed for O_2 production has enhanced adsorption capacity due to Li^+ ions presence.

Besides, the zeolites have also shown to be suitable for ammonia adsorption. However, due to strong adsorption of ammonia to the zeolite, temperature increase is required for regeneration. Therefore, instead of PSA the **temperature swing adsorption (TSA)** is required for ammonia removal. For example, to

	H_2O	NH_3	H_2	N_2
Boiling temp. (°C)	100	-33.34	-252.9	-195.8
Freezing temp. (°C)	0	-77.73	-259.2	-210
Critical temp. (°C)	374	405.56	-239.9	-146.9
Critical pressure (bar)	220.7	112.8	13	34

Table A.1: Critical properties of H_2 and other components present in the ammonia decomposition product stream

regenerate the 5A zeolite packing in the adsorber, the column has to be heated up to 300-350°C [122]. Also, the Li-X zeolite in the TSA unit makes it possible to reduce ammonia concentration up to 0.01-0.02 ppm and N_2 concentration to <100ppm, with 5.7wt% adsorption capacity, and has to be heated up to 300°C for regeneration [103].

B. Cryodistillation

In case of cryodistillation, the difference in boiling point of molecules in the gas mixture is used for separation. As the gasses in the mixture are highly volatile, very low temperatures are required to facilitate the separation. Cryodistillation is a mature technology, which remains as the main method for mass production of air products, such as O_2,N_2 and Ar[63]. Cryodistillation is especially efficient when any of the following criteria are required namely (i) large quantities of product gas (>100 tons/day), (ii) high purities of gas (>99.5% for oxygen production) and (iii) high pressures of the product. Each of these criteria are also important for hydrogen-from-ammonia production, as it requires large product quantities, has strict quality requirements of the hydrogen network and elevated pressures can reduce the costs of downstream compression up to the network pressure.

Working Principle

The fundamental processes of cryodistillation are: (i) compression of gas mixture, (ii) gas purification, (iii) heat exchange, (iv) distillation and finally (v) the compression of product gas to required pressure (see figure A.12)[63].

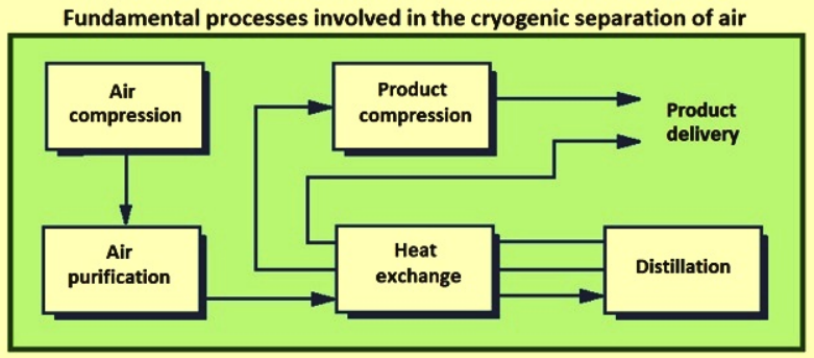

Figure A.12: The Fundamental steps of cryodistillation process, for air as an example gas mixture [63]

In case of applying cryodistillation for the gas mixture from the ammonia cracker, the properties of components have to be considered carefully. Table A.1 lists the properties of the components present in the reactor downstream.

For H_2 recovery from mixtures with N2, NH_3, and water traces, the significant difference in the boiling points of H2 and N2 of 57.1 °C creates a feasible VLE-based separation. However, such temperatures might induce the solidification of NH_3 and traces of H_2O as their freezing point is much higher than the boiling point of H_2 (−252.9 °C) at atmospheric pressure. Therefore, NH_3 (and H_2O traces) have to be removed from the mixture prior to cryodistillation process in a separate unit.

Pd Membrane code	Thickness [μm]	H_2 perm. [mol/s/m^2/Pa]	Pressure exp.	H_2/N_2 select.
1	$\sim$ 1	$2.22 \cdot 10^{-6}$	0.80	5210
2	$\sim$ 6-8	$1.15 \cdot 10^{-6}$	0.72	68960

Table A.2: Performance of Pd membrane at 450°C and 1 bar pressure difference across the membrane [37]. Ideal H_2/N_2 selectivity given at different thickness of selective layer.

Cryogenic temperatures and Hydrogen-Nitrogen Separation
After removing ammonia and water traces, the remaining nitrogen-hydrogen mixture can be separated by cryodistillation. Before entering the distillation unit, the mixture is cooled in the heat exchanger by the product and waste streams from the distillation column, which is an important step for energy recovery. To obtain cryogenic temperatures, the refrigeration process uses compressor-expander systems, to remove energy from the gas mixture stream through expansion, while compressing the product streams [63] (which reduces the downstream H_2 compression costs). To obtain relatively high purity of H_2 purity (98%), the distillation column has to operate at very low temperatures, due to low boiling point of H_2. In the previous research on hydrogen purification, cryodistillation at -149.5°C only attained the purity of 88% H_2[64]. Therefore, low operating temperatures are required, which brings high energy consumption.

C. Membrane Separation
In this section different types of membranes are reviewed on their hydrogen separation performance. Also, the use of membranes is reviewed for ammonia-cracker downstream purification of H_2.

Membrane Types
Membrane separation depends on the molecular structure of the membrane. The driving force for diffusion of gas through membrane is defined by pressure, concentration or electric potential gradient across the membrane. Each membrane type faces trade-off between permeability and selectivity. Various types of materials are used in the development of hydrogen-selective membranes, such as polymer membranes and inorganic membranes. Inorganic membranes can be further grouped into two types, (porous) molecular sieve membranes (such as carbon, zeolite and ceramic) and (dense) metallic membranes (Pd, Pt, V etc.)[123]:

- **Polymeric Membranes** are known for their energy efficiency, low production costs and convenience of use. There are glassy and rubber types of polymers membranes. The glassy membranes show better selectivity than rubber due to the adequate voids in the molecular structure, which govern the diffusivity of the penetrant gas [62]. However there is a trade-off between high selectivity and permeability for this membrane type. While polymeric membranes are economical and technologically useful, they are bounded by their performance, known as the (empirically defined) Robeson limit [124]. Also, polymer membranes have low thermal stability and weaker structure compared to inorganic membranes, and therefore a short lifespan [62].
- **Molecular Sieve Membranes** Overall, ceramic, zeolite, and carbon-based membranes are showing promise for H2 separation. Ceramic membranes are well-established and have high permeability and selectivity, but have manufacturing issues which are still unsolved on lab scale. Zeolite and carbon-based membranes have potential for high H2 permeability and selectivity, but they are brittle and require complex production processes, making them too expensive and hard to scale up [62].
- **Metallic Membranes**, Pd membranes in particular, are known as the most efficient membranes for hydrogen separation,due to excellent solubility of H_2 in a wide temperature range, having both high selectivity, permeability and stable performance in the range of 400-500°C. The Pd metal membranes show the unrivaled performance of H_2/N_2 selectivity, while having higher permeation than other membrane types in the list [37], see table A.2. Due to these characteristics most recent ammonia cracking membrane reactor researches have been focused solely on Pd-based membranes. However, high costs and scarcity of Pd (see figure A.7) form a barrier for large scale application.

D. Operating Conditions
Based on the reviewed membrane types, Pd membranes show the best performance on hydrogen selectivity. Pd-based membranes are commonly fabricated on ceramic porous supports, such as alumina

tubes [37] to withstand pressure difference across the membrane. The Pd-based membrane can withstand temperatures of 300-600°C and feed pressures up to 12 bar [125]. However below 400 °C they are prone to hydrogen embrittlement, while at temperatures above 500°C cracking at support-metal interface occurs due to thermal expansion mismatch.

The biggest issue of using membranes downstream of the reactor, next to the high costs of palladium, is the resulting low pressure of hydrogen in the permeate. To compress the produced gas to hydrogen network pressure, a lot of compression energy is required. The comparative study of membrane separation and cryodistillation for separation and purification of syngas-derived hydrogen was performed.Based on its economic evaluation, membrane separation is nearly twice as expensive than cryodistillation because of the high cost of required compressors [126]. Therefore, membrane technology utilizes most of its advantages when integrated in the reaction process, not as a separate downstream purification unit.

E. Membrane H_2/NH_3 and H_2/N_2 Selectivity

The report by Jiang J.[66] published the paper with the data on membrane selectivity of Pd based membrane, compared to modified MFI zeolite membrane and carbon molecular sieve membrane. The results are depicted in the figure A.13 below:

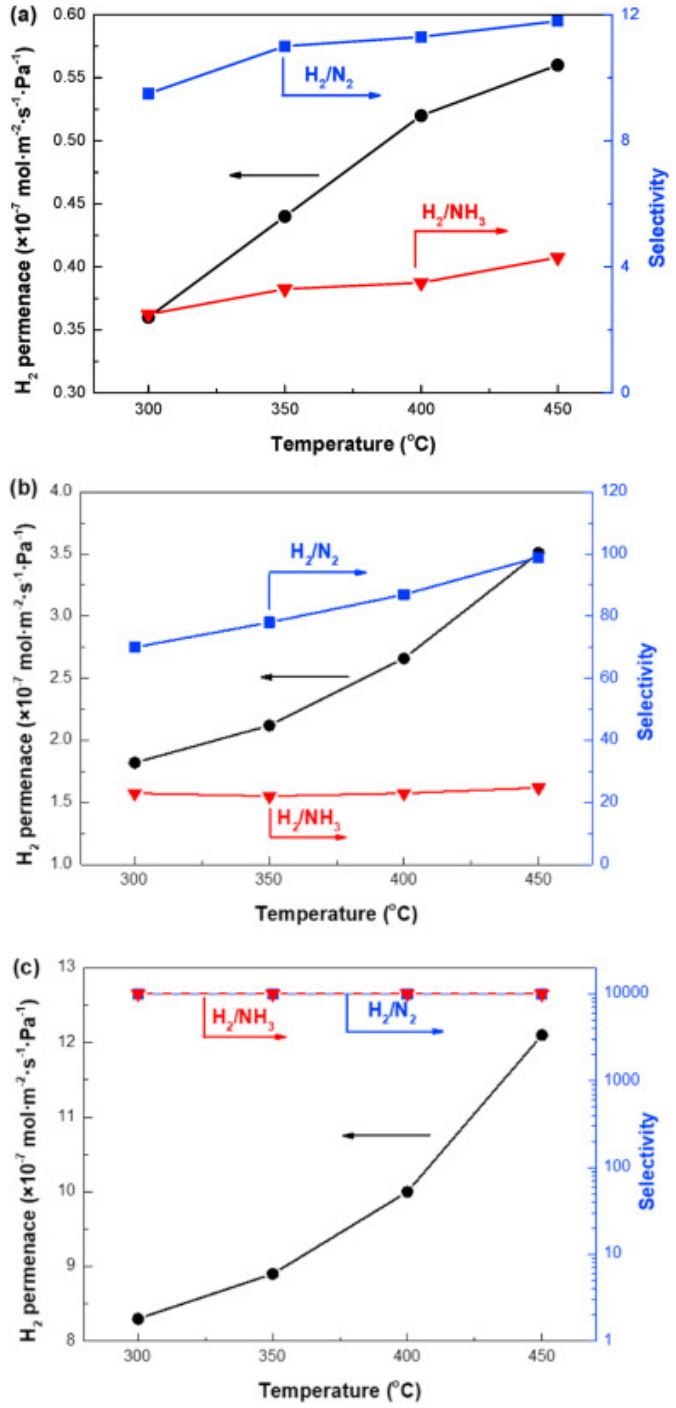

Figure A.13: Ternary mixture gas (5%NH3/71%H2/24%N2) separation with modified MFI membrane, carbon molecular sieve and Pd/Ag membranes at different temperatures and pressure drop of 7 bar: (a) modified MFI membrane; (b) carbon molecular sieve membrane; (c) Pd/Ag membrane.[66]

A.7. Hydrogen Compression

To be admitted to hydrogen network, purified hydrogen has to be pressurized up to 50 bar [17]. The required pressure ratio is dependent on the exit pressure of the purification unit. Also, the target for large-scale hydrogen production capacity of ammonia cracking plant is set at 100 tons/day, which is around 50000 Nm^3/h, which is at comparable scale to the large-scale electrolysis plant production. Therefore, the selection of a applicable compression technology is required, which is able to handle such throughputs.

In this chapter the technologies with a potential for large-scale hydrogen distribution by pipeline are reviewed[67]: mechanical compression (section **??**) and electrochemical compression (section **??**).

A. Mechanical Compression

Mechanical compression is the most mature and common method of gas compression. In this method the gas is compressed by mechanical 'positive displacement' devices, such as by turbomachinery, piston or flexible membrane devices[127], which are used on industrial scale. The compression is facilitated by reduction of confined volume of contained hydrogen. Thus, mechanical energy is converted into gas energy. As the energy of the gas increases, the number of collisions of particles H_2 increases, which leads to an increase in gas pressure [67].

There are various configurations of mechanical compressors currently available, such as reciprocating piston, diaphragm, centrifugal, linear and liquid ring compressors. However, for large-scale hydrogen production, only two types of compressors [7] can handle the required capacity:

- **Reciprocating Compressor** is the most frequently used compression topology, especially attractive when high pressure ratios are required. It can handle hydrogen flow up to 4800 Nm^3/h[7]. It uses a piston to compress a gas to deliver it at high pressure (see figure A.14 of a commercial reciprocating compressor by Ariel). They are best applied for the purpose of production of highly compressed hydrogen, and are only available compressors to reach H_2 1000 bar[7], when a multi-stage configuration is used[67]. However, with increase in scale for large scale production bigger and heavier components are required. To limit the resulting mechanical stresses for piston-type compression, reciprocal compressor must operate at lower speeds. It forms a barrier, as large flow rates are required for large scale production. Other limitations for reciprocal compressors are complex manufacturing processes, high maintenance costs due to moving components, ineffective cooling during compression [69], and pressure variations causing vibrations, noise, and even explosions.

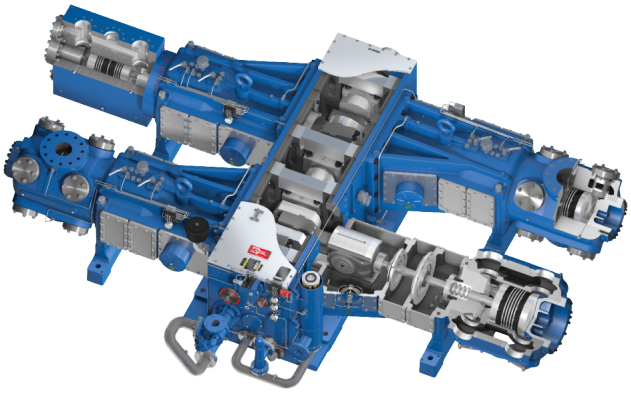

Figure A.14: Large-Scale Reciprocating Compressor by Ariel[128]

- **Centrifugal Compressor**

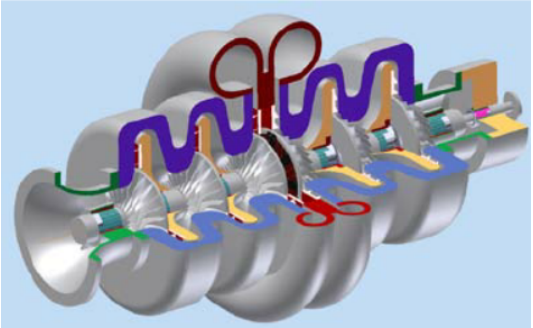

Figure A.15: Large-Scale Centrifugal Hydrogen Compressor [129]

B. Electrochemical Compression

The innovative electrochemical compressor works by the same principle as the proton exchange membrane (PEM) fuel cell, see figure A.16. The process of compression consists out of three main steps:

1. low pressure hydrogen is fed to the anode side of the fuel cell, where it is split in protons and electrons (Eq.A.4)

$$H_2 \rightarrow 2H^+ + 2e^- \tag{A.4}$$

2. The protons than go through the solid polymer electrolyte membrane to the cathode side, while electrons go externally through the electrical circuit, controlled by potential difference from electric power supply.
3. The protons and electrons recombine at cathode side (Eq. A.5), resulting in pressure pressure.

$$2H^+ + 2e^- \rightarrow H_2 \tag{A.5}$$

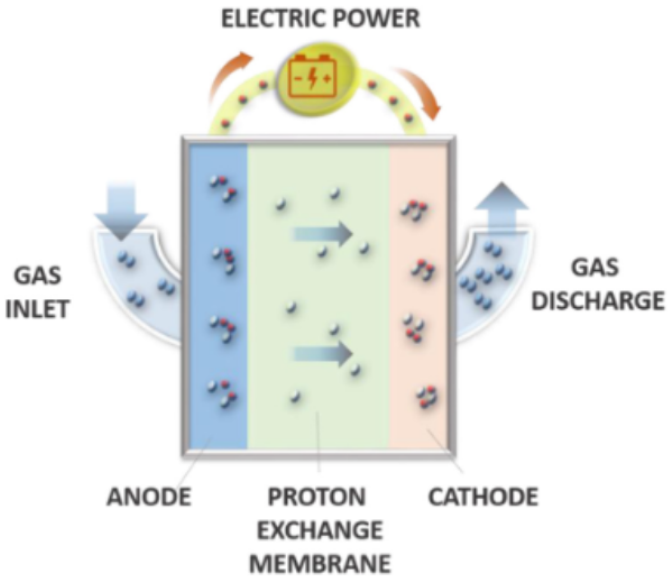

Figure A.16: Working Principle of Electrochemical Compressor[67]

The compression performance is entirely dependent on the supplied voltage to the electrochemical compressor. Nernst Equation (Eq. A.6) gives the relationship between the supplied voltage and the achieved pressure ratio:

$$E_{cell} = E_0 + \frac{RT}{2F} ln \frac{p_c}{p_a} \tag{A.6}$$

with $\frac{p_c}{p_a}$ as result pressure ratio, E_0 as the cell potential at standard conditions (considered in electrochemical compression), R as gas constant, T as absolute temperature and F as the charge of 1 mol of electrons [67]. According to the equation, in theory 0.0386 V is enough to increase pressure from 1 to 50 bar.

In practice, however, more voltage is required due to electric resistance of the proton exchange membrane, which is the main limiting factor of the electrochemical compressor. Another issue of using electrochemical compression is the increasing permeation of molecular hydrogen through the membrane in case of high pressure ratio, what decreases the efficiency of the compressor. Nevertheless, electrochemical compressor shows great advantages when operated at moderate pressures and low flow rates, and is considered highly efficient in comparison with mechanical compression. Also, this method requires no moving parts, which is very attractive for processes where vibrations and noise need to be eliminated. Last but not least, electrochemical compressors are simultaneously able to purify hydrogen from impurities[70]. This synergy is very attractive for small scale production of hydrogen.

However on large scale, electrochemical compressors have not yet reached the level of maturity and reliability to become competitive with traditional compressors. Currently, the maximum lifetime of the commercially available polymeric membranes is below 5 years [71].

B

Process Simulation

B.1. Kinetic Model: Catalyst Properties & Experimental Conditions

For validation of the kinetics the physical properties of the catalyst had to be accurately defined. The physical properties were defined through the steps of catalyst production. The Ni/Al_2O_3 was created in four steps [89]:

1. The commercial cordierite monolith is taken as the catalyst basis.
2. The Al_2O_3 catalyst support layer coating was applied on top of the monolith.
3. The active layer of nickel particles was applied on top of the catalyst.
4. The monolith structure was crushed and filled into the reactor as packed bed.

The physical propeties and operating conditions of the catalyst are derived from the experimental setup by Armenise. S. [89]. Both physical properties and experimental conditions are listed in Table B.1 below:

Table B.1: Properties of the Ni/Al2O3/monolith based packed bed, from experiments by Armenise.S. [89] [90]

Catalyst Physical Properties and Experimental Conditions		
Experiment Setup		
		Unit:
Weight of experimental packed bed:	2,779	gm
Volume reactor (D=15mm , L=15mm)	2,651	mL
Basis (cordierite monolith)	2,600	gm
Support Layer Washcoat (Al2O3)(6 wt% of the packing)	0,156	gm
Active Layer (Nickel Particles) (15% of the support layer)	0,023	gm
Properties of the Catalyst (Derived from setup):		
		Unit:
Density Packed Bed:	1048,632334	**kg/m3**
Density Catalyst Layer:	67,68534239	**kg/m3**
Experimental Conditions:		
		Unit:
Temperature Range:	**500-1000**	**°C**
Pressure:	**1**	**bar**
GHSV:	35000,0	cm3g-1h-1
	12324,0	h-1
Flow rate:	100,0	mL/min
Residence Time (Derived from GHSV, flow rate, and packed bed geometry)	**4,43**	sec

B.2. Reactor Packed Bed Sizing Procedure

After validation of the catalyst model at the pressure of interest, the initial sizing of the reactor was performed with the following steps:

1. **Selection of Operating Conditions**: The first step involved selecting thermodynamic conditions for reactor sizing. This began with assuming a uniform temperature for the PFR simulation of the experimental setup configuration. Temperature of 983 K was taken as reference temperature. Pressure was taken as 1bar.
2. **Required flow rate**: To ensure 100 TPD of hydrogen product, the required NH3 reactant feed flow was set to 640 TPD. From stoichiometry, 630 TPD of ammonia is required to obtain 100 TPD, as 90% of H2 recovery by H2 purification is assume.
3. **Packing Volume Derivation**: The volume of the catalyst packing was calculated by the following equation.

$$Packing Volume = Packing volume experimental setup * \frac{Required\ NH3\ Flow\ rate}{NH_3\ flowrate\ experimental\ setup} \quad \text{(B.1)}$$

4. **Tubing Configuration**: Based on the determined packing volume, an estimation of the internal structure of the reactor was made, paying particular attention to the tubing configuration. The tubing configuration was selected in accordance with the API 560 standard for sizing fired heater-reformers. According to this standard, the inner diameter of industrial reformer tubes typically falls within the range of 4 to 6 inches, with lengths varying from 10 to 15 meters. The number of tubes is determined by the residence time, derived from the GHSV (Gas Hourly Space Velocity) of the experimental setup.

$$GHSV = \frac{STP\ Process\ Gas\ Volumetric\ Flow\ rate}{Active\ Catalyst\ Layer\ Volume} \quad \text{(B.2)}$$

By following these steps, the process of reactor sizing was systematically conducted, ensuring alignment with experimental conditions. The scaling procedure, together with the resulting reactor configuration, is visualised in the figure B.1 below:

Experiment Case Stream Properties			
Stream name:		FEED STREAM	PRODUCT STREAM
Total Mass Flo	tons/day	1,20E-04	1,20E-04
H2	tons/day	1,42E-12	2,03E-05
N2	tons/day	1,98E-11	9,42E-05
NH3	tons/day	1,20E-04	5,84E-06
Volume Flow	cum/sec	5,98E-07	1,17E-06

Product Scale Factor: 5,32E+06

Target Case Stream Propertes			
Stream name:		FEED STREA	PRODUCT STREAM
Total Mass Flo	tons/day	640,0	640,0
H2	tons/day	0,0	108,1
N2	tons/day	0,0	500,8
NH3	tons/day	640,0	31,1
Volume Flow	cum/sec	3,2	6,2

Experimental Setup Properties	
Packing Vol. (m3)	2,65E-06
$L_{reactor}$(m)	1,50E-02
$D_{Reactor}$ (m)	1,50E-02
Vol. Flow (m3/s)	5,98E-07
Stream velocity (m/s)	3,38E-03
residence time (s)	4,44
GHSV (h-1)	12324

Derived Multi-Tubular Reactor Properties		
Packing Vol. (m3)	14,48	
NUMBER OF TUBES	145	
L_{Tube} (m)	12,00	
D_{tube} (m)	0,1016*	*4 inches
Vol. Flow (m3/s)	3,27	
Stream velocity (m/s)	2,71	
residence time (s)	4,43	
GHSV (h-1)	12324	

Figure B.1: The derivation procedure for the reactor packed bed sizing. The reactor is sized by scaling the experimental packed bed size to obtain the required H_2 production rate, while maintaining the same residence time of the process stream inside the catalyst packing. Operating conditions during scaling: P = 1 bar, T = 973K (700°C)

B.3. Reactor Modelling: Optimum Temperature Derivation from Heat Balance of the Idealized Process Model

After the reactor is sized, its optimum operating temperature has to be determined. The optimum temperature would lead to the minimum fresh NH_3 fuel requirement for heat supply to the reactor and heat exchanger system. To estimate the optimal NH_3 decomposition reactor temperature, which would potentially minimize the required amount of ammonia flow from the feed, the simplified model of the process plant was simulated in Aspen Plus V12 (see flowsheet in Figure B.2).

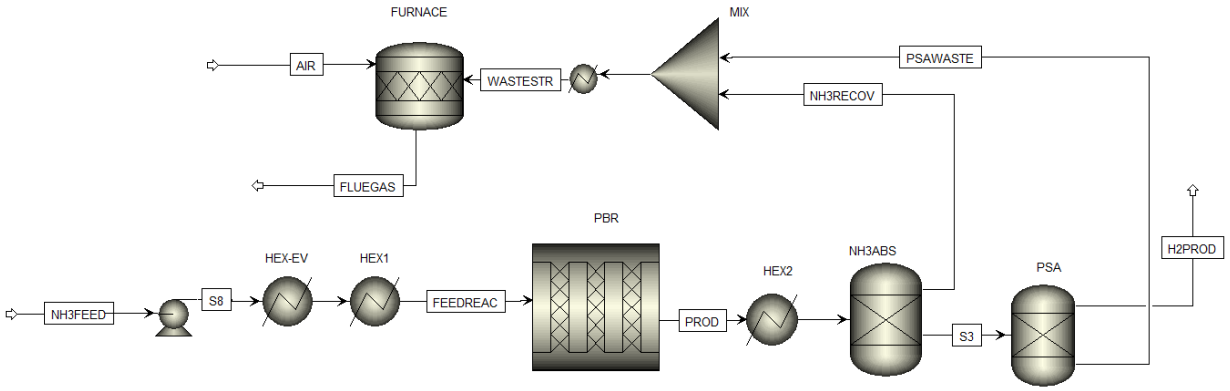

Figure B.2: Simplified process plant flowsheet for minimization of additional heat supply. Made in Aspen Plus V12

The model consists out of 7 main process units, which play as simplified representations of the main process plant subsystems:

1. **Packed Bed Reactor (PBR)**: This unit represents a multi-tubular ammonia cracking reactor. It is simulated as an isothermal plug flow reactor. Its temperature is determined by the outlet temperature prescribed in the HEX1 heater block specifications. It uses the reactor geometry and kinetic model determined during PFR sizing in Subsection 4.2.1. The reactor pressure was set at 10 bar.
2. **Fired Heater (FURNACE)**: This block is a stoichiometric reactor model, which simulates the combustion of the waste stream from H_2 purification. Its heat duty is determined by the the combustion reactions of H_2 and NH_3:

	Fractional conversion	Fractional Conversion of Component	Stoichiometry
	1	NH3	2 NH3 + 1,5 O2 --> 3 H2O(MIXED) + N2(MIXED)
	1	H2	2 H2 + O2 --> 2 H2O(MIXED)

Reference condition

	Rxn No.	Reference component	Heat of reaction	Reference Temperature	Reference Pressure	Reference Phase
			kJ/kmol	K	bar	
	1	NH3	-316801	298,15	1,01325	Vapor
	2	H2	-286000	298,15	1,01325	Vapor

The inputs for this reactor are the air flow(AIR) and the H2 purification waste stream (WASTESTR) blend from simplified H2 purification blocks PSA and NH3ABS. The fuel mixture comprises NH_3, H_2, and N_2 from the waste streams of the purification units. The net duty produced by the FURNACE is

quantified by setting both the input (AIR, WASTESTR) and output stream temperatures (FLUEGAS) at 30°C.

3. **Feed Stream Evaporator (HEXEV)**: Heater Block. After liquid ammonia (NH3FEED) is pumped up to 10 bar, it is evaporated by increasing its temperature up to 30 °C.
4. **Feed Stream Pre-Heater (HEX1)**: Heater Block.The evaporated NH_3 stream is preheated up to operating temperature of PBR. In this model, the output temperature of HEX1 is communicated to PBR as constant temperature along the reactor length. **The analysis of temperature sensitivity of heat duties of defined units is performed by varying the temperature of this block.**
5. **Product Stream Cooler (HEX2)**: Cooler Block. The product stream (PROD) from the PBR is cooled down to 30 $ircC$ before entering the product purification unit NH3ABS.
6. **Ammonia Absorber Unit (NH3ABS)**: Component Separator Block. In this unit, unreacted ammonia is recovered and is directed for combustion in in FURNACE. 100% recovery of ammonia is assumed.
7. **Pressure Swing Adsorber Unit (PSA)**: Component Separator Block. H_2-rich stream from absorber unit (S3) undergoes purification from nitrogen in the PSA system. It's simulated as a simple separator, assuming a 90% recovery of H_2. The waste stream (PSAWASTE), containing unrecovered 10% of produced H_2, is directed to FURNACE as combustion fuel.

For this model, a sensitivity analysis was conducted by varying the output temperature of HEX1, which in turn determines the temperature inside the PBR. The objective was to observe the impact on both the net heat duty in the furnace (FURNACE) and the sum of net heat duties of all heat exchange blocks (HEX-EV, HEX1, HEX2) and the reactor (PBR). The obtained temperature sensitivity plot is plotted in figure B.3.

Through temperature sensitivity analysis, it is observed that the total heat duties produced and consumed are in balance at a reactor temperature of 962 K (or 689 °C), see Figure B.3. The reactor operation at this temperature region is assumed to minimize the fresh NH_3 fuel requirement for the ammonia cracker.

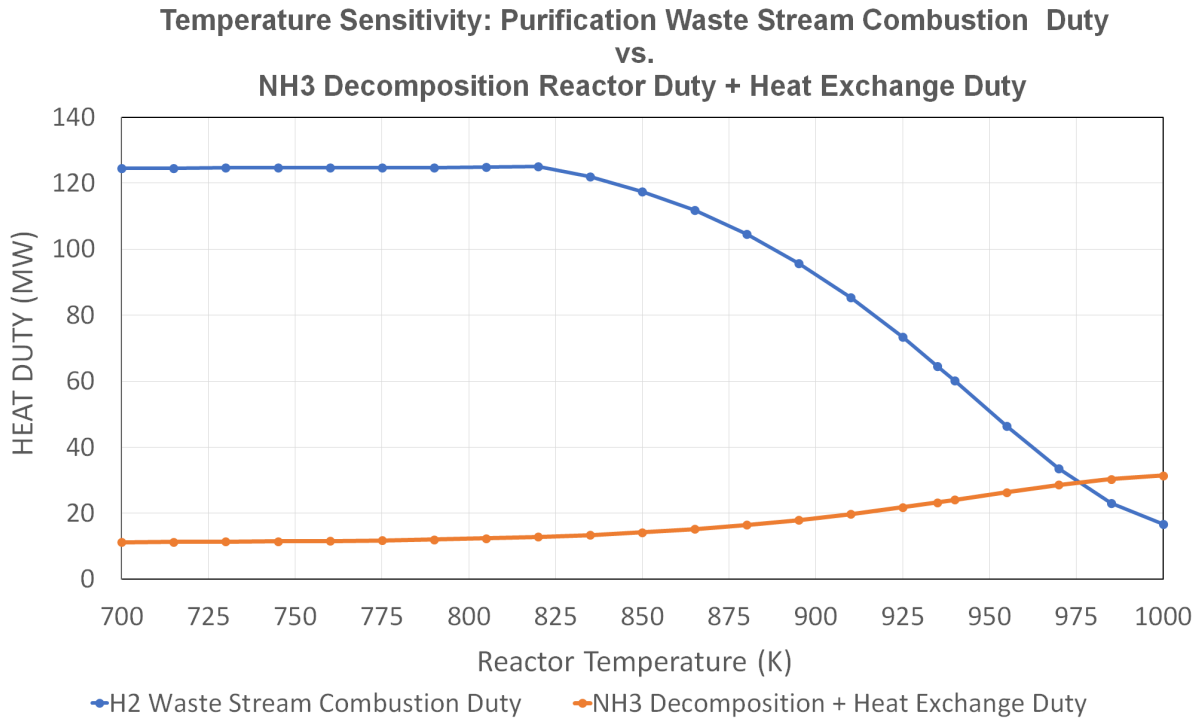

Figure B.3: Temperature sensitivity plot for total duty of H_2 purificationwaste stream combustion and the sum of NH_3 decomposition and required heat exchange duties. The heat balance is pinpointed at T = 962 K (or 689°C).

In the plot shown in Figure B.3, it's evident that the furnace duty and the net duty of the major heat exchangers and of the reactor, cross at a temperature of 962K (689°C). This choice minimizes the

additional ammonia feedstock required for generating heat in the furnace. This establishes it as the optimal temperature for the simulated simplified process plant scenario. This temperature serves as the reference point for further detailed design of the fired heater-cracker system and for subsequent simulation of the entire process plant. To maintain this temperature in the reactor, the furnace is required to transfer at least 30 megawatt of heat to the process.

B.4. Ammonia Cracker Modelling: Isothermal PFR Model Stream Properties from Aspen Plus

Table B.2: The inlet stream (REACFEED) and outlet stream(REACPROD) composition of the isothermal PFR reactor (at P = 10 bar, T = 689°C, F_{NH3} = 640 TPD), modelled in Step 1 of ammonia cracker design.

STREAMS:		REACFEED	REACPROD
Temperature	°C	660	689
Pressure	bar	10	10
Mole Fractions:			
NH3		0,99499	0,0397
H2		1E-05	0,718
N2		1E-05	0,239
H2O		0,00499	0,0026
Mass Flow:	tons/day	640	640
NH3	tons/day	636,6	48,8
H2	tons/day	0	104,3
N2	tons/day	0	483,5
H2O	tons/day	3,4	3,4

B.5. Fired Heater: Determined Fuel, Oxidant and Flue Gas streams of the Fired Heater side of the Ammonia Cracker by Aspen EDR

Table B.3: Compositions and Flowrates of the entering and produced streams in the fired heater.

Fired Heater Burner Streams:		Fuel Stream		Oxidant Stream	Flue Gas
Mole Fractions		**Fresh NH3 Feedstock**	**H2 Purif. Wastestream**	**AIR**	**FLUE GAS**
NH3		99,5%	12%	0%	0
H2		0%	21%	0%	0
N2		0%	67%	79%	76%
H2O		0,5%	0%	0%	23%
O2		0%	0%	21%	1,1%
Mass Flows	**tons/day**	**68**	**518**	**1160**	1746
NH3	**tons/day**	67,8	48,8	0	0
H2	**tons/day**	0	10	0	0
N2	**tons/day**	0	457	890	1442,5
H2O	**tons/day**	0,4	1,63	0	280,2
O2	**tons/day**	0	0	270	23,1

B.6. Fired Heater: Overall Summary from Aspen EDR

Fired Heater Efficiency Related Parameters Overall Efficiency = (Total heat absorbed by all process streams in heater)/(heat released from fuel combustion + sensible heat from fuel and oxidant)

Firebox Efficiency = (Heat absorbed by process stream in firebox)/(heat released from fuel combustion + sensible heat from fuel and oxidant)

Heat released from fuel combustion (W) = flowrate of fuel (kg/s) * Lower calorifcic value of fuel (J/kg).

Sensible heat = Flowrate x (Enthalpy (at inlet temp) - Enthalpy(at 25C))

Figure B.4: Fired Heater Performance Results, copied from Aspen EDR

FiredHeater Summary

Heater duty	kW	35433,8
Overall efficiency (%)	-	89,03
Firebox efficiency (%)	-	51,45
Fuel efficiency (%)	-	88,87
Fuel flowrate	kg/s	1,4708
Oxidant flowrate	kg/s	18,5194
% Excess air		7,862245
Heat from combustion of fuel	kW	39872
Firebox well-stirred gas temperature	°C	939
Bridgewall gas temperature	°C	753
Stack flue gas inlet temperature	°C	173
Stack flue gas outlet temperature	°C	132
Stack oxygen, mass percent, dry	-	1,34
Estimated draught loss	Pa	

Figure B.5: Fired Heater Firebox and Convection Bank Performance Results, copied from Aspen EDR

		Firebox	Bank 1
Process stream number		1	2
Stream name		1	2
Process stream duty	MW	20,575	14,859
Process stream inlet temperature	°C	660	-34
Process stream outlet temperature	°C	668	339
Process stream pressure drop	bar	0,40512	0,49327
Process stream inlet vapor mass fraction	-	1	0
Process stream outlet vapor mass fraction	-	1	1
Process stream mass flux	kg/s/m²	850,66	163,64
Average heat flux	kW/m²	28,6	59,11
Peak tube wall temperature	°C	763	461
Peak fin tip temperature	°C		584
Flue gas inlet temperature	°C		753
Flue gas outlet temperature	°C		180
Flue gas max.mass velocity (mass flux)	kg/s/m²		1,88
Bare tube area	m²	719,4	251,4
Total tube area	m²	719,4	3354,5
Ratio total area / bare tube area	-	1	13,35

B.7. Process Stream Overview for the Firebox and the Convection Bank

Figure B.6: Process Stream Overview for the Firebox and the Convection Bank. The Stream 1, representing the reactor process stream, is increased from 640 TPD upto 1000 kg/s(86400 TPD) to minimize the process stream enthalpy change for heat flux prediction. The Stream 2 is representing the process stream of liquid ammonia, evaporated and preheated by the fluegas stream leaving the firebox.

Process | Inlet+Outlet Properties

		Stream 1	Stream 2
Stream name		1	2
Process stream duty	kW	20575,3	14858,4
Process stream inlet temperature	°C	660	-34
Process stream outlet temperature	°C	668	339
Process stream inlet pressure (abs)	bar	10,2	11
Process stream outlet pressure (abs)	bar	9,79488	10,50673
Process stream pressure drop	bar	0,40512	0,49327
Process stream pressure drop scaling	-	0,1465	1
Process stream inlet vapor mass fraction	-	1	0
Process stream outlet vapor mass fraction	-	1	1
Process stream flowrate (inlet)	kg/s	1000	6,7199
Process stream inlet specific enthalpy	kJ/kg	-1272	-4278,8
Process stream outlet specific enthalpy	kJ/kg	-1251,4	-2067,7

B.8. Hydrogen Purification

A. Hydrogen Purification: Absorber-Stripper System Stream Results

Table B.4: Absorber and Stripper Stream Results from Aspen Plus

ABSORBER STREAMS					
		FEEDGAS	SOL2ABS	NH3RICH	PUREGAS
Temperature	C	30,00	30,00	46,03	30,32
Pressure	bar	9,79	9,79	9,84	9,79
Mole Fractions					
NH3		0,0370	4,29E-05	0,042097	6E-6
H2		0,7203	1,09E-43	2,80E-06	0,747149
N2		0,2401	6,59E-45	6,25E-07	0,249053
H2O		0,0026	0,999957	0,9579	0,003792
Mass Flows	tons/day	640,0	1100	1144	595,8
NH3	tons/day	45,6	0,045	45,63964	0,0066751
H2	tons/day	104,9	0	0,000359	104,9357
N2	tons/day	486,1	0	0,001115	486,08382
H2O	tons/day	3,4	1100	1099	4,76

STRIPPER STREAMS				
		SRBFEED	NH3LEAN	NH3REC
Temperature	C	82	102,8661	34,83876
Pressure	bar	1,00	1,05	1,00
Mole Fractions				
NH3		0,042096501	4,30E-05	0,967492
H2		0,0000	1,10E-43	6,44E-05
N2		0,0000	6,61E-45	1,44E-05
H2O		0,9579	1,00E+00	3,24E-02
Mass Flows	tons/day	1144,2132	1097	47,21316
NH3	tons/day	45,6	0	46
H2	tons/day	0,0	0,000	0,000359
N2	tons/day	0,0	0	0,001115
H2O	tons/day	1098,6	1097	1,616647

B. Pressure Swing Adsorption Streams

Table B.5: Results from the PSA component separator

PSA STREAMS				
		ABSPROD(FEED)	PSA-PROD	PSAWASTE
Mole Fractions				
NH3		0,0000059	0,0000086	0
H2		0,7471	0,9746	0,2410
N2		0,2491	0,0199	0,7590
H2O		0,0038	0,0055	0
O2		0	0	0
Mass Flows	tons/day	592,6	125,3	467,3
NH3	tons/day	0,0070018	0,007	0
H2	tons/day	104,3730061	93,936	10,4373006
N2	tons/day	483,4773556	26,640	456,8371785
H2O	tons/day	4,7457876	4,746	0
O2	tons/day	0	0	0

B.9. Membrane Reactor: Effect of Pressure Ratio on H_2 Recovery and NH_3 Conversion

For the Pd-Au membrane, the effect of absolute pressure difference between permeate and retentate on NH_3 conversion and hydrogen product recovery is visualized in the figure B.7[38]. This behaviour is determined by the experiments done by (Cerrillo J., 2022 [38]). It is visible that with increasing the absolute pressure ratio between the membrane retentate and permeate, both the NH_3 conversion and recovery of produced H_2 in the permeate increase.

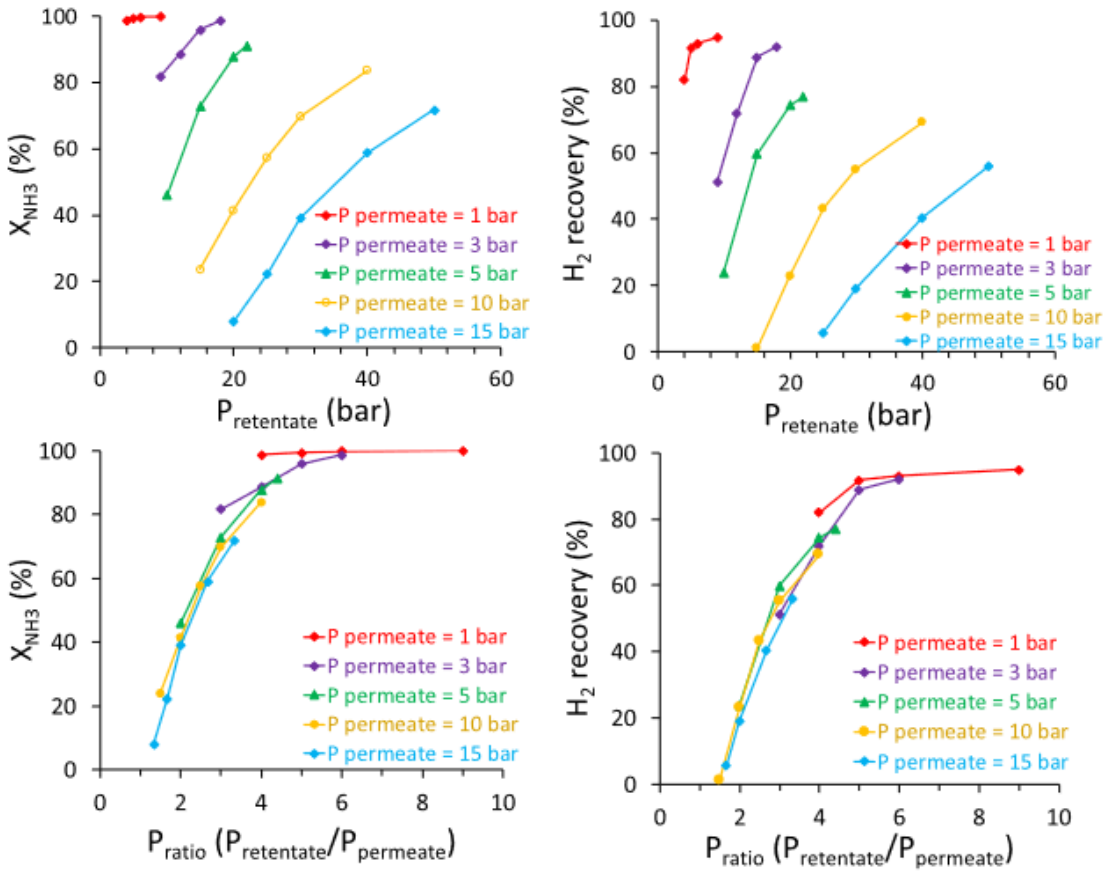

Fig. 6. Effect of the permeate pressure using different retentate pressures on conversion and H_2-recovery. Reaction conditions: 0.5%Ba-CoCe catalyst: 10 g (350–500 µm) diluted with 10 g of SiC – 680 µm. Ammonia flow rate 200 N mL min^{-1}, T = 485 °C , $P_{retentate}$ = 4–50 bar, $P_{permeate}$ = 1–15 bar.

Figure B.7: The effect of the permeate pressure using different retentate pressures on conversion and hydrogen recovery, is visualised. Experimental results by (Cerrillo, J. 2022)[38].

B.10. Membrane Reactor: Membrane Module Sizing from Reference Case

In the figure below the Pd-membrane properties and sizing assumptions are compared side by side to the reference case taken from the published experimental case by (Kim,2022) [40], which reports the highest reported hydrogen permeation reported.

Reference Case Taken from Paper by Kim [37]	
Area of membrane unit:	0,0175 m2
NH3 feed flow rate (@ 30 degC, 5barg) :	2365 ml/min
Corresponding mass flow rate	0,015 TPD
F/A (feed flow/mem.area)	13.5 ml min-1cm-2
Pressure Ratio	6.67
Retentate Pressure	6 bar
Permeate Pressure	0.9 bar
Membrane thickness:	4 µm
H2/N2 selectivity	335
H2/NH3 selectivity	unreported by Kim [37], reported to be the same order of magnitude by Ji Jiang [58]
H2 Recovery at given flowrate	approx. 90%
Reactor Temp	703 K
NH3 conversion without membrane module (Ru-based catalyst)	30%
NH3 conversion with membrane module	98%

Upscaled case for this study	
Area of membrane unit:	763 m2
mass flow rate	640 TPD
F/A (feed flow/mem.area)	13.5 ml min-1cm-2
Pressure Ratio	7,5
Retentate Pressure	15 bar; 30 bar; 60 bar
Permeate Pressure	2 bar; 4 bar; 8 bar
Membrane thickness:	1
H2/N2 selectivity	300
H2/NH3 selectivity	300
H2 Recovery at given flowrate	approx 90%
Reactor Temp	773 K
NH3 conversion without membrane module (Ni/Al2O3 in a monolith-structured catalyst bed, by Armenise 2010)	20% (from literature, at 1 bar pressure)
NH3 conversion with membrane module	97-99% (from Aspen Plus outputs for different retentate pressures)

Figure B.8: Comparison of membrane sizing and properties in the up-scaled case and the reference case by (Kim,2022)[40]. Note": on the right table (up-scaled case) the membrane thickness is 1μm

C

Economic Analysis

C.1. Case I: Equipment Cost List

Table C.1: Case I: Equipment Cost List

CASE I: EQUIPMENT PRICE LIST		Exch. Rateof Dollar to Euro = 1.05 CEPCI 2023: 803,2	
ITEM CODE	**NAME**	**COST BARE MODULE (CEPCI 2023)**	**SOURCE & NOTES**
REFORMER	**AMMONIA CRACKING**	**€23,5 mln**	
	Fired Heater-Cracker	€ 17.900.000,00	Scaling fromP=10 bar; 35.4 MW; Stainless Steel
	Catalyst Packing	€ 5.640.000	14.1m3 catalyst bed; NiAl2O3-crushed monolith, Initial cost assumption = 400€/dm3
PSA	**HYDROGEN PURIFICATION**	**€4,0 mln**	
PSA-COMP	Compressor	€ 2.621.282,80	Aspen Economic Analyzer V12: Assumed equivalent to downstream compressor cost
	Adsortption Towers (2x)	€ 419.404,74	Assumed equivalent to ABS-Tower in Ammonia Recovery @ 10 bar operating pressure
DRY	DRYING UNIT	**€ 1.000.000**	Assumption
	AMMONIA RECOVERY	**€,6 mln**	
B2	Solvent Cooler	€ 57.234,40	Aspen Economic Analyzer V12
	Stripper-condenser	€ 54.987,33	Aspen Economic Analyzer V12
	Stripper-cond. acc.	€ 16.654,81	Aspen Economic Analyzer V12
	Stripper-reboiler	€ 55.251,69	Aspen Economic Analyzer V12
	Stripper-reflux pump	€ 7.798,68	Aspen Economic Analyzer V12
STRIPPER	Stripper tower	€ 132.313,25	Aspen Economic Analyzer V12
ABSORBER	Absorption tower	€ 209.702,37	Assumption (scaled from stripper column; cost scale factor with pressure = 0.2)
B6	Solvent Stream Heat Exchanger	€ 41.504,86	Aspen Economic Analyzer V12
	HEAT RECUPERATION	**€,7 mln**	
B8	HEX-1	€ 341.027,16	Aspen Economic Analyzer V12
HEX-2	HEX-2	€ 156.238,02	Aspen Economic Analyzer V12
HEX-3	COOLER	€ 48.774,81	Aspen Economic Analyzer V12
B10	COOLER-extra	€ 128.347,82	Aspen Economic Analyzer V12
B4	HEATER	€ 14.539,92	Aspen Economic Analyzer V12
	COMPRESSION	**€5,2 mln**	
C1	COMPRESSOR-1 (+ intercooling)	€ 2.621.282,80	Aspen Economic Analyzer V12
C2	COMPRESSOR-2 (+ intercooling)	€ 2.621.282,80	Aspen Economic Analyzer V12
	MISCELLANEOUS	**€1,0 mln**	
SCR	SCR UNIT	**€ 1.000.000**	Assumption
PUMP	LIQ NH3 PUMP	**€ 30.402,61**	Scaled from Sinott&Towler
	TOTAL EQUIPMENT COST:	**€35,1 mln**	

C.2. Case II: Equipment Cost List

Table C.2: Case II: Equipment cost list for various membrane module retentate pressures (15 bar, 30 bar, 60 bar)

SCENARIO II: EQUIPMENT PRICE LIST		Exch. Rateof Dollar to Euro = 1.05;			CEPCI 2023: 803,2
ITEM CODE	NAME	COST BARE MODULE (CEPCI 2023)			SOURCES & NOTES:
		Case 1: 15 bar retentate	Case 2: 30 bar retentate	Case 3: 60 bar retentate	
	AMMONIA CRACKING	**€ 21,0 mln**	**€ 21,2 mln**	**€ 24,2 mln**	
	REFORMER-FURNACE	€ 15.341.089	€ 15.514.641	€ 18.566.599	P=10 bar; 33 MW; Stainless Steel
	Catalyst Packing: (Unit: Volume: dm3)	€ 5.640.000	€ 5.640.000	€ 5.640.000	Catalyst (NiAl2O3-monolith reference). Initial cost assumption = 400 EUR/dm3; Same catalyst loading assumed as for base case.
	MEMBRANE-INTEGRATION	**€ 3,0 mln**	**€ 3,0 mln**	**€ 3,0 mln**	**From Literature: Support + 90% Selective Layer Recycling. Selective layer thickness: 1µm**
	TSA AMMONIA REMOVAL	**€ ,3 mln**	**€ ,3 mln**	**€ ,3 mln**	
	2 TSA Columns	€ 264.692	€ 264.692	€ 349.960	Assumption: cost of the stripper in base case (operation at P atm and elevated temperatures)
	HEAT RECUPERATION	**€ ,2 mln**	€ ,1 mln	€ ,2 mln	
	EVAP-HEX	**€ 36.491**	€ 29.880	€ 136.841	Aspen Economic Analyzer V12
	HEX-1	€ 31.996	€ 39.003	€ 67.561	Aspen Economic Analyzer V12
	B1 (HEX-2)	€ 155.087	€ 34.640	€ 31.017	Aspen Economic Analyzer V12
	B18	€ 14.940	€ 14.940	€ 14.544	Aspen Economic Analyzer V12
	COOLER	€ 139.221	€ 70.999	€ 100.747	Aspen Economic Analyzer V12
	COMPRESSION SYSTEM	**€ 10,2 mln**	**€ 6,4 mln**	**€ 5,4 mln**	
	COMP-1	€ 5.112.451	€ 3.186.357	€ 2.678.127	Aspen Economic Analyzer V12
	COMP-2	€ 5.112.451	€ 3.186.357	€ 2.678.127	Aspen Economic Analyzer V12
	MISC	**€ 1,0 mln**	**€ 1,1 mln**	**€ 1,2 mln**	
	PUMP1	**€ 30.674**	€ 91.095	€ 159.847	Aspen Economic Analyzer V12
	SCR Unit	€ 1.000.000	€ 1.000.000	€ 1.000.000	Aspen Economic Analyzer V12
	TOTAL EQUIPMENT COST:	**€ 35,7 mln**	**€ 32,0 mln**	**€ 34,3 mln**	

C.3. Reactor Modelling: Catalyst Kinetics Model Employed

During the selection of an appropriate catalyst, the models were taken from three different sources.

- Ni/Al2O3/monolith catalyst: Taken from the paper from 2013 by Armenise S. [89]. This paper was making the kinetic model of the reaction rate for the ammonia decomposition kinetics of the Ni/Al2O3/monolith catalyst. The kinetic models were based on Langmuir isotherm assumption. There, multiple reaction, adsorption and desorption stages were taken into account (see figure C.1 depicting stages).

$$\text{(i)}\ NH_3 + * \overset{k'_0, k'_{-0}}{\longleftrightarrow} NH_3*$$
$$\text{(ii)}\ NH_3* + * \overset{k'_1, k'_{-1}}{\longleftrightarrow} NH_2* + H*$$
$$\text{(iii)}\ NH_2* + * \overset{k'_2, k'_{-2}}{\longleftrightarrow} NH* + H*$$
$$\text{(iv)}\ NH* + * \overset{k_1, k_{-1}}{\longleftrightarrow} N* + H*$$
$$\text{(v)}\ \frac{3}{2}\left[2H* \overset{k'_{H_2}, k'_{H_2}}{\longleftrightarrow} H_2 + 2*\right]$$
$$\text{(vi)}\ \frac{1}{2}\left[2N* \overset{k'_{N_2}, k'_{-N_2}}{\longleftrightarrow} N_2 + 2*\right]$$

Figure C.1: Reaction Stages for ammonia decomposition over Ni/Al2O3/monolith catalyst[89]

It was derived by Armenise S. that desorption of adsorbed nitrogen atoms to the catalyst is the controlling step, and other stages are attaining the chemical equilibrium. The piece on value of reaction constants and final reaction rate expression is copied from [89] to figure **??**. The values of these constants were experimentally derived. The table with data on conditions on 13 conducted experiments is put in figure C.2

Experiment	$W/F_{NH_3,0}$ (g s mol^{-1})	$p_{NH_3,0}$ (atm)	$p_{H_2,0}$ (atm)	$p_{Ar,0}$ (atm)
1	13 921.9	0.031	0.494	0.475
2	3333.4	0.108	0.786	0.107
3	1342.5	0.219	0.664	0.117
4	1407.3	0.233	0.767	0.000
5	729.2	0.302	0.456	0.242
6	1029.5	0.303	0.697	0.000
7	739.1	0.376	0.624	0.000
8	568.0	0.439	0.561	0.000
9	831.6	0.515	0.000	0.485
10	431.0	0.507	0.493	0.000
11	380.0	0.737	0.263	0.000
12	420.3	0.849	0.151	0.000
13	444.3	1.000	0.000	0.000

Figure C.2: Enter Caption

Based on the research results, the writers concluded that the case where all of the adsorption and desorption steps are taken into account gives the most accurate estimation of the prepared catalyst.

The term * denotes a vacant site, and NH_3*, NH_2*, NH*, N* and H* are the adsorbed species. If all the above reactions are equilibrated, the constants of equilibrium can be expressed in terms of concentration of adsorbed species as:

$$K_0 = \frac{k'_0}{k'_{-0}} = \frac{[NH_3*]}{p_{NH_3}[*]} \quad (3)$$

$$K_1 = \frac{k'_1}{k'_{-1}} = \frac{[NH_2^*]\,[H^*]}{[NH_3^*]\,[*]} \quad (4)$$

$$K_2 = \frac{k'_2}{k'_{-2}} = \frac{[NH*]\,[H*]}{[NH_2*]\,[*]} \quad (5)$$

$$K_3 = \frac{k'_3}{k'_{-3}} = \frac{[N*]\,[H*]}{[NH*]\,[*]} \quad (6)$$

$$K_{H_2} = \frac{k'_{-H_2}}{k'_{H_2}} = \frac{[H*]^2}{pH_2[*]^2} \quad (7)$$

$$K_{N_2} = \frac{k'_{-N_2}}{k'_{N_2}} = \frac{[N*]^2}{pN_2[*]^2} \quad (8)$$

If it is supposed that the desorption on N*, stage (vi), is slow but reversible, and the rest of the stages attains the equilibrium (named Case A), then eqn (8) does not apply and the reaction rate will be given by:

$$(-r_{NH_3}) = k'_{N_2}[N*]^2 - k'_{-N_2}pN_2[*]^2 \quad (9)$$

Figure C.3: Equilibrium constants expression and the reaction rate expression from [89]

This reaction-rate kinetics was modelled in two ways. THe reactin rate unit for this model is given in $\frac{mol}{g_{cat}*s*atm^{\alpha+\beta}}$

- **LHHW kinetics model:** First it was modelled in explicit form of Langmuir-Hinshelwood-Hougen-Watson (LHHW) kinetics model, which considers the rate of adsorption during catalytic decomposition. From derivation of the fractional coverage (θ) of all the adsorbed species, the LHHW model was formulated (see figure C.4)

$$(-r_{NH_3}) = \frac{k_A\left(\frac{K_0^2K_1^2K_2^2K_3^2}{K_{H_2}^3}\right)\frac{p_{NH_3}^2}{p_{H_2}^3}\left(1-\frac{1}{K_{eq}}\frac{p_{N_2}p_{H_2}^3}{p_{NH_3}^2}\right)}{\left(1+\sqrt{K_{H_2}p_{H_2}}+K_0p_{NH_3}\left(1+\frac{K_1}{\sqrt{K_{H_2}p_{H_2}}}\left(1+\frac{K_2}{\sqrt{K_{H_2}p_{H_2}}}\left(1+\frac{K_3}{\sqrt{K_{H_2}p_{H_2}}}\right)\right)\right)\right)^2}$$

Figure C.4: Adsorption/Desorption rate considering (LHHW) model by Armenise S.[89]

- **Temkin Pyzhev kinetics model:** As alternative for this explicit LHHW model, a more simple powerlaw model was derived. It was done by mapping of data of 13 different experiments

with various flow rates and inlet feed NH3/H2/Ar(inert) ratios (figure C.2 to a simple power-law formula, which is also known as Temkin-Pyzhev model (see figure C.5.

$$\left(-r_{NH_3}\right) = 4.859 \times 10^8 \exp\left(-\frac{202835}{RT}\right)\left(\frac{{p_{NH_3}}^{0.73}}{{p_{H_2}}^{0.64}}\right) \qquad (81)$$

Figure C.5: Temkin-Pyzhev model by Armenise S.[89]

The power-law model did not have the reaction equilibrium constant K_{eq}. It was done due to the reaction through all of the conducted experiments being far from equilibrium, making the value of K_eq virtually 0. For the modelling of the reactor in chapter **??** on process modelling this assumption was taken into account during reactor sizing by ensuring same residence time of process fluid in the packed bed.

A. Kinetic Models Validation in MathCad

The expressions for both approaches of kinetics modelling were initially plugged into Aspen Plus V12 Packed bed reactor. However, they did not give the realistic output. Therefore the models were reproduced in MathCad to check the models. See the screenshots of mathcad file below.

Initially the reaction rate for the powerlaw model by Armenise S.[89] was plotted over mole fraction of ammonia in a mixture (figureC.6).

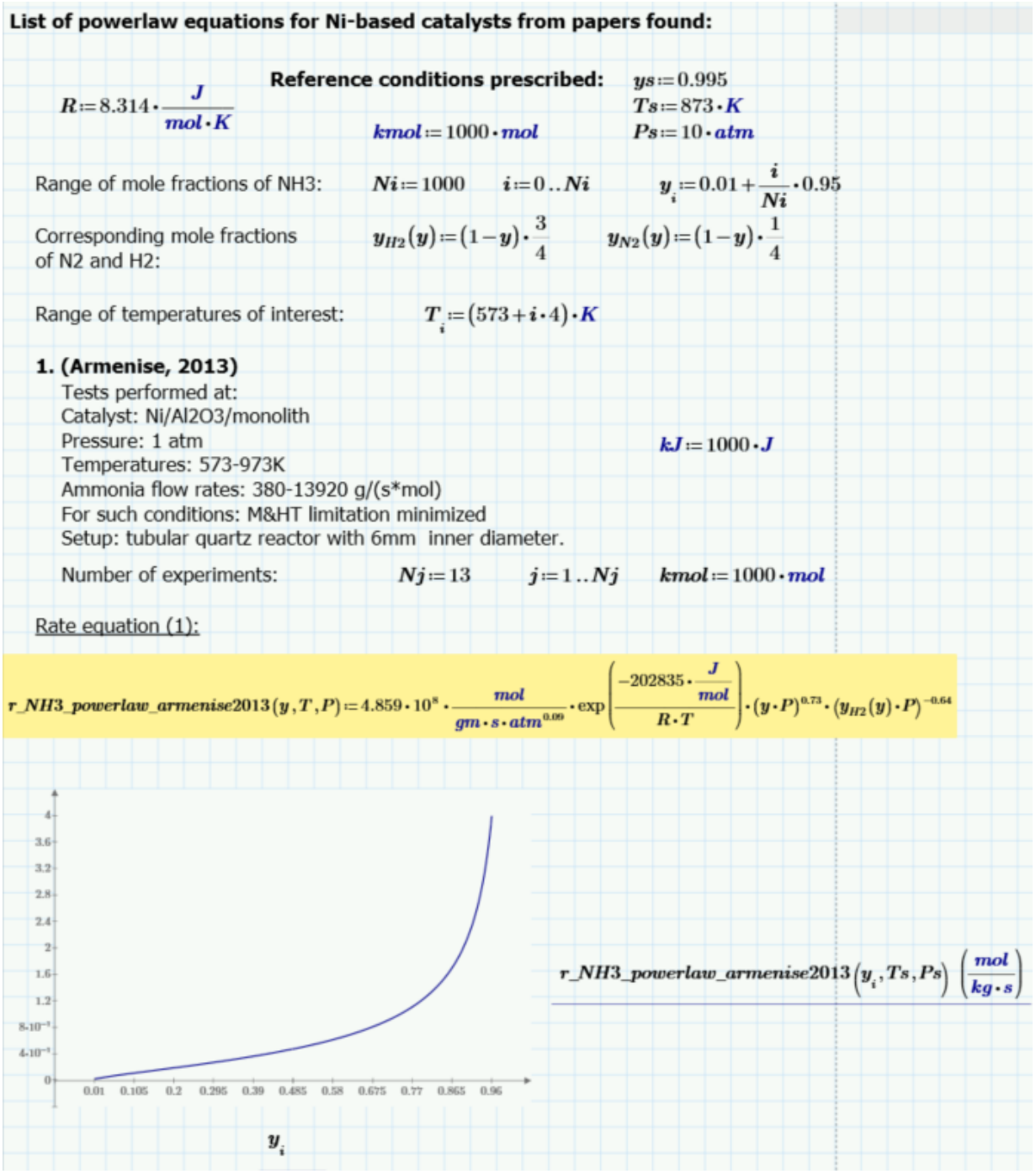

Figure C.6: powerlaw model by Armenise

Then all of the 13 experimental cases were formulated (C.7) and plotted (C.9).

Figure C.7: Parameters for all 13 experimental conditions

The figure C.9 clearly shows that the derived powerlaw expression is indeed the average of the performed experiments. Only two of the experiments were clearly much off. However, the experimental conditions themselves (figure C.2) do not provide a strong reason for such a deviation. It might be only attributed to the experimantal inaccuracy, based on the data provided in the paper.

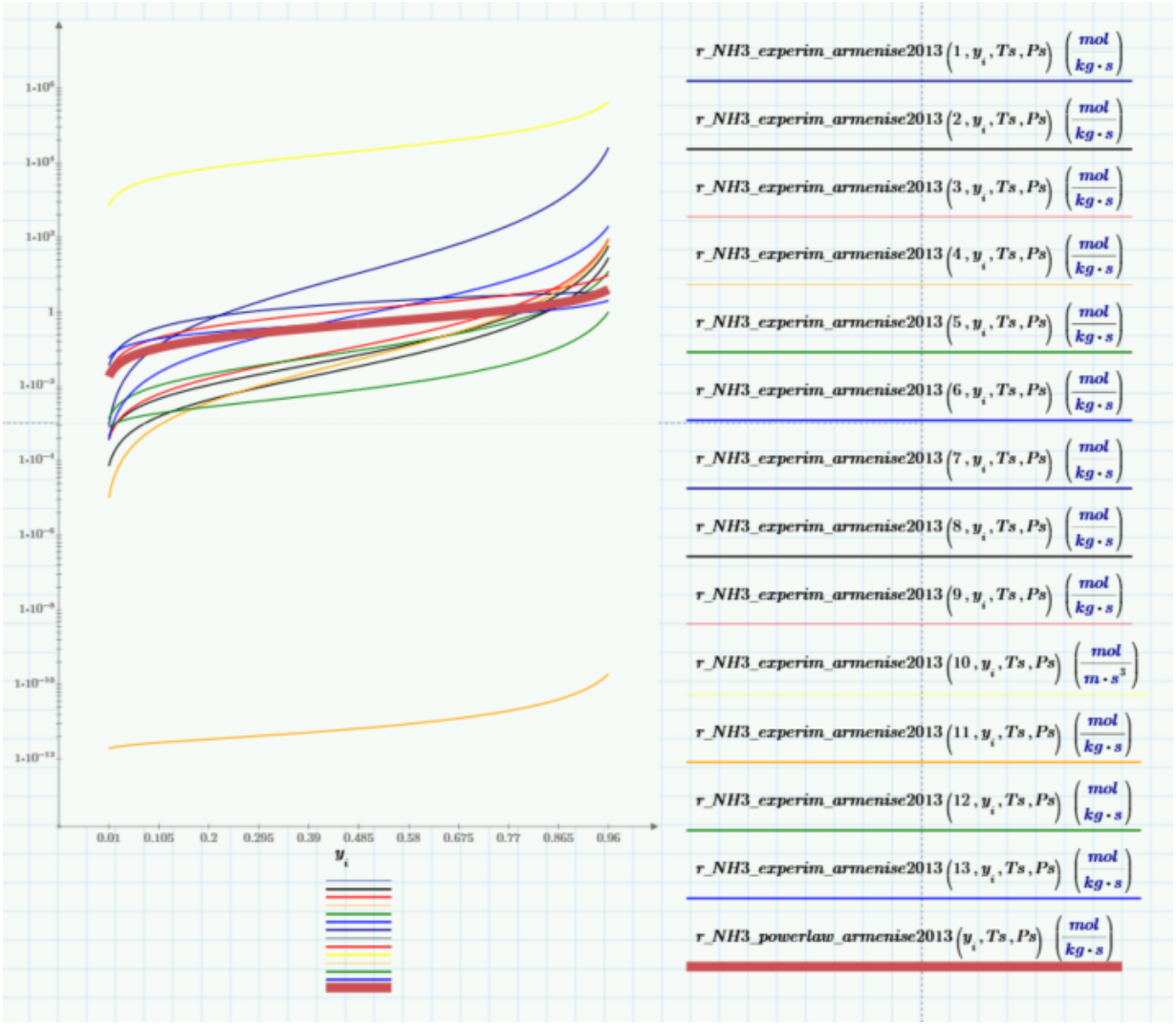

Figure C.8: Enter Caption

Figure C.9: the derived powerlaw expression is indeed the average of the performed experiments

Then, the LHHW model expression was formulated by defining all of the equilibrium constants from the paper (figure **??**) and expressing reaction rate as the LHHW model provided in the literature (C.4). See the expression in Mathcad format in figure **??**.

Figure C.10: Equilibrium constants expressions for the LHHW model by Armenise [89]

$$r\_NH3\_lhhw\_armenise2013(y,T,P) := \frac{k\_A(T)\cdot\left(\frac{K\_0(T)^2\cdot K\_1(T)^2\cdot K\_2(T)^2\cdot K\_3(T)^2}{K\_H2(T)^3}\right)\cdot\frac{(y\cdot P)^2}{(y_{H2}(y)\cdot P)^3}\cdot\left(1-\frac{1}{K\_eq\_est(T)}\cdot\frac{(y_{N2}(y)\cdot P)\cdot(y_{H2}(y)\cdot P)^3}{(y\cdot P)^2}\right)}{\left(1+\sqrt{K\_H2(T)\cdot y_{H2}(y)\cdot P}\cdot 1+K\_0(T)\cdot y\cdot P\cdot\left(1+\frac{K\_1(T)\cdot atm}{\sqrt{K\_H2(T)\cdot y_{H2}(y)\cdot P}}\cdot\left(1+\frac{K\_2(T)\cdot atm}{\sqrt{K\_H2(T)\cdot y_{H2}(y)\cdot P}}\cdot\left(1+\frac{K\_3(T)\cdot atm}{\sqrt{K\_H2(T)\cdot y_{H2}(y)\cdot P}}\right)\right)\right)\right)^2}$$

Figure C.11: LHHW model by Armenise [89] in MathCad

An important result was obtained from the comparison of powerlaw and LHHW model by armenise. The plot on figure C.12 clearly shows, that the powerlaw expression based on the published data contains errors, as the reaction rate produced by LHHW was at least 10^{25} times less when filling in the published parameters.
Therefore, the LHHW model had to be, unfortunately, left behind and only the powerlaw expression was used for modelling, as it does come across as the average of the experimental data.

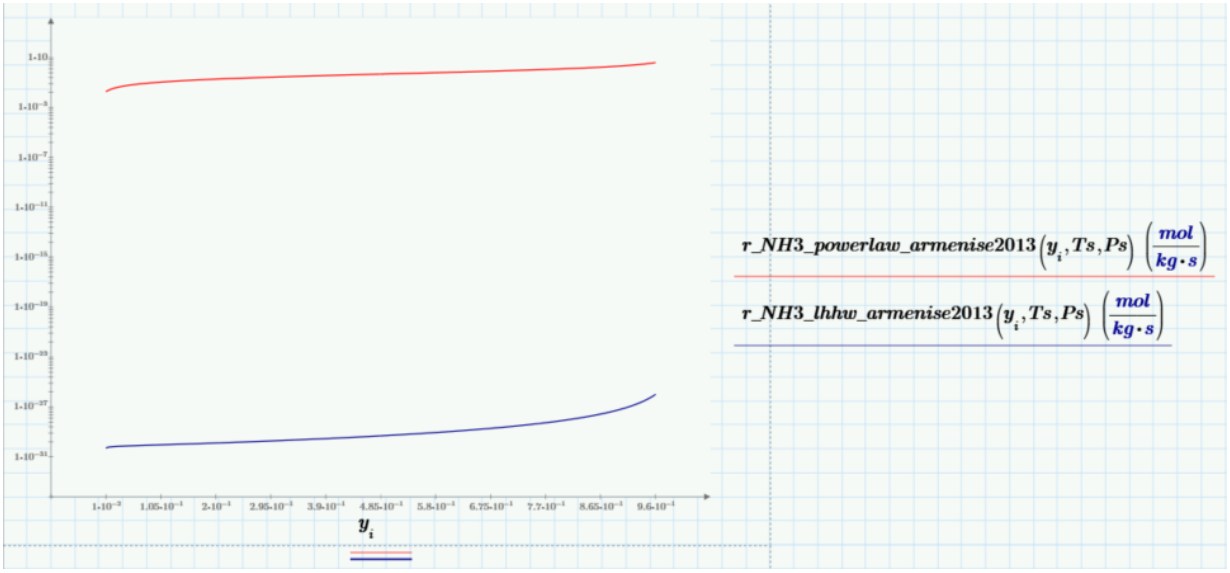

Figure C.12: LHHW model shows much lower reaction rate than powerlaw, which coincides well with the experiments. Conclusion:LHHW model can not be reproduced accurately with the published data

- The second paper which was used to find the kinetics of the Ni/Al2O3 Catalyst was published by Chellappa in 2002 [130]. There, **Ni-Pt/Al2O3 catalyst** was analysed for NH3 decomposition for hydrogen production for PEM fuel cell application. The first plot on the figure **??** that the reaction rate is in the same order of magnitude as the one by Armenise [89]. However, the reaction rate expression is much more simple as there the reaction rate is solely dependent on the partial pressure of ammonia, which is assumed to be a too strong simplification of the kinetics. Therefore, this kinetic model was abandoned.

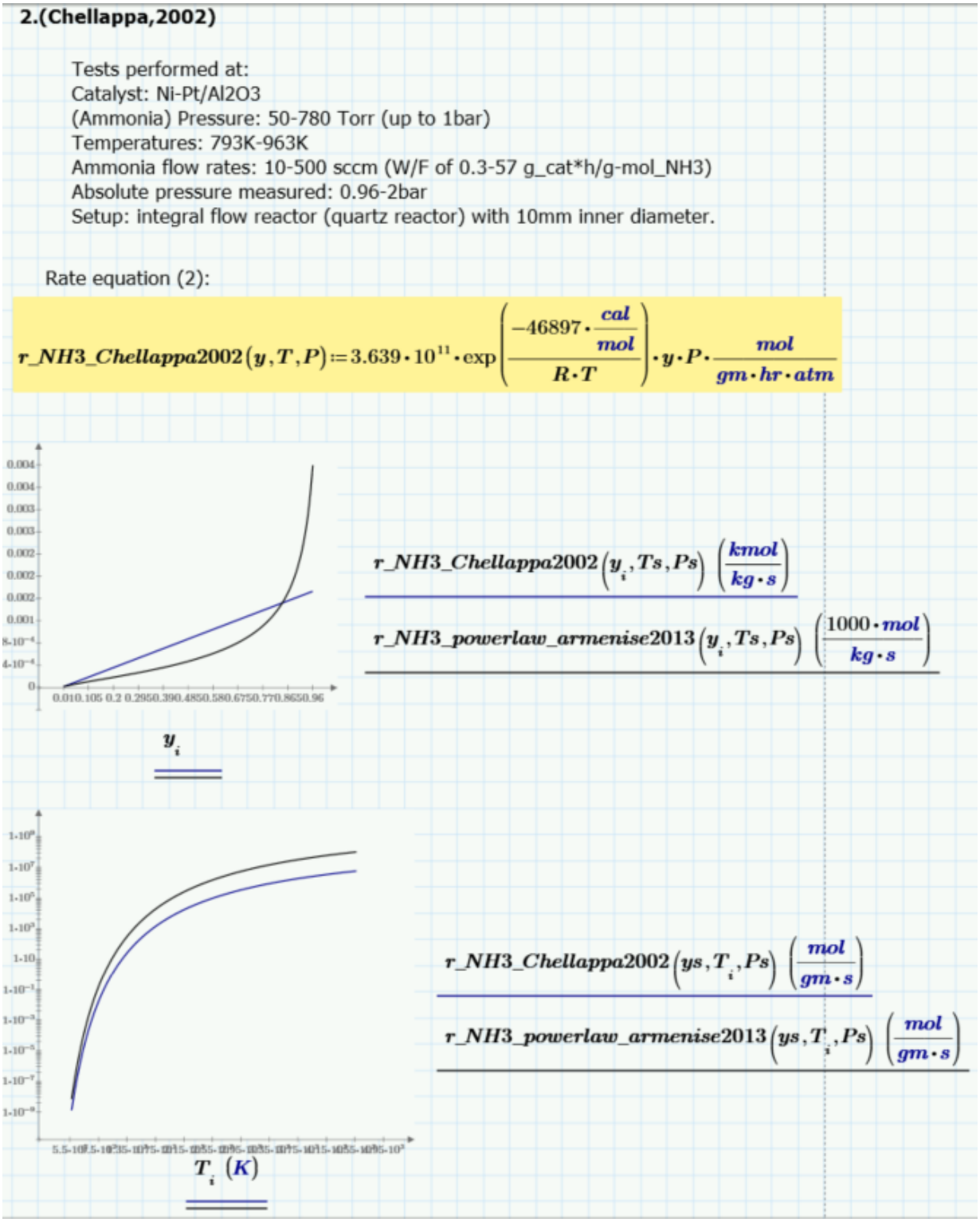

Figure C.13: Reaction Rate of the Catalyst published by Chellappa[130]. Comparison with Armenise [89]

- The paper by Zhang J.[131] was researching ammonia cracking with a Ni-La/Al2O3 catalyst (figure C.14. However, The issue with that paper was that it calculates the reaction rate per 'nanoparticle' of a used catalyst. No information is provided about the configuration of the catalyst packing. Therefore, this paper was abandoned.

3. (Wang, 2019)

Tests performed at:
Catalyst: Ni _1.20/La_0.32-Al2O3
(Ammonia) Pressure: 0.01bar-0.25bar permeate pressure. **1 bar** at retentate.
Temperatures: 373-573K
Ammonia flow rates: 600 sccm (7.59mg/s)
Absolute pressure measured: 1bar at retentate
Setup: Simulation. Conceptual solar-driven hydrogen decomposition. Ni _1.20/ La_0.32-Al2O3 catalyst reactor. The ammonia continuously flows into the tube at a constant molar ratio. Hydrogen is transported through the HPM driven by the pressure difference of hydrogen between inside and outside membrane.The HPM reactor equipment is shown in Fig. 2, and the outer (R0) and inner radii (Rin) of the palladium membrane are 1 cm and 0.95 cm, respectively.

MULTIPLE ERRORS IN UNITS DETECTED. Links lead to non-existing sources (in open source) ***UNUSABLE***

Th reaction rate is given in mol/s per nanoparticle Ni0 (see source of the model (Zhang 2005):https://www.sciencedirect.com/science/article/pii/S0926860X05006538?casa_token=k9YQCi_tmv8AAAAA:d2n-WlNeHXpdgZz5uzaFwTvFm1FAak0NAejA8xzg_QOaswQg393YSNZQ6EctuiYbFajSawJZjlM)

$$r_A = k\cdot\left[\left(\frac{P_{NH_3}^2}{P_{H_2}^3}\right)^{\beta} - \frac{P_{N_2}}{K_{eq}^2}\left(\frac{P_{H_2}^3}{P_{NH_3}^2}\right)^{1-\beta}\right]$$

$$k = k_0 e^{-Ea/RT_0}$$

$$beta2019 := 0.166$$

$$k0\_2019 := 13.51\cdot 10^6 \cdot \frac{mol\cdot bar^{0.166}}{s} \qquad Ea\_2019 := 107.1\cdot 1000\cdot \frac{J}{mol}$$

$$k\_2019(T) := k0\_2019\cdot \exp\left(\frac{-Ea\_2019}{R\cdot T}\right)$$

$$r\_NH3\_Wang2019(y,T,P) := k\_2019(T)\cdot\left(\left(\frac{(y\cdot P)^2}{(y_{H2}(y)\cdot P)^3}\right)^{0.166} - \frac{y_{N2}(y)\cdot P}{K\_eq\_est(T)}\cdot\left(\frac{(y_{H2}(y)\cdot P)^3}{(y\cdot P)^2}\right)^{0.834}\right)$$

Figure C.14: Kinetic model over Ni-nanoparticles from [131]

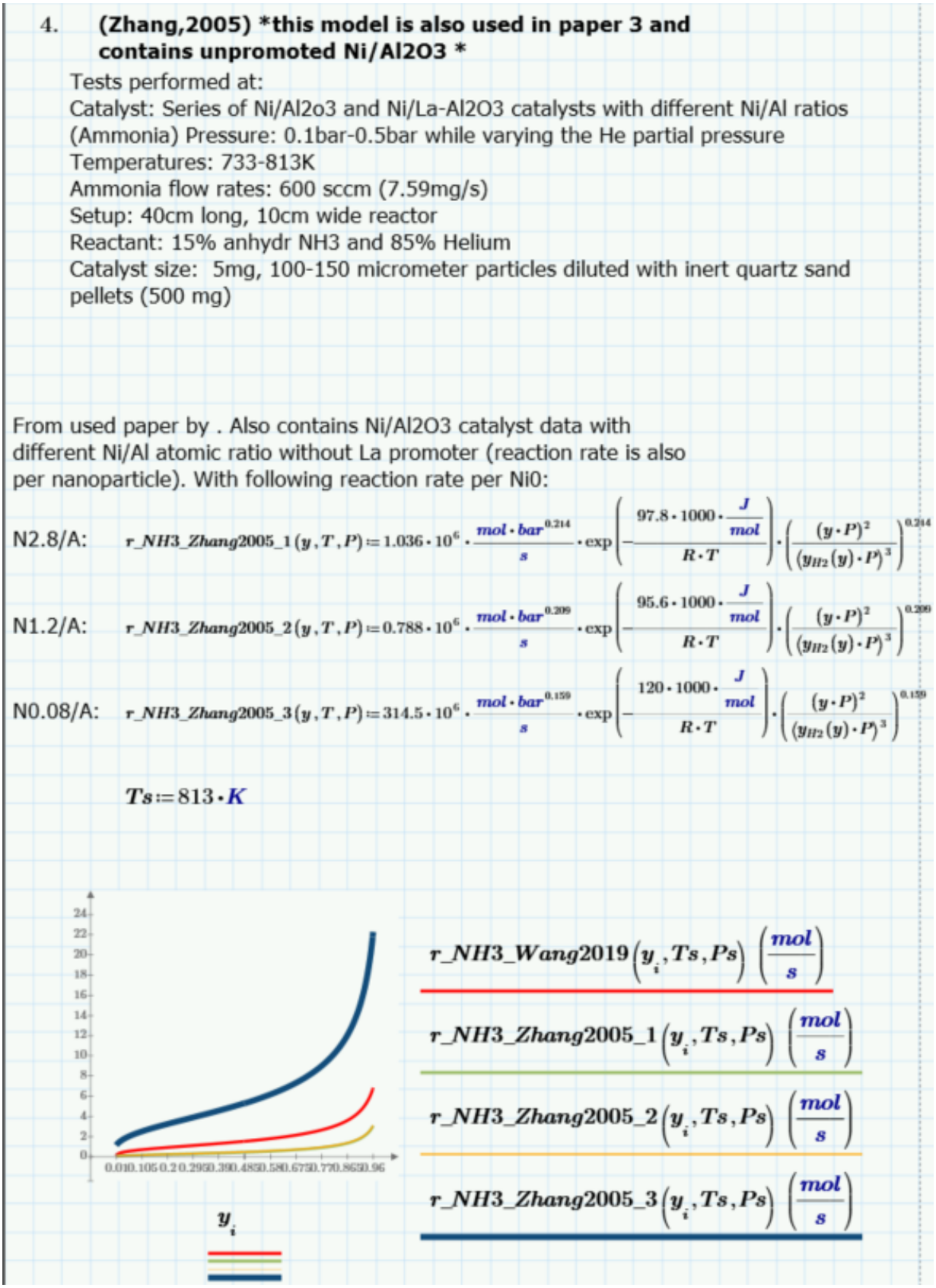

Figure C.15: Enter Caption

Based on all of the reviewed papers of kinetics, only the ones by Armenise,2013 and Chellappa, 2002 were giving realistic outputs in the same order of magnitude. Their units had to be converted to the Aspen standards (see figure C.16 for parameters in Aspen format)

In the end, only the paper by Armenise [89] appeared to be applicable due to its consideration of various reaction mechanisms and reproducability. Therefore, it was selected as the model of choice for the packed bed of the ammonia cracker in this research paper.

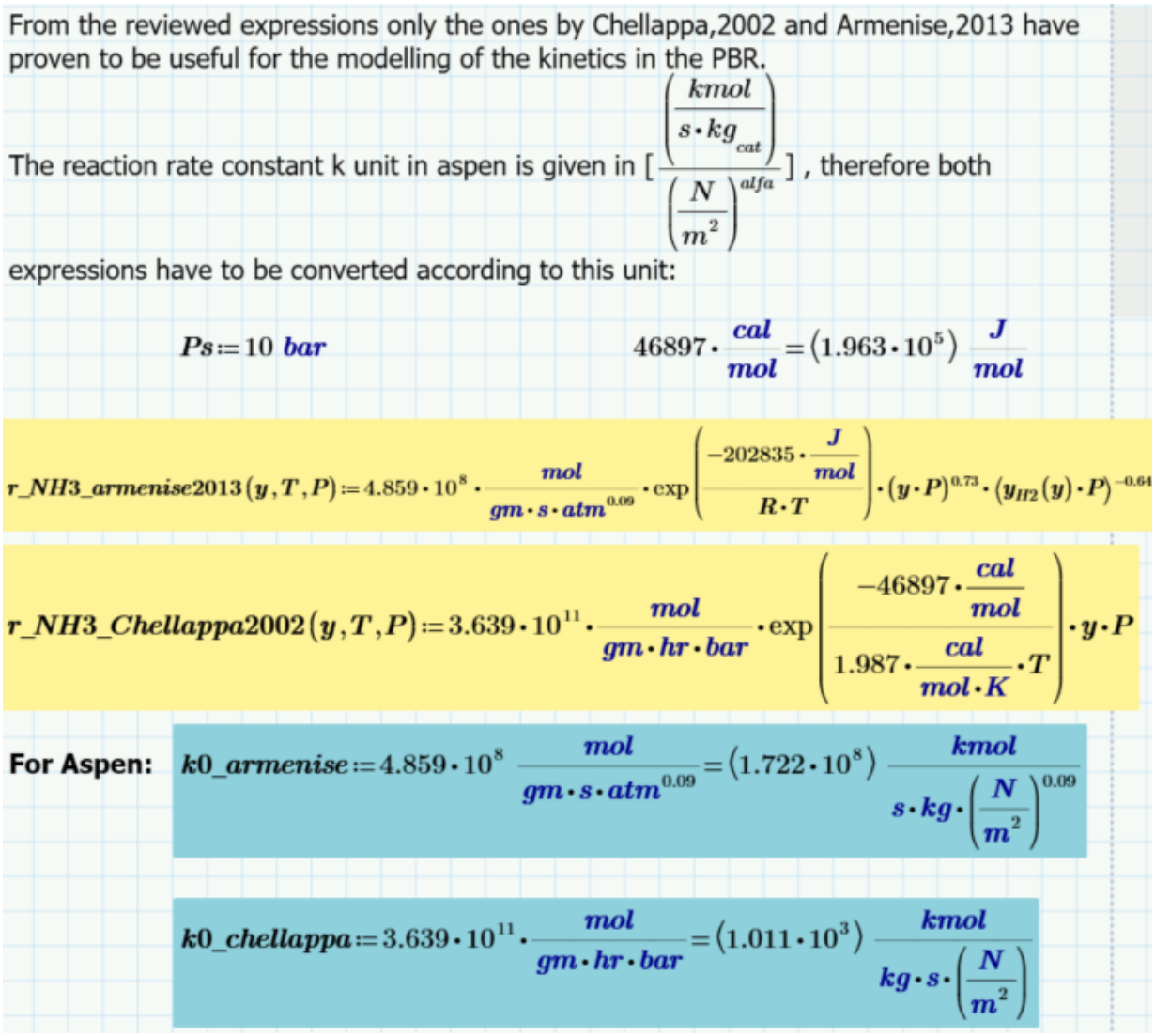

Figure C.16: Enter Caption

D

Stream Data of Aspen Plus Process Simulations

Table D.1: Case I (conventional Technology) - stream properties from Aspen Plus

Stream ID	Temperature (°C)	Pressure (bar)	Molar Vap.Fr.	Mole Flow (kmol/day)	Mass Flow (TPD)
ABSPROD	30	10	1,0	63258	596
AIR	30	1	1,0	36476	1160
COOLED	30	10	0,0	55241	1097
FLUEGAS	780	1	1,0	61341	1745
H2-DRY	30	10	1,0	43407	121
H2-PROD	20	50	1,0	43407	121
HUMID	30	10	0,0	238	5
LEAN	103	1	0,0	55241	1097
NH3-1	-34	1	0,0	34082	640
NH3-2	-34	1	0,0	3629	68
NH3-FUEL	30	1	1,0	3629	68
NH3-REC	35	1	1,0	2484	47
NH3ABS	46	10	0,0	57725	1144
PSA-PROD	30	10	1,0	43645	126
PSA-REST	30	10	1,0	19613	470
PSAWASTE	29	1	1,0	19613	470
REACFEED	660	10	1,0	34082	640
REACPROD	684	10	1,0	65590	640
S1	-34	10	0,0	34082	640
S2	347	10	1,0	34082	640
S3	659	10	1,0	34082	640
S4	419	10	1,0	65590	640
S5	87	10	1,0	65590	640
S6	30	10	1,0	65590	640
S7	46	1	0,0	57725	1144
S8	82	1	0,0	57725	1144
S9	65	1	0,0	55241	1097
S10	66	10	0,0	55241	1097

Table D.1 continued from previous page

Stream ID	Temperature (°C)	Pressure (bar)	Molar Vap.Fr.	Mole Flow (kmol/day)	Mass Flow (TPD)
S11	20	50	1,0	21704	61
S13	20	10	1,0	21704	61
S14	20	10	1,0	21704	61
S15	20	50	1,0	21704	61
S17	20	10	1,0	43407	121
SOLVENT	30	10	0,0	55392	1100
STACK	115	1	1,0	61341	1745
TANKNH3	-34	1	0,0	37711	708
WASTE	30	1	1,0	22096	517
WATER	30	10	0,0	151	3

Table D.2: Case I (Conventional Technology) - stream mole fractions from Aspen Plus

Stream ID	NH3	H2	N2	H2O	O2
ABSPROD	0,00	0,75	0,25	0,00	0,00
AIR	0,00	0,00	0,79	0,00	0,21
COOLED	0,00	0,00	0,00	1,00	0,00
FLUEGAS	0,00	0,00	0,76	0,23	0,01
H2-DRY	0,00	0,98	0,02	0,00	0,00
H2-PROD	0,00	0,98	0,02	0,00	0,00
HUMID	0,00	0,00	0,00	1,00	0,00
LEAN	0,00	0,00	0,00	1,00	0,00
NH3-1	0,99	0,00	0,00	0,00	0,00
NH3-2	0,99	0,00	0,00	0,00	0,00
NH3-FUEL	0,99	0,00	0,00	0,00	0,00
NH3-REC	0,97	0,00	0,00	0,03	0,00
NH3ABS	0,04	0,00	0,00	0,96	0,00
PSA-PROD	0,00	0,97	0,02	0,01	0,00
PSA-REST	0,00	0,24	0,76	0,00	0,00
PSAWASTE	0,00	0,24	0,76	0,00	0,00
REACFEED	0,99	0,00	0,00	0,00	0,00
REACPROD	0,04	0,72	0,24	0,00	0,00
S1	0,99	0,00	0,00	0,00	0,00
S2	0,99	0,00	0,00	0,00	0,00
S3	0,99	0,00	0,00	0,00	0,00
S4	0,04	0,72	0,24	0,00	0,00
S5	0,04	0,72	0,24	0,00	0,00
S6	0,04	0,72	0,24	0,00	0,00
S7	0,04	0,00	0,00	0,96	0,00
S8	0,04	0,00	0,00	0,96	0,00
S9	0,00	0,00	0,00	1,00	0,00
S10	0,00	0,00	0,00	1,00	0,00

Table D.2 continued from previous page

Stream ID	NH3	H2	N2	H2O	O2
S11	0,00	0,98	0,02	0,00	0,00
S13	0,00	0,98	0,02	0,00	0,00
S14	0,00	0,98	0,02	0,00	0,00
S15	0,00	0,98	0,02	0,00	0,00
S17	0,00	0,98	0,02	0,00	0,00
SOLVENT	0,00	0,00	0,00	1,00	0,00
STACK	0,00	0,00	0,76	0,23	0,01
TANKNH3	0,99	0,00	0,00	0,00	0,00
WASTE	0,11	0,21	0,67	0,00	0,00
WATER	0,00	0,00	0,00	1,00	0,00

Table D.3: Case II (Emerging Technology , 30 bar retentate case) - stream properties from Aspen Plus

	Temperature (°C)	Pressure (bar)	Molar Vap. Frac	Mole Flows (kmol/hr)	Mass Flows (TPD)
AIR	30	1	1,0	1733	1200
DES-NH3	20	4	1,0	0	0
F-1	29	1	1,0	1028	537
FLUEGAS	447	1	1,0	2835	1797
H2CLEAN	20	4	1,0	2073	103
MEMFEED1	500	30	1,0	3023	640
MEMFEED2	500	30	1,0	1868	581
MEMFEED3	500	30	1,0	1316	552
NH3-TSA	30	4	1,0	0	0
NH3DEC	-34	1	0,0	1566	640
NH3FUEL	-34	1	0,0	147	60
NH3MIX	30	1	1,0	147	60
NH3TANK	-34	1	0,0	1713	700
NH3WARM	450	30	1,0	1566	640
PERMH2-1	500	4	1,0	1203	59
PERMH2-2	500	4	1,0	582	29
PERMH2-3	500	4	1,0	288	15
RET	30	4	1,0	1028	537
RET1	500	30	1,0	1819	581
RET2	500	30	1,0	1285	552
RET3EXIT	500	30	1,0	1028	537
S1	-33	30	0,0	1566	640
S2	66	30	0,5	1566	640
S3	66	30	1,0	1566	640
S4	416	30	1,0	1566	640
S5	76	4	1,0	2074	103
S6	20	4	1,0	2074	103
S7	20	4	1,0	1037	51

Table D.3 continued from previous page

	Temperature (°C)	Pressure (bar)	Molar Vap. Frac	Mole Flows (kmol/hr)	Mass Flows (TPD)
S8	20	4	1,0	1037	51
S9	30	50	1,0	1037	51
S10	30	50	1,0	1037	51
S11	30	50	1,0	2073	103
S14	25	1	1,0	0	0
S15	30	1	1,0	147	60
S17	77	30	1,0	1028	537
STACK	150	1	1,0	2835	1797
TOTAL-H2	500	4	1,0	2074	103

Table D.4: Case II (Emerging Technology, 30 bar retentate case) - stream mole fractions from Aspen Plus

Stream ID	NH3	H2	N2	O2	H2O
AIR	0,00	0,00	0,79	0,21	0,00
DES-NH3	1,00	0,00	0,00	0,00	0,00
F-1	0,03	0,23	0,74	0,00	0,00
FLUEGAS	0,00	0,00	0,78	0,04	0,18
H2CLEAN	0,00	1,00	0,00	0,00	0,00
MEMFEED1	0,04	0,72	0,24	0,00	0,00
MEMFEED2	0,03	0,57	0,40	0,00	0,00
MEMFEED3	0,02	0,40	0,58	0,00	0,00
NH3-TSA	1,00	0,00	0,00	0,00	0,00
NH3DEC	1,00	0,00	0,00	0,00	0,00
NH3FUEL	1,00	0,00	0,00	0,00	0,00
NH3MIX	1,00	0,00	0,00	0,00	0,00
NH3TANK	1,00	0,00	0,00	0,00	0,00
NH3WARM	1,00	0,00	0,00	0,00	0,00
PERMH2-1	0,00	1,00	0,00	0,00	0,00
PERMH2-2	0,00	1,00	0,00	0,00	0,00
PERMH2-3	0,00	0,99	0,00	0,00	0,00
RET	0,03	0,23	0,74	0,00	0,00
RET1	0,06	0,54	0,40	0,00	0,00
RET2	0,05	0,37	0,58	0,00	0,00
RET3EXIT	0,03	0,23	0,74	0,00	0,00
S1	1,00	0,00	0,00	0,00	0,00
S2	1,00	0,00	0,00	0,00	0,00
S3	1,00	0,00	0,00	0,00	0,00
S4	1,00	0,00	0,00	0,00	0,00
S5	0,00	1,00	0,00	0,00	0,00
S6	0,00	1,00	0,00	0,00	0,00
S7	0,00	1,00	0,00	0,00	0,00
S8	0,00	1,00	0,00	0,00	0,00

Table D.4 continued from previous page

Stream ID	NH3	H2	N2	O2	H2O
S9	0,00	1,00	0,00	0,00	0,00
S10	0,00	1,00	0,00	0,00	0,00
S11	0,00	1,00	0,00	0,00	0,00
S14	1,00	0,00	0,00	0,00	0,00
S15	1,00	0,00	0,00	0,00	0,00
S17	0,03	0,23	0,74	0,00	0,00
STACK	0,00	0,00	0,78	0,04	0,18
TOTAL-H2	0,00	1,00	0,00	0,00	0,00